

SISO - MIMO Applications and Analysis of Visible Light Communications Systems

ANIL YESILKAYA

Bachelor of Science in Electronics Engineering, Kadir Has University, 2014

A thesis submitted in partial fulfillment for the
degree of Master of Science
in the
Graduate School of Science and Engineering

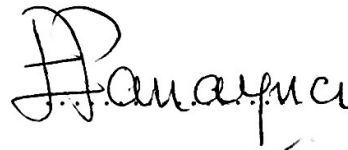
Kadir Has University

June, 2016

SISO - MIMO Applications and Analysis of Visible Light Communications
Systems

APPROVED BY:

Prof. Dr. Erdal Panayirci
(Thesis Supervisor)



Assoc. Prof. Dr. Serhat Erkucuk



Asst. Prof. Dr. Ertugrul Basar



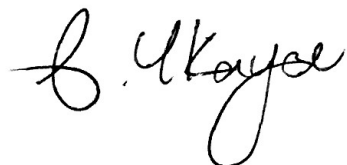
DATE OF APPROVAL: Day.Month.Year

31/05/2016

“I, Anıl Yeşilkaya, confirm that the work presented in this thesis is my own. Where information has been derived from other sources, I confirm that this has been indicated in the thesis.”

Author's Signature

ANIL YEŞİLKAYA

A handwritten signature in black ink, appearing to read 'A. Yeşilkaya', written in a cursive style.

ABSTRACT

SISO - MIMO Applications and Analysis of Visible Light Communications Systems

Rapid development in technology and increasing necessity to reach information instantaneously saturates RF bands rapidly. Because of that, it can be seen that we are gradually approaching upper limits of the band. It can be said that, operating beyond that upper limit would be hard and unfeasible for 5th generation mobile systems (5G). At this point, it is needed to develop alternative telecommunication systems to RF technology. VLC could be the most appropriate and appealing solution for researchers due to its unregulated visible light band. In this context, determination of the real VLC channel models would play vital role on bit error rate performance of the communication systems. The main objective of this thesis is to introduce this novel and interesting topic to the researchers and investigating performances of SISO and MIMO OFDM based VLC systems in realistic channel models obtained in Zemax environment. Besides, novel transmission model is proposed in the thesis and analyzed and simulated in great detail. Obtained performances of SISO-MIMO OFDM based VLC systems are compared with reference systems and conclusions are offered about the results.

Keywords: Visible Light Communications (VLC), Orthogonal Frequency Division Multiplexing (OFDM), Asymmetrically Clipped Optical OFDM (ACO-OFDM), Indoor Channel Modeling, High Rate Optical OFDM (HRO-OFDM), VLC Indoor Channel Modeling, MIMO systems, MIMO-OFDM, MAP estimation.

ÖZET

SISO - MIMO Görünür Işıklı Haberleşme Sistemlerinin Uygulamaları ve Analizi

Gelişen teknolojiler ve bilgiye olan hızlı ve artan gereksinimler nedeniyle kablosuz mobil haberleşmeye tahsis edilen radyo frekans (RF) bantlarının gittikçe ve hızla dolmakta ve bu nedenle de yavaş yavaş RF frekans bandının üst sınırlarına doğru yaklaşılmakta olduğu görülmektedir. Dolayısıyla, 5G için belirlenebilecek muhtemel frekans bantlarının ötesinde daha yüksek frekans bantlarında çalışmanın son derece güç veya olanaksız hale geleceği anlaşılmaktadır. Bu durumda RF teknolojisine alternatif olabilecek ve bu teknolojiye paralel optik tabanlı bir takım yeni haberleşme teknolojilerinin geliştirilmesi için araştırma ve geliştirme çalışmalarına gereksinim vardır. Bu soruna en uygun çözüm olarak, görünür ışıkla haberleşme (VLC), çok geniş ve regüle edilmemiş bir frekans bandına sahip olması nedeniyle, ilginç bir teknoloji olarak öne çıkmakta olup üzerinde yoğun araştırma ve geliştirme çalışmaları sürdürülmektedir. Bu bağlamda, VLC sistemlerinin kullanılacağı kanal ortamının gerçek modelinin ortaya çıkarılması ve ayrıca bu kanal üzerinden yapılan iletişim başarımının belirlenmesi büyük önem taşımaktadır. Bu tezin temel amacı, kablosuz mobil haberleşme konusunda odaklanan araştırmacılara bu güncel ve ilginç alanı ayrıntılarıyla tanıtmak ve özellikle optik SISO ve MIMO tabanlı optik OFDM yöntemleri için detaylı bir analiz sağlamanın yanı sıra yüksek veri hızlarına erişebilen yeni ve özgün bir VLC sistemin tasarımını sunmaktır. Önerilen sistemlerin başarımı Zemax yazılımı yardımıyla modellenen gerçek optik kanallar üzerinden bilgisayar benzetimleri yoluyla incelenerek diğer var olan SISO ve MIMO VLC sistemlerle karşılaştırılarak incelenmiştir.

Anahtar Kelimeler: Görünür Işıklı Haberleşme (VLC), Dikey Frekans Bölmeli Çokul-

lama (OFDM), Asimetrik Kırpılmış Optik OFDM (ACO-OFDM), Kapalı Alan Kanal Modelleme, Yüksek Hızlı Optik Dik Frekans Bölmeli Çoğullama (HRO-OFDM), VLC Kapalı Alan Kanal Modelleme, MIMO sistemler, MIMO-OFDM, MAP kestirimi.



ACKNOWLEDGEMENTS

First and foremost, I would like to offer my sincerest gratitude to my supervisor Prof. Dr. Erdal Panayirci, head of the Kadir Has University electrical and electronics engineering department for providing me great opportunity to work with his very prestigious research group. It has been honor to be a part of this top line team. I appreciate all his support, time and efforts on my education. His endless energy and motivation inspired me to become not only a good engineer but also a good person.

I gratefully acknowledge the Kadir Has University, Department of Electrical - Electronics Engineering funding and Prof. Dr. Erdal Panayirci's research grant from the TUBITAK COST 2515 Project, "MIMO –OFDM Based Visible Light Communications", Project No. 113E307 for providing me financial support throughout my graduate studies. I have served as a teaching assistant in the Department of Electrical - Electronics Engineering at Kadir Has University and a research assistant in Prof. Panayirci's project in the last two years.

Many thanks also to Asst. Prof. Ertugrul Basar, Assoc. Prof. Serhat Erkucuk, Asst. Prof. Habib Senol and Asst. Prof. Arif Selcuk Ogresci for their valuable contributions to my graduate education.

And finally, I would like to say a heartfelt thank you to my parents and my sister for their patience and encouragement which helped me to become a good scientist.

TABLE OF CONTENTS

ABSTRACT	iv
ÖZET	v
ACKNOWLEDGEMENTS	vii
LIST OF FIGURES	xii
LIST OF TABLES	xviii
LIST OF SYMBOLS/ABBREVIATIONS	xx
1. Introduction	1
1.1. History of OWC	1
1.2. Towards 5G Wireless Cellular Networks	1
1.3. Thesis Contributions	3
1.4. Thesis Outline	4
2. Indoor Optical Wireless Communication	5
2.1. IM/DD Structure	5
2.1.1. LED as a Transmitter	6
2.1.2. Photo-diode as a Receiver	7
2.2. VLC Channel Impulse Response Modeling	7
2.2.1. Sequential Ray-tracing Approach	8
2.2.1.1. Selection of materials	10
2.2.1.2. Selection of light sources	10
2.2.1.3. Selection of detectors	10
2.3. Numerical Results	11
2.4. Conclusions	13
3. Analysis of OFDM Based Indoor OWC Systems	16
3.1. SISO Based O-OFDM Systems	17
3.1.1. ACO-OFDM Based IM/DD OWC Systems	17

3.1.1.1.	VLC Channel Impulse Response Modeling	20
3.1.1.2.	Selection of materials	20
3.1.1.3.	Selection of Light Sources and Detectors	21
3.1.1.4.	Channel Impulse Response	21
3.1.1.5.	ACO-OFDM	22
3.1.1.6.	Computer Simulation Results	26
3.1.1.7.	Conclusions	26
3.1.2.	DCO-OFDM Based IM/DD OWC Systems	28
3.1.2.1.	Introduction	28
3.1.2.2.	VLC Channel Impulse Response Modeling	29
3.1.2.3.	DCO-OFDM System Structure	29
3.1.2.4.	Computer Simulation Results	33
3.1.2.5.	Conclusions	35
3.2.	MIMO Based Optical OFDM Systems	35
3.2.1.	Enhanced Unipolar OFDM (eU-OFDM)	35
3.2.1.1.	Introduction	36
3.2.1.2.	Realistic VLC Channel Modeling	37
3.2.1.3.	MIMO Enhanced Unipolar OFDM (MIMO-eU-OFDM) System	42
3.2.1.4.	Computer Simulation Results	46
3.2.1.5.	Conclusions	47
3.2.2.	Red-Green-Blue OFDM (RGB-OFDM)	49
3.2.2.1.	Introduction	49
3.2.2.2.	System Structure	51
3.2.2.3.	MIMO Channel Model	54
3.2.2.4.	Frequency Selective MIMO Channel Model	56
3.2.2.5.	Design of a MAP Estimator	57
3.2.2.6.	Eigenvalue decomposition for circulant matrices	58
3.2.2.7.	Simulations and Results	59

3.2.2.8. Conclusions	59
4. Realization of Indoor Optical Wireless Communication Systems	61
4.1. 1st Generation (1G) RZ-OOK Based VLC System	62
4.1.1. Transmitter	63
4.1.2. Optical Channel	64
4.1.3. Receiver	64
4.1.4. Experimental Results	66
4.1.5. Conclusions	67
4.2. 2nd Generation (2G) 4-PAM Based VLC System	69
4.2.1. Transmitter	70
4.2.1.1. DAQ (Data Acquisition) Board	71
4.2.1.2. LED Current Driver	71
4.2.1.3. Power LED	71
4.2.2. Optical Channel	72
4.2.3. Receiver	73
4.2.4. Experimental Results	73
4.2.4.1. SER Graph of 4 level system (Ideal Channel)	74
4.2.4.2. Comparison of SER Graph in 4 Level System with Realistic Channel and Ideal Channel	74
4.2.4.3. SER Graph of 8 level system (Ideal Channel)	75
4.2.5. Conclusions	75
4.3. 3rd Generation (3G) OFDM Based Optical Wireless Communication System	77
4.3.1. Optical OFDM for VLC in IM/DD Systems	78
4.3.2. Implementation of the Optical OFDM System	78
4.3.3. Transmitter	80
4.3.3.1. Choosing the LED Positions	80
4.3.3.2. Amplifier and Use of Current Source as Bias	81
4.3.3.3. ADLINK DAQ Board	81

4.3.4. Visible Light Communications Channel	82
4.3.5. Receiver	83
4.3.6. ACO-OFDM Modulation and Demodulation Processes	84
4.3.7. VLC System Based on LTE Standard	85
4.3.8. Experimental Results	86
4.3.9. Conclusions & Future Works	89
5. Conclusions	91
APPENDIX A:	92
REFERENCES	97
A.1. Curriculum Vitae	104
A.2. Publications	104
A.2.1. National Journal Papers	104
A.2.2. International Conference Papers	104
A.2.3. National Conference Papers	105

LIST OF FIGURES

Figure 1.1.	OWC Timeline	2
Figure 2.1.	Intensity Modulation / Direct Detection (IM/DD) Structure	6
Figure 2.2.	Spectral reflectances of various materials for IR and VL bands respectively.	8
Figure 2.3.	Spectral reflectances of reference materials in VL band	11
Figure 2.4.	Geometry of source and detector	12
Figure 2.5.	Inputs and outputs of Zemax environment	12
Figure 2.6.	Scenarios under consideration	13
Figure 2.7.	Spectral reflectance of plaster	13
Figure 2.8.	CIRs for different configurations, (a) CIR for configuration A, (b) CIR for configuration B, (c) CIR for configuration C, (d) CIR for configuration D, (e) CIR for configuration E, (f) CIR for configuration F	14
Figure 3.1.	Optical OFDM system's development	16
Figure 3.2.	IM/DD OFDM	17
Figure 3.3.	ACO OFDM Frame Structure	18

Figure 3.4.	ACO OFDM Block Diagram	18
Figure 3.5.	Structure and CIR of Configuration A	22
Figure 3.6.	Structure and CIR of Configuration B	23
Figure 3.7.	BER performance of Configuration A	27
Figure 3.8.	BER performance of Configuration B	27
Figure 3.9.	DCO Block Diagram	29
Figure 3.10.	BER performance of Configuration A	34
Figure 3.11.	BER performance of Configuration B	34
Figure 3.12.	Configuration A (receivers located in center), B (receivers located in corners) and C (receivers at the left corner, chair and laptop exists)	38
Figure 3.13.	The PDP's for configuration C	40
Figure 3.14.	Channel frequency responses for configuration C	41
Figure 3.15.	Wiring topology between communication access point and luminaries	42
Figure 3.16.	Cabling topology in configuration C via CAT-5	42

Figure 3.17.	Channel impulse response for configuration C including the delays caused by cabling	43
Figure 3.18.	eU-OFDM signal generation for $L = 3$ layers	44
Figure 3.19.	MIMO-eU-OFDM system model for $T \times R$ Optical MIMO System	46
Figure 3.20.	Performance of MIMO-eU-OFDM and V-BLAST-DCO-OFDM for 2×2 MIMO system	47
Figure 3.21.	Performance of MIMO-eU-OFDM and V-BLAST-DCO-OFDM for 4×4 MIMO system	48
Figure 3.22.	RGB OFDM Block Diagram	51
Figure 3.23.	Office room scenario	55
Figure 3.24.	Simulated relative spectral distributions of the RGB and white LEDs respectively	55
Figure 3.25.	BER vs. SNR Results for ZF and MAP Estimators with L=1 and L=2 tap channels	59
Figure 3.26.	MSE vs. BER Result for ZF and MAP Estimator with L=2 tap channel	60
Figure 4.1.	1^{st} , 2^{nd} and 3^{rd} Generation OWC Systems	61
Figure 4.2.	RZ-OOK Transmitter Structure	63

Figure 4.3.	Flowchart of RZ-OOK MATLAB audio transmission algorithm	63
Figure 4.4.	RZ-OOK Receiver Structure	64
Figure 4.5.	Photograph of receiver circuitry	65
Figure 4.6.	Flowchart of RZ-OOK MATLAB receiver algorithm for audio	65
Figure 4.7.	Photograph of CP2102 USB TO UART Bridge	66
Figure 4.8.	Distance vs BER graphs for; 64K white LED w/o lens (upper left), 64K blue LED w/ lens (upper right), 64k white LED w/ lens (lower left) and BER vs SNR graph for 64K white LED w/ lens (lower right).	68
Figure 4.9.	Sent and received signal shapes for various distances (yellow is sent signal and blue is received signal)	68
Figure 4.10.	PAM based VLC System Schematic	69
Figure 4.11.	Transmitter part of the 2nd generation PAM based VLC system	70
Figure 4.12.	String that converted voltage values.	71
Figure 4.13.	CIR obtained by optical illumination software environment	72
Figure 4.14.	Decision algorithm at the receiver	73
Figure 4.15.	Receiver part of the 2nd generation PAM based VLC system	74

Figure 4.16.	4 Level SER vs. SNR in different distances	75
Figure 4.17.	4-Level SER vs. SNR, Ideal vs. Realistic Channel	76
Figure 4.18.	8 Level SER vs. SNR in different distances	76
Figure 4.19.	Basic Indoor VLC System Working Principle	78
Figure 4.20.	Block diagram of receiver-transmitter parts of an ACO-OFDM system	79
Figure 4.21.	1G (left) and 2G (right) VLC Systems	79
Figure 4.22.	The general view of third generation VLC system	80
Figure 4.23.	LED light sources	81
Figure 4.24.	560B Laser Diode Driver as a current source	81
Figure 4.25.	ADLINK USB-1902 device and input/output connections	82
Figure 4.26.	Demonstration of how the system works	82
Figure 4.27.	ACO OFDM Block Diagram for channel estimation	83
Figure 4.28.	Block diagram of ACO-OFDM system	84
Figure 4.29.	Block diagram of ACO-OFDM system	85

Figure 4.30. Message signal and received message signal 86



LIST OF TABLES

Table 2.1.	Comparison of RF and VLC systems	6
Table 2.2.	Parameters of given configurations in Fig. 2.6	14
Table 2.3.	Different material types for empty room	14
Table 2.4.	Channel parameters of scenario-1	15
Table 2.5.	Channel parameters of scenario-2	15
Table 3.1.	Channel Configurations	22
Table 3.2.	Channel Configurations	39
Table 3.3.	Channel parameters for configurations A, B and C	40
Table 3.4.	Spectral Efficiencies of various modulation methods	51
Table 3.5.	RGB OFDM Signal Generation Rule	52
Table 3.6.	Simulation Parameters	56
Table 3.7.	Channel Parameters for Office room with secondary light scenario including human body and furniture	56

Table 4.1.	Results for audio transmission with white power LED	66
Table 4.2.	Results for image transmission with white power LED	67
Table 4.3.	Results for image transmission with blue power LED	67
Table 4.4.	Transmitter loop-up table for 2G system	70
Table 4.5.	Results for, DC Bias: 280mA, sample rate: 150K, N: 2048	87
Table 4.6.	Results for, DC Bias: 280mA, sample rate: 100K, N: 2048	87
Table 4.7.	Results for, DC Bias: 280mA, sample rate: 100K, N: 4096	88
Table 4.8.	Results for, DC Bias: 500mA, sample rate: 150K, N: 2048, M: 4	88
Table 4.9.	Results for, DC Bias: 500mA, sample rate: 150K, N: 2048, M: 16	88
Table 4.10.	Results for, DC Bias: 500mA, sample rate: 150K, N: 2048, M: 64	88
Table 4.11.	Results for, DC Bias: 500mA, sample rate: 150K, N: 4096, M: 4	89
Table 4.12.	Results for, DC Bias: 500mA, sample rate: 150K, N: 1024, M: 4	89
Table 4.13.	QPSK wire modulation with various subcarriers	89

LIST OF SYMBOLS/ABBREVIATIONS

χ^2	: Chi-square distribution
$\delta(.)$: Dirac delta function
η	: Noise
γ_m	: SNR
\hat{P}_f	: The probability of misdetection of overall system
λ_i	: Threshold values
τ_i	: i th component of the multipath delay
E_b	: Energy per bit
E_p	: Mean pulse energy
H_0	: Hypothesis that the primary system is not present
H_1	: Hypothesis that the primary system is present
h_i	: i th multipath coefficient
j	: Number of situation
K	: Number of sensors
L	: Number of component of multipath delay
L_r	: Number of rake fingers
M	: Number of bands
N_f	: Number of frames
$P_{e,j}$: Probability of error for j th situation
$P_{e,m}$: Probability of error for m th link
$P_{f,T}$: Total probability of false alarm for one sensor
$P_{md,T}$: Total probability of misdetection for one sensor

T_i : Integration duration

T_s : Signal duration

W_{rx} : Noise bandwidth of the receiver front end

A/D : Analog-to-Digital

ACO-OFDM : Asymmetrically Clipped Optical Orthogonal Frequency Division Multiplexing

AWGN : Additive white Gaussian noise

BPSK : Binary Phase Shift Keying

CIR : Channel Impulse Response

D/A : Digital-to-Analog

DAQ : Digital Acquisition

DCO-OFDM : Direct Current Biased Optical Orthogonal Frequency Division Multiplexing

eU-OFDM : Enhanced Unipolar Orthogonal Frequency Division Multiplexing

FFT : Fast Fourier Transform

ICI : Inter-carrier Interference

IFFT : Inverse Fast Fourier Transform

IM/DD : Intensity Modulation and Direct Detection

IR : Infra-red

ISI : Inter-symbol Interference

LED : Light Emitting Diode

LiFi : Light fidelity

LOS : Line of Sight

MAP : Maximum-a-Posteriori

MIMO : Multiple Input Multiple Output

NLOS : Non-Line of Sight

OFDM : Orthogonal Frequency Division Multiplexing

OWC : Optical Wireless Communications

P/S : Parallel-to-Serial

PAPR : Peak-to-Average-Power Ratio

PD : Photo-diode

PDF : Probability Density Function

PHY : Physical layer

QAM : Quadrature amplitude modulation

RGB : Red-green-blue

RZ-OOK :Return-zero On-Off Keying

S/P : Serial-to-Parallel

SISO Single Input Single Output

SNR : Signal-to-Noise Ratio

U-OFDM : Unipolar Orthogonal Frequency Division Multiplexing

VL : Visible Light

VLC : Visible Light Communications

WiFi : Wireless fidelity

WLAN : Wireless local area network

ZF : Zero Forcing

1. Introduction

1.1. History of OWC

OWC is one of the oldest technologies that mankind is still using. It is known that around 800 BC, ancient Romans and Greeks were using reflection of sunlight and fire beacons for signaling purposes. Around 150 BC, American Indians were using smoke patterns to communicate over long distances. French inventor Claude Chappe invented optical telegraph better known as semaphore telegraph in 1792. In 1880, Alexander Graham Bell invented photo-phone to transmit his voice by simply employing vibrating mirrors to modulate the sunlight and selenium cell at the receiver to demodulate voice signals [1]. Invention of the laser beam in 1960, new area called FSO emerged and lasers are employed for space communications. Over the last decade 10Gbps data rate is achieved between satellites using FSO link [2]. Two of the most important vulnerabilities of the FSO links investigated as atmospheric effects and fog. In 1979, indoor OWM systems are investigated by Gfeller and Bapst [3]. In 1993, open standard for infrared communications (IrDA) is developed and used by many devices. 2000's could be the junction that, almost 2900 years of technology revives by using modern electronic components. It started with OMEGA project in 2008 and standardized in 2009 by IEEE under the name of 802.15.7 protocol. Rapid development of opto-electronics devices helped significantly to achieve higher data rates. Today's OWC systems with full duplex communications could reach up to 2.5 Gbps by employing WDM techniques. Historical timeline for OWC systems are given in Fig. 1.1.

1.2. Towards 5G Wireless Cellular Networks

Fortune of the telecommunications systems significantly changed in 1947 after invention of transistor by Bardeen, Brattain and Shockley. IC's started to be used in analog/digital signal processing areas. OFDM implementation of DFT/IDFT pair allows OFDM to be easy to implement

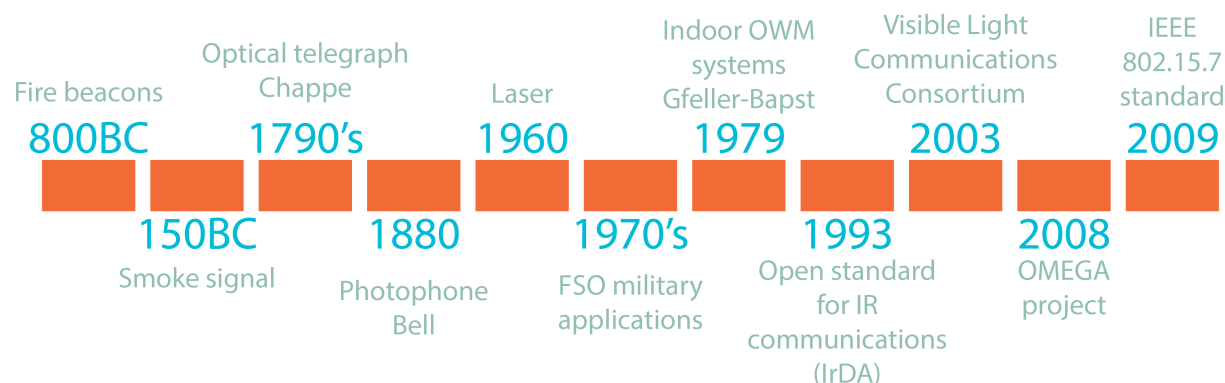


Figure 1.1. OWC Timeline

system in variety of digital signal processing boards (FPGA, DAQ Boards, BeagleBone, Rasberry etc.). Frequency selective behavior of the wireless channels and as a result ISI pushed researchers and engineers to combat with multi-path propagation. OFDM became one of the widely applied scheme among multi-carrier transmission methods. Despite the fact that OFDM has many advantages over frequency selective channels, it also has many disadvantages such as, high PAPR and vulnerability to phase noise and frequency offset.

After mobile revolution in 2000's, number of mobile devices are started to increasing exponentially. Internet of things, wearable technologies, smart cities etc. concepts are emerged. Rapid development of mobile devices are started to cause a capacity issues in the network. According to Cisco forecasts, global mobile traffic in 2019 would be around 24.3 exabytes (1 EB = 10^{18} bytes). In spite of the exponential increase of the data demand each year, spectral efficiency gains are degrading exponentially and converges to one. Potential bottleneck in the spectrum, pushes researchers to find new mediums to communicate, millimeter-wave technologies is one of the hottest topics in wireless communications for 5G, 5G+ and 6G systems [4]. TVWS is another technology which would potentially employ TV white space band for WRANs [5]. VLC is another new and complimentary wireless transmission candidate for small-cell levels. The optical APs which named as an attocell, could improve coverage and security while reducing interference with the macro-cellular network. VLC-RF heterogenous networks, channel models and physical layer modulation methods are under investigation by researchers under IEEE 802.15.7 standization

groups. Nonetheless, VLC has various kinds of challenges such as, front-end non-linearities, multi-user communications scenarios, utilization of the optical spectrum, capacity enhancing techniques and multiple access scenarios. This thesis addresses physical layer solutions in both theoretical and practical ways while considering realistic VLC channel models in OWC links.

1.3. Thesis Contributions

This thesis has contributions in three main subjects. Firstly, novel VLC channel modeling approach and obtaining CIRs. Secondly, performing BER vs. SNR analysis of SISO and novel MIMO systems under realistic CIRs. Lastly, realization of VLC systems by experimental setup in real life. In Section 2.2, realistic VLC channel modeling approach proposed by our research group is explained in detail. In Chapter 3, realization process of the VLC systems in experiment setup by utilizing RZ-OOK, PAM and OFDM modulation schemes is given with promising BER vs. SNR results. In Chapter 4, two of the most popular optical OFDM methods for IM/DD system ACO-OFDM and DCO-OFDM are analyzed in detail and their performances investigated under realistic channel models obtained in Section 2.2. In Chapter 4, MIMO is proposed for VLC communications for different modulation techniques. Section 4.2.1 proposes MIMO transmission scheme for one of state-of-the-art spectral efficient unipolar schemes called eU-OFDM. Realistic concerns such as cabling delays between luminaries are considered to model VLC channel. Eventually, MIMO frequency selective sparse channel model is obtained and proposed for MIMO VLC transmission. Finally, in Section 4.2.2, WDM based novel and spectrally efficient transmission scheme called RGB-OFDM is proposed. Through providing this modulation scheme its performance analysis has been conducted for MIMO frequency selective sparse RGB channel models by employing maximum a posteriori detector. It is proposed that, by using time-domain half-Gaussian distribution information of the discrete-time samples gives the optimal detector for such MIMO VLC OFDM systems.

1.4. Thesis Outline

The rest of this thesis is organized as follows. **Chapter 2**, indoor optical wireless communication systems are introduced, including IM/DD structure and non-sequential ray tracing based VLC channel modeling approach.

In **Chapter 3**, OFDM based optical wireless communication systems are elaborated. Section 3.1 presents mathematical background and performances of two most important OFDM based SISO communication systems ACO-OFDM and DCO-OFDM under realistic channel models obtained in Chapter 2. Section 3.2 expands same analysis and performance benchmark for one of the recent invention for unlocking spectral efficiency loss which is called enhanced unipolar OFDM (eU-OFDM) and proposed novel wavelength division multiplexing (WDM) based red-green-blue OFDM (RGB-OFDM).

In **Chapter 4**, real life applications of RZ-OOK, PAM and OFDM systems for optical communication is given. Channel estimation and equalization techniques are introduced for systems of interest. Experimental BER vs. SNR results are given.

Finally, **Chapter 5** concludes the thesis with the crucial findings on this study. The limitations of the work discussed, and future work is presented.

2. Indoor Optical Wireless Communication

2.1. IM/DD Structure

In radio frequency (RF) communication systems we have three fundamental property of an electromagnetic waves that we can carry information on which are, amplitude, frequency and phase. In optical systems as long as we are dealing with the light wave as a information carrying medium, we could only have light intensity to carry information. There is no frequency and phase information on the light wave. So that, non-coherent detectors are used at the receiver part instead of coherent detectors. This type of light intensity modulation and non-coherent reception system called as intensity modulation and direct detection (IM/DD) system. In Fig. 2.1 basic structure of an IM/DD system is given. Generated electrical signals are converted to optical intensity levels by electro-optical converter device which could be simple off-the-shelf LED at the transmitter. Optical intensity levels pass through optical channel where reflection, refraction and noise phenomenons occur. At the receiver front-end simple photo-diodes are employed in reverse biased way to convert optical intensity levels to electrical signals back. The information carrying signal at the transmitter is constrained to be non-negative and real all time, since light intensity levels are inherently positive and real numbers. Constrains for signal $x(t)$ could be given as, $x(t) \geq 0$ and $\Im_{x(t)} = 0$ for $\forall t$. In consequence of, positiveness and realness of the both transmitted and received signals, effect of the optical channel must be positive and real in IM/DD systems. One of the most important advantage of modulating light intensity becomes obvious in high mobility case. In typical RF systems, high mobility causes variation in carrier frequency which is well known phenomenon called Doppler shift. Despite of in IM/DD based systems moving source still introduces Doppler shift in the light's frequency, it would only effect red shift and blue shift in the color. This inherent difference of RF and VL bands comes from the fact that, there is no medium required for the propagation of the light waves. Basic characteristics of non-coherent IM/DD systems and coherent systems are summarized in the Table 2.1.

Table 2.1. Comparison of RF and VLC systems

Typical RF System	Complex & Bipolar	Electromagnetic Radiation Conveys Information	Coherent Detection, Local Oscillator at the Receiver
Optical System	Real & Unipolar	Light Intensity Conveys Information	Non-coherent, Direct Detection

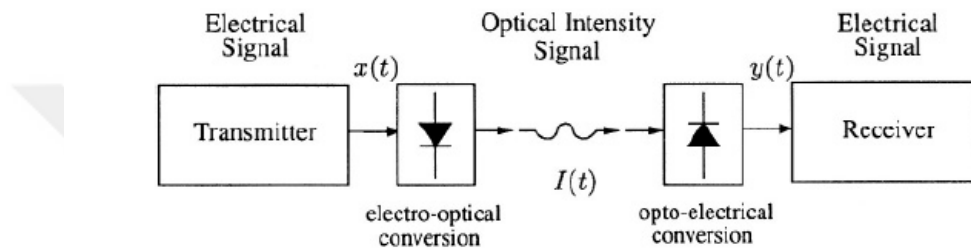


Figure 2.1. Intensity Modulation / Direct Detection (IM/DD) Structure

2.1.1. LED as a Transmitter

Solid state lighting technologies are developed in last decade very fast. Incandescent light sources are replaced by LEDs, OLEDs, amOLEDs etc. Rapid development in the LED technologies has granted huge chance to OWC systems. Deployment ease and expense would be one of the major advantage of the VLC system among other candidate systems. In VLC technology, generic off-the-shelf LEDs operating in the 780-950nm range would be utilized as a transmitter. Modulated electrical signals at the receiver is directly fed into a typical LED, information could be carried on either voltage or current. LED acts as a simple converter which would convert voltage/current values (electrical domain) to optical intensity values (optical domain). Frequency response, non-linear characteristics and self-heating problems are various problems that VLC will face with in near the future. Detailed explanation about lighting sources and their real life performances will be mentioned in next two sections in a great detail.

2.1.2. Photo-diode as a Receiver

Complementary to transmitter device photo-diode device converts optical intensity values to electrical voltage/current values back. Non-linear characteristics of the PD is still an important issue at the receiver side. Opto-electrical devices could be utilized at the PD (optical lenses, filters, retarders etc.). Detailed explanation about photo-diodes and their real life performances will be mentioned in next two sections in a great detail.

2.2. VLC Channel Impulse Response Modeling

OWC comprises VL (visible light) and IR (infra-red) regions of the spectrum as indoor/outdoor wireless communications medium. Visible light communications (VLC) is a branch of OWC operating in the VL (390nm-750nm) band. Intensity Modulation / Direct Detection (IM/DD) method is accepted as the most applicable modulation technique to transmit data over visible light. In IM/DD data are coded on the small intensity fluctuations. At the receiver, photo-detectors capture fluctuations and convert them to digital data [6]. A proper channel model is one of the most important components to have robust, error-free and reliable wireless communications systems. Despite the ever increasing popularity of the visible light communications, there is a lack of a proper VLC channel model. Obtaining an analytical expression for the channel is almost impossible due to the unpredictable changes in the environment.

Reflection and refraction patterns are already well defined for daily life materials however, dynamic parameters are affecting the VLC channel (e.g. moving objects and people, fluctuations in noise sources, unknown reflections of mixed type materials etc.) which complicate the derivation of an analytical expression for the channel model. Obtaining proper channel model ensures designing reliable and robust communication systems. Yet, in the literature most of the researches are using infra-red (IR) channel models or simple additive white Gaussian noise (AWGN) channel to model VLC environment [7, 8]. In [9], IR sources are defined as monochromatic where white

LED's are considered as wide-band sources (380nm-780nm) intrinsically. It could be seen from Fig. 2.2 that wavelength dependent VL channel models are required.

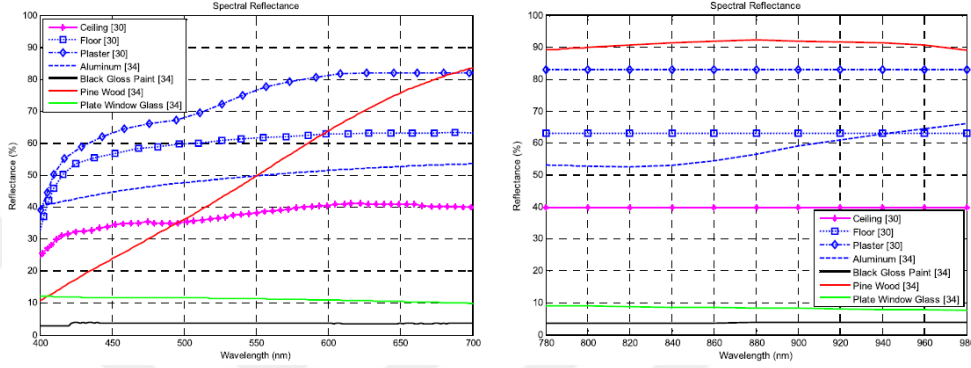


Figure 2.2. Spectral reflectances of various materials for IR and VL bands respectively [10, 9, 11].

For higher data rates VLC channel has frequency selective behavior [10]. Frequency selectivity basically means that channel acts as a simple FIR filter described by coefficients which are called "channel taps" in the communication literature. Obtaining channel taps brings great control over distortion cancellation in the received signal. These channel taps are used to model channel impulse response (CIR) which can be expressed as attenuations and time delays as,

$$h(t) = \sum_{i=1}^N P_i \delta(t - \tau_i) \quad (2.1)$$

where P_i is the power and τ_i is the propagation time of the i^{th} ray, δ is the Dirac delta function and N is the number of rays received in the detector.

2.2.1. Sequential Ray-tracing Approach

As a research group, we present an extensive study on indoor channel modeling for VLC and present channel impulse responses (CIRs) and associated characteristics for a number of indoor environments. This part of the study is based on Zemax; a commercially available optical and illumination design software [12]. Although the main purpose of such software is optical and

illumination system design, we take advantage of the ray tracing features of this software which allows an accurate description of the interaction of rays emitted from the lighting source within a specified and confined space (i.e., room, office, etc).

Zemax is an optical and illumination design software with sequential and non-sequential ray-tracing capabilities. It allows an accurate description of the interaction of rays emitted from the LEDs for a user-defined indoor environment. In non-sequential ray-tracing, rays are traced along a physically realizable path until they intercept an object. The line-of-sight (LOS) response is straightforward to obtain and depends upon the LOS distance. Besides the LOS component, there is a large number of reflections between ceiling, walls, and floor as well as any other objects within the environment. The rays of light hit the other walls and are reflected towards the receiver. The simulation environment is created in Zemax and enables us to specify the geometry of the environment, the objects inside, the reflection characteristics of the surface materials as well as the specifications of the sources (i.e., LEDs) and receivers (i.e., photodiodes). In order to create the simulation environment in Zemax, we need to specify application scenario, room size, position of transmitters and receivers, type of materials and type of sources and detectors.

Based on the obtained CIRs, we can further quantify fundamental channel characteristics. Channel DC gain (H_0) is one of the most important features of the VLC channel. It determines the achievable signal-to-noise ratio (SNR) for fixed transmitter power. The delay profile is composed of dominant multiple line of sight (LOS) links and less number of non-line of sight (NLOS) delay taps. The temporal dispersion of a power delay profile can be expressed by the mean excess delay (τ_0) and the channel root-mean-square (RMS) delay spread (τ_{RMS}). These parameters are given by [10],

$$\begin{aligned}
\int_0^{T_r} h(t)dt &= 0.97 \int_0^{\infty} h(t)dt \\
\tau_0 &= \frac{\int_0^{\infty} t \times h(t)dt}{\int_0^{\infty} h(t)dt} \\
\tau_{RMS} &= \sqrt{\frac{\int_0^{\infty} (t-\tau_0)^2 h(t)dt}{\int_0^{\infty} h(t)dt}} \\
H_0 &= \int_{-\infty}^{\infty} h(t)dt
\end{aligned} \tag{2.2}$$

From (2.2) it can be seen that 97 percent of the power of the CIR is contained in the $[0, T_r]$ interval.

2.2.1.1. Selection of materials. The selection of material for wall, ceiling and floor is particularly important for realistic channel modeling. From NASA database [11] we can choose some realistic materials and apply to our configuration. In Fig.1-5 reflectivity values of bare red brick, pine wood, black gloss paint, plate window glass and plaster have been shown respectively and we can see the reflectivity of each material in VLC band in Fig. 2.3.

2.2.1.2. Selection of light sources. In Zemax, we can select light sources from commercially available devices [13] and [14] such as Cree Inc., OSRAM AG, OPTO Diode Corp., Philips Lighting, Vishay Intertechnology, Panasonic Corporation, StockerYale.

2.2.1.3. Selection of detectors. In Zemax, we can specify different detector parameters (types) including detector color, polar, Rectangle, surface and volume. In Fig. 2.4 you can see the geometry of source and detector with respect to each other.

Main structure of our VL channel modeling methodology is given in Fig. 2.5.



Figure 2.3. Spectral reflectances of reference materials in VL band [11].

2.3. Numerical Results

In our work, we consider an empty rectangular room with dimensions $3m \times 3m \times 3m$ and change the position/rotation of detector, see Fig. 2.6. All related simulation parameters are summarized in Table 2.2 and 2.3. CIRs are provided in Fig. 2.8. Channel parameters are calculated based on CIRs and presented in Tables 2.4 and 2.5. Based on Table 2.4 and 2.5 we can see that:

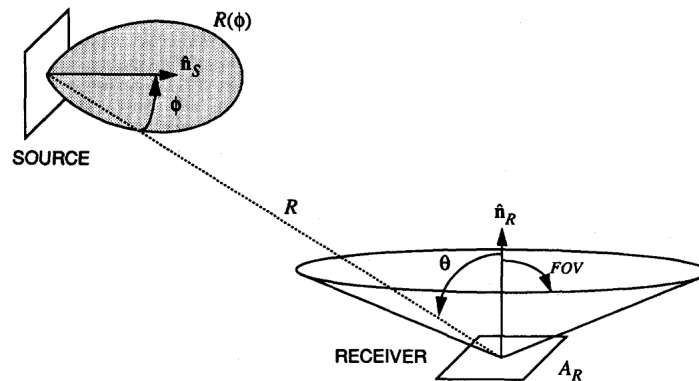


Figure 2.4. Geometry of source and detector

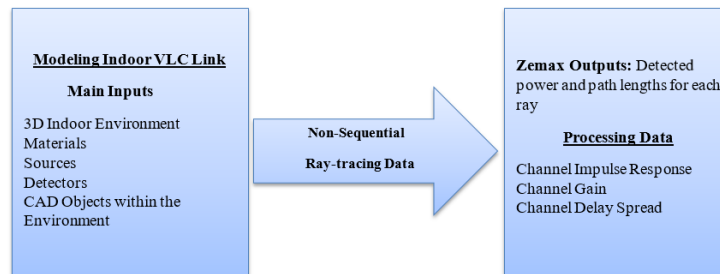


Figure 2.5. Inputs and outputs of Zemax environment

- The position of receiver and transmitter with respect to each other has large effect on CIR and channel parameters. For example by moving the detector to the corner, RMS delay increases because the detector receive more scatter from corner sides. We can see this effect in scenario which the detector has rotation. Also by rotation of the detector, the received power decreases because the detector can not receive scatter from some places (behind the detector).
- CIR and parameters of channel largely depends on material which has been used in our configuration. In scenario F we used material with smaller reflectivity compared to scenario A and we can see the RMS delay decreases because the detector receive less power from wall, floor and ceiling.

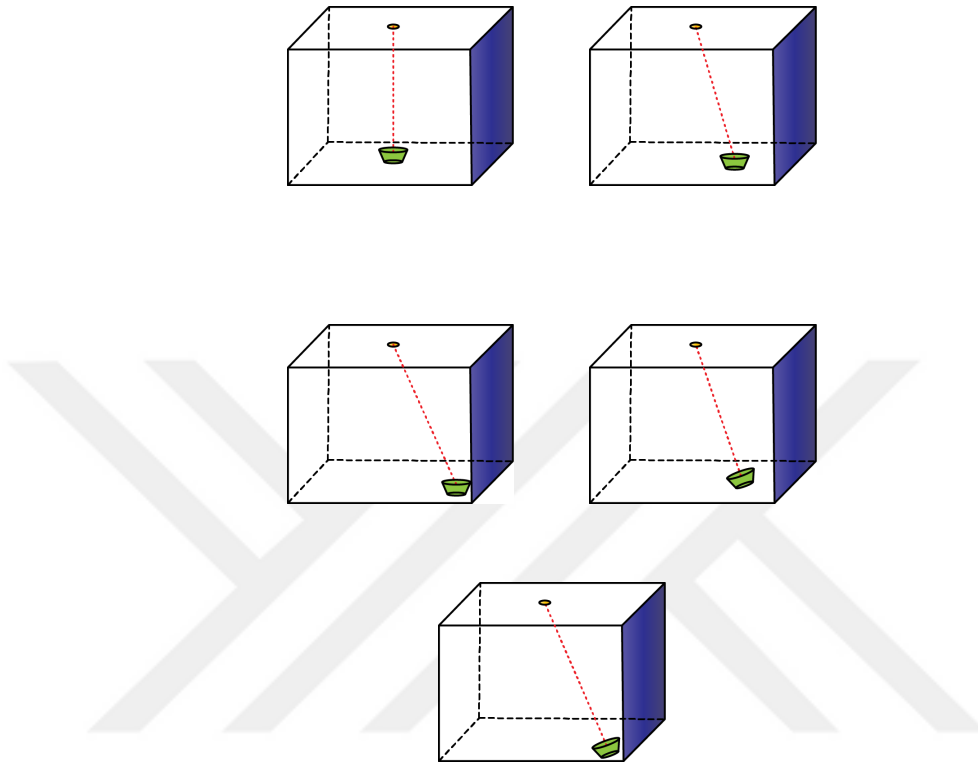


Figure 2.6. Scenarios under consideration

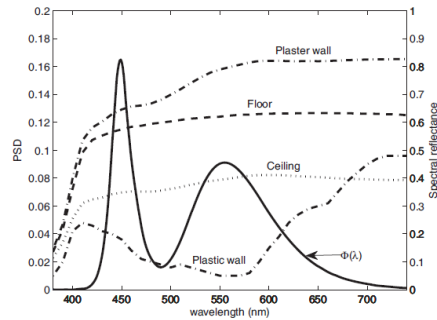


Figure 2.7. Spectral reflectance of plaster [9].

2.4. Conclusions

In this, section we presented an overview of VLC channel structure and approaches for channel modeling. It is greatly emphasized that, IR channel models used in literature is not suitable for visible light communications. Reflectivity is almost constant for IR band for various materials but it is not the case in VL band. Obtaining one closed form expression for VLC channel is

Table 2.2. Parameters of given configurations in Fig. 2.6

Configuration	Specifications	Room size (m ³)	Position of Transmitters (m)	Position of Receiver (m)	Reflectivity
A	Empty Room Bottom 1 Illumination	3x3x3	(0,0,3)	(0,0,0)	Wall: Plaster Ceiling: Plaster Floor: Pine Wood
B	Empty Room Bottom 1 Illumination	3x3x3	(0,0,3)	(0.75,0.75,0)	Wall: Plaster Ceiling: Plaster Floor: Pine Wood
C	Empty Room Bottom 1 Illumination	3x3x3	(0,0,3)	(1.3,1.3,0)	Wall: Plaster Ceiling: Plaster Floor: Pine Wood
D	Empty Room Bottom 1 Illumination (Rotation)	3x3x3	(0,0,3)	(0.75,0.75,0)	Wall: Plaster Ceiling: Plaster Floor: Pine Wood
E	Empty Room Bottom 1 Illumination (Rotation)	3x3x3	(0,0,3)	(1.3,1.3,0)	Wall: Plaster Ceiling: Plaster Floor: Pine Wood

Table 2.3. Different material types for empty room

Config.	Specifications	Room size (m ³)	Position of Transmitters (m)	Position of Receiver (m)	Reflectivity
A and F	Different Material Types	3x3x3	(0,0,3)	(0,0,0)	Wall: Plaster, Ceiling: Plaster, Floor: Pine Wood Wall: Plaster, Ceiling: Plaster, Floor: from Fig. 2.7.

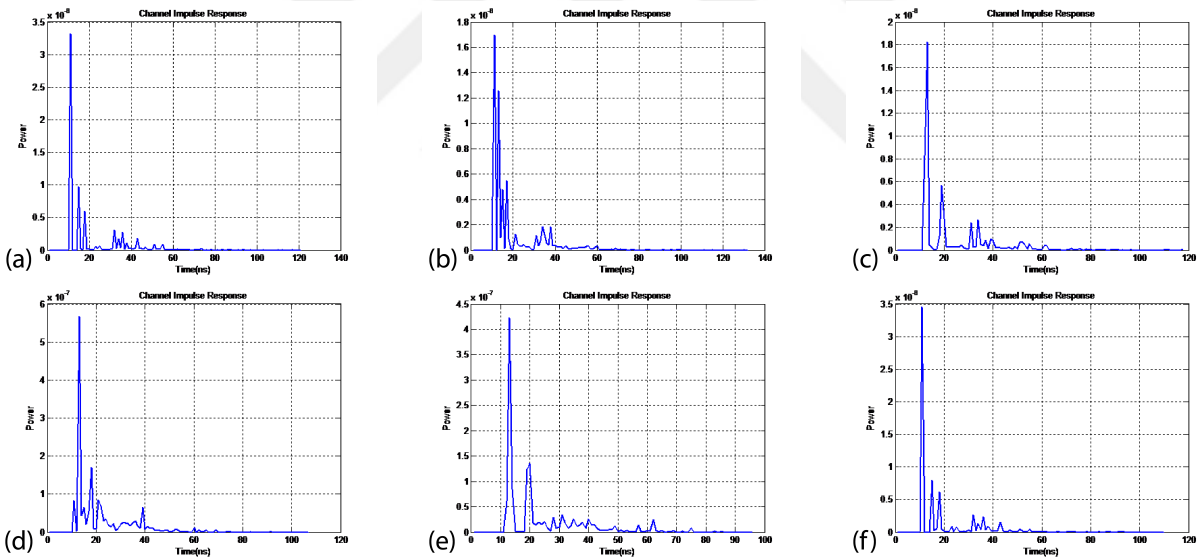


Figure 2.8. CIRs for different configurations, (a) CIR for configuration A, (b) CIR for configuration B, (c) CIR for configuration C, (d) CIR for configuration D, (e) CIR for configuration E, (f) CIR for configuration F

not feasible by now. Size of the parameter space and unpredictable behavior of the parameters makes modeling channel very challenging problem. To obtain appropriate channel model we have utilized optical design and simulation environment called Zemax. By using sequential ray tracing

Table 2.4. Channel parameters of scenario-1

Configuration / Channel Parameters	$T_{DP}(ns)$	$\tau_0(ns)$	$\tau_{RMS}(ns)$	$H_0(ns)$	Comment
A	54	20.48	13.98	6.93e-6	By moving the detector to the corner, RMS delay spread increases and DC gain decreases because the distance between transmitter and detector increases. Also by rotation of detector, DC gain decreases because the detector can not receive scatter from some places(behind the detector).
B	55	20.34	13.61	5.89e-6	
C	60	23.33	15.19	5.54e-6	
D	52	21.7	11.94	1.69e-6	
E	61	23.51	14.07	1.30e-6	

Table 2.5. Channel parameters of scenario-2

Configuration / Channel Parameters	$T_{DP}(ns)$	$\tau_0(ns)$	$\tau_{RMS}(ns)$	$H_0(ns)$	Comment
A	54	20.48	13.98	6.93e-6	Different materials has effect on CIR and channel parameters. In scenario F we have material with spectral reflectance which is smaller than scenario A So the RMS delay decreases by decreasing the reflectivity and received power from reflected paths also decreases.
F	47	18.70	11.86	6.62e-6	

capabilities of the software we have modeled typical daily life scenario rooms. CIRs for VLC are obtained in great detail. Simulations and results are expanded and proposed to 802.15.7r1 IEEE "Short Range Optical Wireless Communications" standardization process. Average delay spread of the scenarios A-E and F is given as 13.758 ns and 11.86 ns respectively. Therefore, for signaling rates 8.43 Mbits/sec the VLC channel is behaving as frequency-selective for given configurations. Since, Gbits/sec data rates are promoted for VLC technology channel appears frequency selective in our point of view. However, still most of the physical layer papers on VLC are considering frequency-flat case. In, [15] there is a solid justification for that why %80 of the total users experiencing frequency flat channel. Consequently, VLC channel model and its frequency selectivity behaviour is still hot and complicated problem.

3. Analysis of OFDM Based Indoor OWC Systems

Discrete multitone (DMT) systems are the baseband equivalent of the OFDM method. Development process of the optical OFDM (O-OFDM) systems are depicted in Fig. 3.1. In [16], multiple-subcarrier transmission for IR systems is investigated for the first time. Using OFDM modulation for VLC systems proposed for the first time in [17]. Bipolarity problem in IM/DD systems solved by adding a DC bias for the first time in also in [17]. However, adding DC bias had causes power inefficiency. One of the state of the art solutions to bipolarity problem without adding DC bias called asymmetrically clipped optical OFDM (ACO-OFDM) proposed in [18]. Another approach to bipolarity by time domain manipulation called Flip-OFDM & Unipolar OFDM (U-OFDM)) are given in the [19, 20]. Recent modulation methods to obtain same spectral efficiency as DCO-OFDM without energy efficiency loss are proposed as eU-OFDM in [21] and for ACO-OFDM in [22]. ACO-OFDM, DCO-OFDM and U-OFDM (Flip OFDM) modulation schemes and their properties are detailed in the next sections.

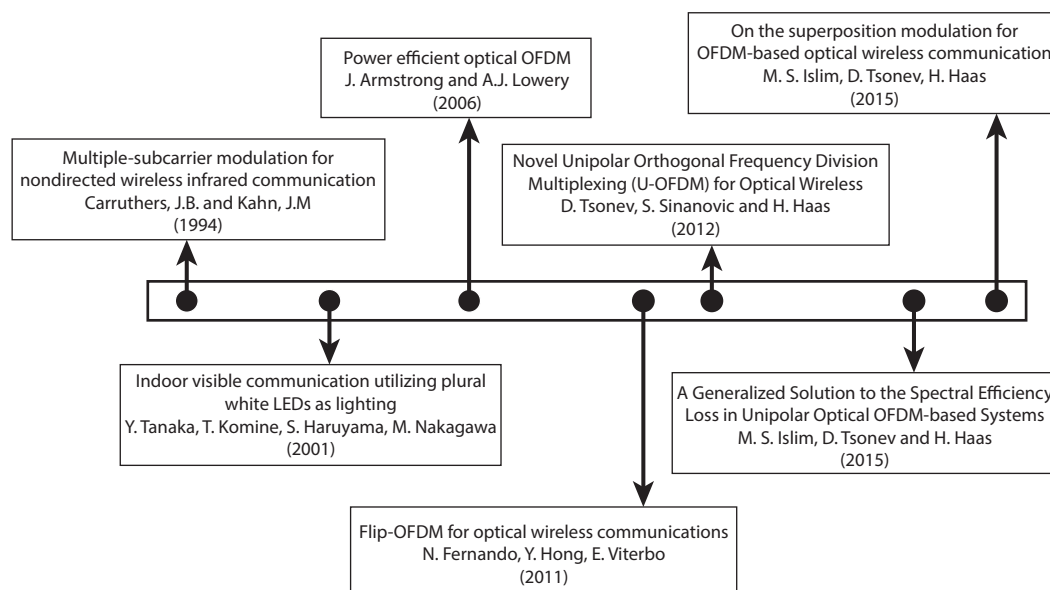


Figure 3.1. Optical OFDM system's development

Typical IM/DD based optical OFDM system depicted in Fig. 3.2. Randomly generated

input bit stream is mapped into M-ary signal constellation space. In IM/DD systems, signals are restricted to be real and positive. Reality satisfied by conjugate symmetry. Then, IFFT imposed on the parallel stream. Obtained real but bipolar time domain samples are processed such a way that, result becomes real and unipolar (positive) signal. IM/DD suitable time domain samples are sent via off-the-shelf LEDs. Optical channel brings multipath fading. At the receiver, received signal processed in parallel manner and FFT is imposed. Message signal could be obtained by channel equalization and symbol detection processes at the receiver.

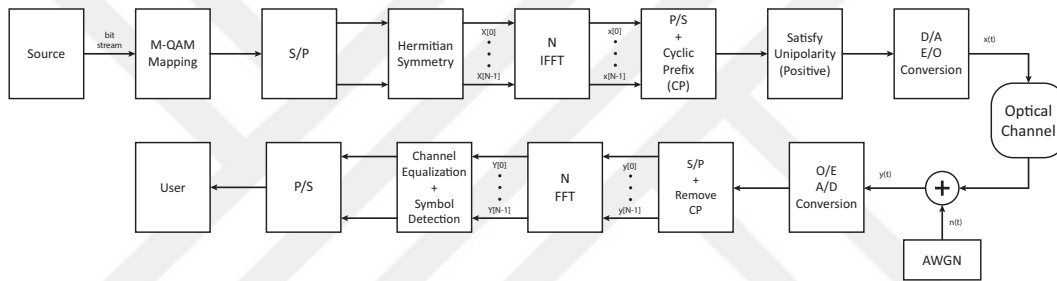


Figure 3.2. IM/DD OFDM

3.1. SISO Based O-OFDM Systems

3.1.1. ACO-OFDM Based IM/DD OWC Systems

One of the state-of-the-art non DC biased unipolar OFDM method proposed in [18] known as asymmetrically clipped optical OFDM (ACO-OFDM). ACO-OFDM has approximately 8dB better optical power efficiency compared with DC biased optical OFDM (DCO-OFDM). However, it has half of the spectral efficiency that DCO-OFDM has in return. Spectral efficiency of ACO-OFDM could be given as, $N \log_2 M$ bits/Hz. N and M are number of subcarriers in OFDM frame and number of constellation points respectively. Basic idea behind the ACO-OFDM is given in the Fig. 3.3.

Accordingly in ACO-OFDM, real number problem solved by applying conjugate symmetry

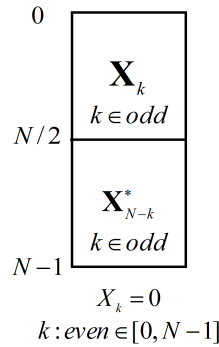


Figure 3.3. ACO OFDM Frame Structure

which is better known as Hermitian symmetry. Detailed proof of why Hermitian symmetry gives real signals given in the Appendix. In the sequel, unipolarity problem is solved by using state-of-the-art DFT property. As a result of this property, if we modulate only the odd subcarriers and set even ones to zero we would have, $x[n + \frac{N}{2}] = -x[n]$. Proof of DFT property is detailed in the Appendix. Transmitter and receiver block diagram for ACO OFDM is given in Fig. 3.4

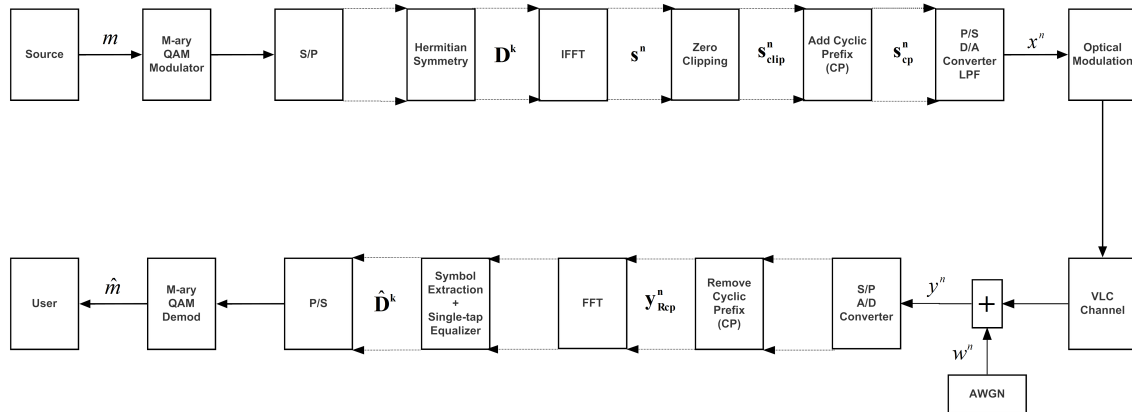


Figure 3.4. ACO OFDM Block Diagram

As it can be seen from Fig.3.4 m information bit stream is mapped onto normalized power M-QAM constellation where M presents the number of constellation points. Resultant frequency domain signal $real(\mathbf{X}) \sim \mathcal{CU}(0, \frac{\sigma^2}{2})$ and $imag(\mathbf{X}) \sim \mathcal{U}(0, \frac{\sigma^2}{2})$ where \mathcal{CU} represent complex uniform distribution, variance of the mapped signal is $\sigma^2 = 1$, $real(\cdot)$ and $imag(\cdot)$ shows the real and imaginary parts of the signal respectively. FFT of the signal \mathbf{X} is taken. From central limit the-

orem (CLT) distribution of the resulting time-domain signal would be Gaussian distribution with some variance which could be calculated from Parseval's Theorem. CLT and Parseval's Theorem are detailed in the Appendix. Resulting time domain real and bipolar signal is $\mathbf{x} \sim \mathcal{N}(0, \frac{\sigma^2}{2N})$. Probability distribution function (pdf) of \mathbf{x} is given as, $f_x(w) = \frac{\sqrt{N}}{\sqrt{\pi\sigma^2}} e^{-\frac{Nw^2}{\sigma^2}}$.

Along this thesis FFT/IFFT operations are taken as,

$$\begin{aligned} DFT : \quad X[k] &= \sum_{n=0}^{N-1} x[n] e^{-\frac{j2\pi kn}{N}} \quad \text{for } k = 0, \dots, N-1 \\ IDFT : \quad x[n] &= \frac{1}{N} \sum_{k=0}^{N-1} X[k] e^{\frac{j2\pi kn}{N}} \quad \text{for } n = 0, \dots, N-1 \end{aligned} \quad (3.1)$$

Basic transformation between \mathbf{X} and \mathbf{x} could be given as, $\mathbf{X} = \mathbf{W}\mathbf{x}$ and $\mathbf{x} = \frac{1}{N}\mathbf{W}^{-1}\mathbf{X}$ where \mathbf{W} and \mathbf{W}^{-1} are DFT and inverse DFT matrices respectively.

From (3.1), if we substitute, $n = n + N/2$

$$x[n + N/2] = \frac{1}{N} \sum_{k=0}^{N-1} X[k] e^{j2\pi k(n+N/2)/N} = \frac{1}{N} \sum_{k=0}^{N-1} X[k] e^{j2\pi kn/N} e^{j\pi k} \quad (3.2)$$

For odd k 's(subcarriers), $e^{j\pi k} = -1$ and for even k 's(subcarriers), $e^{j\pi k} = 1$. If we split (2) to two parts as even and odd subcarriers.

$$x[n + N/2] = \underbrace{\frac{1}{N} \sum_{k, \text{even}} X[k] e^{j2\pi kn/N} \underbrace{e^{j\pi k}}_1}_{\frac{1}{N} \sum_{k, \text{even}} X[k] e^{j2\pi kn/N}} + \underbrace{\frac{1}{N} \sum_{k, \text{odd}} X[k] e^{j2\pi kn/N} \underbrace{e^{j\pi k}}_{-1}}_{-\frac{1}{N} \sum_{k, \text{odd}} X[k] e^{j2\pi kn/N}} \quad (3.3)$$

If we set all even subcarriers to zero, $X[k] = 0$, if k is even. Then,

$$x[n + N/2] = -x[n] \quad \text{for odd } k' \text{'s} \quad (3.4)$$

Similarly, if set all odd subcarriers to zero $X[k] = 0$, if k is odd. We have,

$$x[n + N/2] = x[n] \quad \text{for even } k's \quad (3.5)$$

From (4) and (5) we can easily see that, some important property occurred. If we look at (4) closely we can easily see that. Each time sample has its negative copy $N/2$ shifted in discrete-time domain. It is one of the most important idea behind ACO-OFDM. Each time sample have its negative sample in same OFDM frame. We can apply zero clipping to the OFDM frame and recover entire OFDM frame with negative samples without loss of information[?]. For instance lets assume we have N subcarriers. In that case,

$$x[\frac{N}{2}] = -x[0], x[\frac{N}{2} + 1] = -x[1], x[\frac{N}{2} + 2] = -x[2], \dots, x[N - 1] = -x[\frac{N}{2} - 1].$$

3.1.1.1. VLC Channel Impulse Response Modeling. Our study is based on Zemax[®] which is an optical and illumination design software with sequential and non-sequential ray-tracing capabilities [12]. It allows accurate description of the interaction of rays emitted from the LED's for a user defined environment. In non-sequential ray-tracing, rays are traced along a physically realizable path until they intercept an object. The line-of-sight (LOS) response depends on the LOS distance. Besides the LOS component there is a large number of reflections from the ceiling, walls, floor and as well as objects within the environment. The simulation environments and scenarios created in Zemax[®] is then used to simulate the ACO-OFDM systems.

3.1.1.2. Selection of materials. The selection of material for wall, ceiling and floor is particularly important for realistic channel modeling [23]. NASA optics database [11] has variety of materials and their reflection coefficients obtained from experiments. In our computer simulations some realistic materials for the indoor channel models have been chosen and investigated. Particularly, several curves for the reflection coefficient of the plaster wall - ceiling and floor combination is given in Fig. 2.7.

3.1.1.3. Selection of Light Sources and Detectors. Zemax[®] software includes variety of commercially available devices [13] and [14] such as Cree Inc., OSRAM AG, OPTO Diode Corp., Philips Lighting, Vishay Intertechnology, Panasonic Corporation, StockerYale.

In Zemax[®], we can specify different detector parameters (types) including detector color, polar, Rectangle, surface and volume. Figs. 3.1.1.4-3.1.1.4 show different locations of sources and detectors with respect to each other, described by Configuration A and B.

3.1.1.4. Channel Impulse Response. Channel impulse response (CIR) is expressed as

$$h(t) = \sum_{i=1}^N P_i \delta(t - \tau_i) \quad (3.6)$$

where P_i is the power and τ_i is the propagation time of the i^{th} ray, δ is the Dirac delta function and N is the number of rays received in the detector. Based on the obtained CIR, we can further quantify the fundamental channel characteristics. Channel DC gain (H_0) is one of the most important features of the VLC channel. It determines the achievable signal-to-noise ratio (SNR) for fixed transmitter power. The delay profile is composed of dominant multiple LOS links and less number of NLOS delay taps. The temporal dispersion of a power delay profile can be expressed by the mean excess delay (τ_0) and the channel root-mean-square (RMS) delay spread (τ_{RMS}). These parameters are given by [24, 23],

$$\int_0^{T_r} h(t) dt = 0.97 \int_0^{\infty} h(t) dt \quad (3.7)$$

$$\tau_0 = \frac{\int_0^{\infty} t \times h(t) dt}{\int_0^{\infty} h(t) dt} \quad (3.8)$$

$$\tau_{RMS} = \sqrt{\frac{\int_0^{\infty} (t - \tau_0)^2 h(t) dt}{\int_0^{\infty} h(t) dt}} \quad (3.9)$$

$$H_0 = \int_{-\infty}^{\infty} h(t) dt \quad (3.10)$$

Table 3.1. Channel Configurations

Config.	Room size (m^3)	Position of Transmitter (m)	Position of Receiver (m)	Reflectivity
A	5x5x3	(0, 0, 3)	(1.7, 1.9, 0.7)	Wall: 0.8 Ceiling: 0.8 Floor: 0.3
B	7x7x3	(0, 0, 3)	(3.3, 3.3, 0)	Wall: Plaster Ceiling: Plaster Floor: Pine Wood
	T_{tr} (ns)	τ_0 (ns)	τ_{RMS} (ns)	H_0
A	67	34.43	14.50	1.06e-6
B	87	39.51	20.92	6.97e-7

We are considering the configurations A and B in the Table 3.1.1.4. Configurations are simply 5m x 5m x 3m and 7m x 7m x 3m sized empty rooms with different reflectivities. Transmitters are located at the center of the ceiling (0,0,3) and receivers are at the corner with different altitudes.

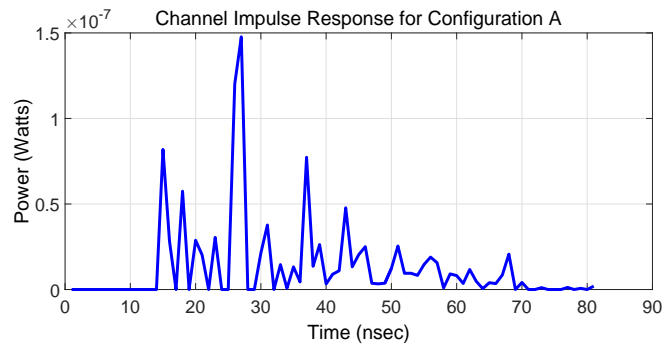
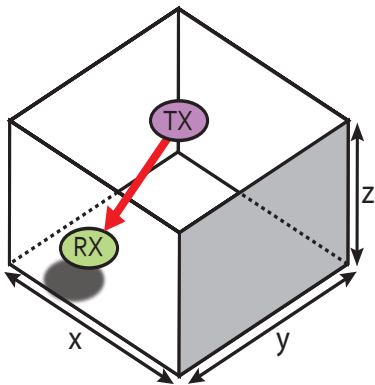


Figure 3.5. Structure and CIR of Configuration A

3.1.1.5. ACO-OFDM. In the ACO-OFDM system only the odd subcarriers carry information bits while the even subcarriers ensure that the transmitted OFDM signal is strictly non-negative.

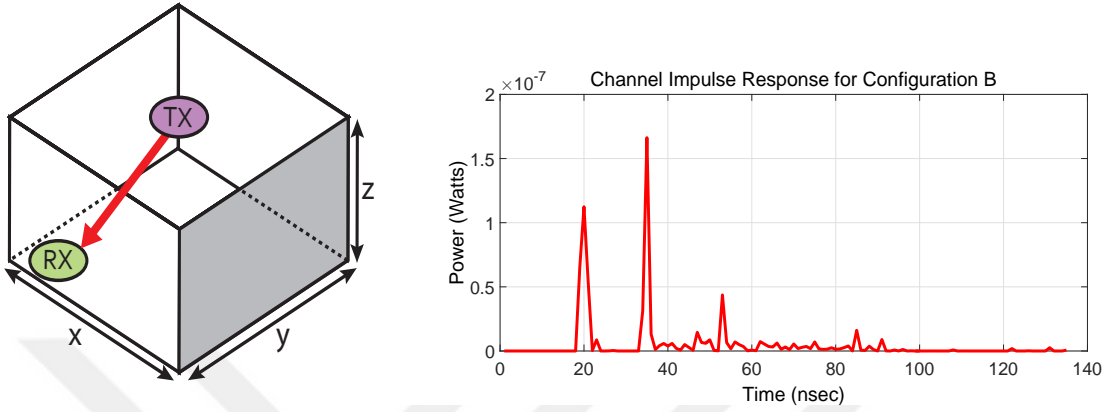


Figure 3.6. Structure and CIR of Configuration B

Random generated source bits are transmitted in the blocks of duration of T_{sym} , modulated in M-QAM modulator and processed parallel in further blocks with blocks of duration $T_s = T_{sym}/N$. N is the total number of actively used subcarriers and for simplicity it has taken as equal to IFFT block size. The frequency domain modulated input signal of IFFT, $\mathbf{X} = [X_0, X_1, X_2, \dots, X_{N-1}]^T$ meets the Hermitian symmetry and comprises only odd subcarriers. The 0^{th} (DC) and $(N/2)^{th}$ subcarriers are set to zero to avoid any complex term and satisfy Hermitian symmetry [25, 18]

$$X[k] = \begin{cases} 0 & , k \text{ is even} \\ X_{N-k}^* & , k \text{ is odd} \end{cases} \quad (3.11)$$

where $*$ denotes the complex conjugation. Throughout this paper, lowercase letters will be used for time-domain signals and uppercase for discrete frequency-domain signals. The resulting real, bipolar and anti-symmetric time-domain IFFT signal is given by, $x = [x_0, x_1, \dots, x_{N-1}]^T$.

$$x[n] = \frac{1}{N} \sum_{k=0}^{N-1} X[k] e^{j \frac{2\pi kn}{N}} \quad (3.12)$$

where N is the number of points in IFFT and $X[k]$ is the k^{th} subcarrier of signal \mathbf{X} . Due to Hermitian symmetry and zero insertion process, the number of data symbols carried by subcarriers in ACO-OFDM is only $N/4$. A cyclic prefix (CP) is then added to the discrete time samples, where N_{CP} is denoted by the length of the CP. N_{cp} must be greater or equal to the maximum delay spread. In our simulations, N_{CP} is taken as $N_{CP} \geq L_h$ where L_h is the length of the impulse response of the optical channel. Negative part of the signal clipped to generate real and unipolar signal is given by

$$[x[n]]_c = \begin{cases} x[n] & \text{if } x[n] \geq 0 \\ 0 & \text{if } x[n] < 0. \end{cases} \quad (3.13)$$

The clipping noise is generated after clipping will fall only on the even subcarriers and will not affect the transmitted symbols carried by odd subcarriers. There is no need to add a DC bias to the clipped signal in the conventional system so that, the ACO-OFDM technique is more power efficient in terms of peak to average power ratio (PAPR) [18]. For a large number of subcarriers, the amplitude of the unclipped ACO-OFDM signal can be approximated by a Gaussian distribution [26]. Thus, the amplitude distribution of the clipped signal $[x[n]]_c$ is the half-Gaussian

$$p_{x_c}(x) = 0.5 \delta(x) + \frac{u(x)}{\sigma_x \sqrt{2\pi}} e^{-\frac{x^2}{2\sigma_x^2}}$$

where σ_x is the standart deviation of the unclipped Gaussian distributed signal, $\delta(\cdot)$ is the Dirac delta function and $u(\cdot)$ is the unit step function. The average transmitted power $P_{opt,ACO}$ of the above clipped signal is given by

$$P_{opt,ACO} = E\{x_c\} = \int_{-\infty}^{\infty} xp_{x_c}(x) dx = \frac{\sigma_x}{\sqrt{2\pi}} \quad (3.14)$$

It is assumed that D/A converter and optical modulator are ideal so that optical-electrical conversion constant ζ and electrical-optical conversion constant R are chosen as $\zeta = R = 1$. At the receiver, optical detector and A/D converter detects and converts the optical signals to electrical signals. Received signal contains amplified/attenuated components as well as inter-symbol interference (ISI) and AWGN. Received time-domain signal has the form of,

$$y(t) = x(t) \star h(t) + w(t) \quad (3.15)$$

where \star denotes the linear convolution operation, $h(t) = [h(0)h(1) \dots h(L_h - 1)]^T$ is the L -path impulse response of the optical channel and $w(t)$ is an AWGN that represents sum of the receiver thermal noise as well as electrical equivalent of optical shot noise. Ambient noise radiation is modeled as DC and can be filtered out. It is important to notice that the AWGN being added in the electrical domain and overall noise power is denoted by σ_n . In this paper, ideal zero-forcing (ZF) equalizer is employed at the receiver to mitigate the effect of the channel and the resulting BER performances are obtained for different signal constellations.

At the receiver, photodetector and A/D converter converts to signal to electrical domain back. After A/D converter, removing the CP, the discrete-time received signal y is taken the Fast Fourier Transform (FFT) to convert it back to frequency-domain signal from which the original data is obtained by a simple one-tap zero forcing equalizer.

3.1.1.6. Computer Simulation Results. In this section, computer simulation for the bit error rate (BER) performances of ACO-OFDM systems are investigated in the presence of realistic indoor optical channel models obtained by Zemax[®] software and compared with the AWGN channels with QPSK (4 QAM) and 16 QAM signaling formats. 256 subcarriers and N_{CP} is equal to the length of the CIR were used in the simulations. For ACO-OFDM systems, the relationship between the optical power defined in (3.14) and the electrical power is $P_{opt,ACO} = \sqrt{P_{elec,ACO}/\pi}$. Normalizing the optical power we have [?],

$$\frac{E_{b_{opt,ACO}}}{N_0} = \frac{1}{\pi} \frac{E_{b_{elec,ACO}}}{N_0}. \quad (3.16)$$

Fig.5 is for the case where the realistic channel configuration A is employed in ACO-OFDM as well as where an AWGN channel is employed. The four plots show the results for QPSK and 16-QAM constellations on the ACO-OFDM subchannels. The plots show the BER versus $E_{b,elec}/N_0$. From these plots it is observed the the performance results given in the literature for the BER versus $E_{b,elec}/N_0$ in the presence of only AWGN channels is far being realistic for the real optical communication channels. Consequently, it is utmost important and necessary to obtain and model realistic indoor optical channel models for efficient design of VLC systems in real applications. Similar results were obtained in Fig. 6 for the the realistic channel configuration B except the BER curves are shifted according to the different properties of the configurations in terms of the room size, coating material types, locations of transmitter and receiver.

3.1.1.7. Conclusions. In this paper, ACO-OFDM, a recently developed modulation scheme for IM/DD systems is analyzed in the presence of realistic indoor optical channel models for two different channel configurations obtained by the Zemax[®] software. The BER performance of the ACO-OFDM system is investigated in the presence of the indoor optical channel impulse responses obtained for these two configurations as well as for different QAM constellations and compared with that of the AWGN channels. It was concluded that there are substantial performance differ-

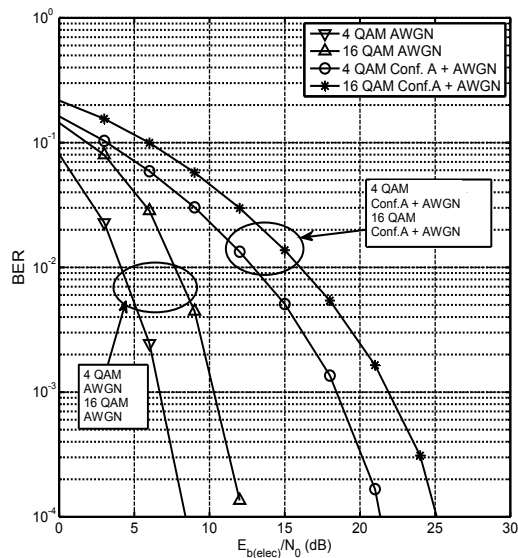


Figure 3.7. BER performance of Configuration A

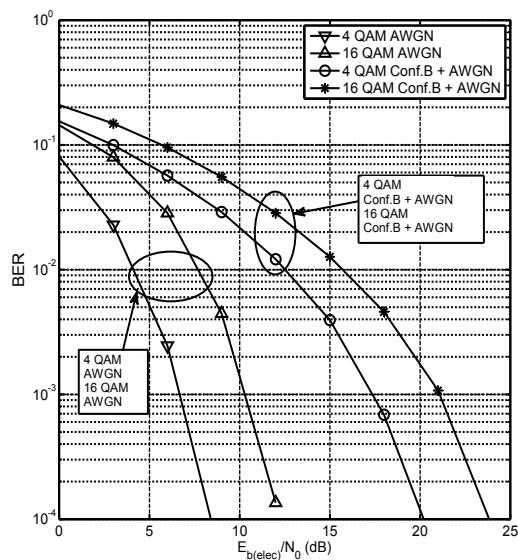


Figure 3.8. BER performance of Configuration B

ences between the cases where an indoor optical channel or an AWGN channel model is used. Consequently, we also concluded that it is not suitable to use the performance results of these types of systems solely based on the AWGN channel assumption for the ACO-OFDM scheme in

designing such systems.

3.1.2. DCO-OFDM Based IM/DD OWC Systems

Visible light communication (VLC) involves the dual use of illumination infrastructure for high speed wireless access. Since indoor optical channels exhibit frequency selectivity, multicarrier communication, particularly orthogonal frequency division multiplexing (OFDM), is used to handle the resulting intersymbol interference in VLC systems. In optical OFDM, modifications are made on the conventional OFDM to ensure the non-negativity of optical signals. One of the commonly used techniques for this purpose is direct-current biased optical OFDM (DCO-OFDM). In this paper, first two indoor channel models obtained for visible light communications (VLC) are introduced using non-sequential ray tracing simulation tools of the Zemax[®] software. Integrating these realistic VLC channel models in our simulations, we then demonstrate the effects of indoor coating (floor, ceiling, etc) material types and receiver/transmitter locations on the BER performance.

3.1.2.1. Introduction. Orthogonal frequency division multiplexing (OFDM) is now increasingly being considered as a modulation technique for optical systems [?, ?] since it has better optical power efficiency than conventional modulation schemes. In conventional OFDM, the transmitted signals are bipolar and complex. But bipolar signals cannot be transmitted in an intensity modulated/direct detection (IM/DD) optical wireless system, because the intensity of light cannot be negative. OFDM signals designed for IM/DD systems must therefore be real and nonnegative. Direct-current biased OFDM (DCO-OFDM) is one of the forms of OFDM for IM/DD systems [27]. In DCO-OFDM, a DC bias is added to the signal to make it positive and all the subcarriers carry data symbols. Consequently, bandwidth efficiency of the overall DCO-OFDM system is less efficient than the conventional OFDM system operating in electrical wireless domain.

The performance of the DCO-OFDM has been investigated in [7] where flat channel is as-

sumed with additive white Gaussian noise (AWGN). The motivation of our work is to investigate the error rate performance of DCO-OFDM in more realistic settings. For this purpose, we follow the channel modeling approach introduced in [24, 23] where ray-tracing based indoor channel models are proposed using the commercially available optical and illumination design software Zemax[®]. We consider two scenarios involving empty rooms with dimensions of 5m x 5m x 3m and 7m x 7m x 3m for different floor/ceiling coating materials as well as different transmitter/receiver locations. First, we obtain the channel impulse responses (CIRs) for the indoor scenarios under consideration, then use these CIRs to determine the performance of the DCO-OFDM scheme with computer simulations.

3.1.2.2. VLC Channel Impulse Response Modeling. Channel modeling approach is given in ACO-OFDM, "VLC Channel Impulse Response Modeling" part in great detail.

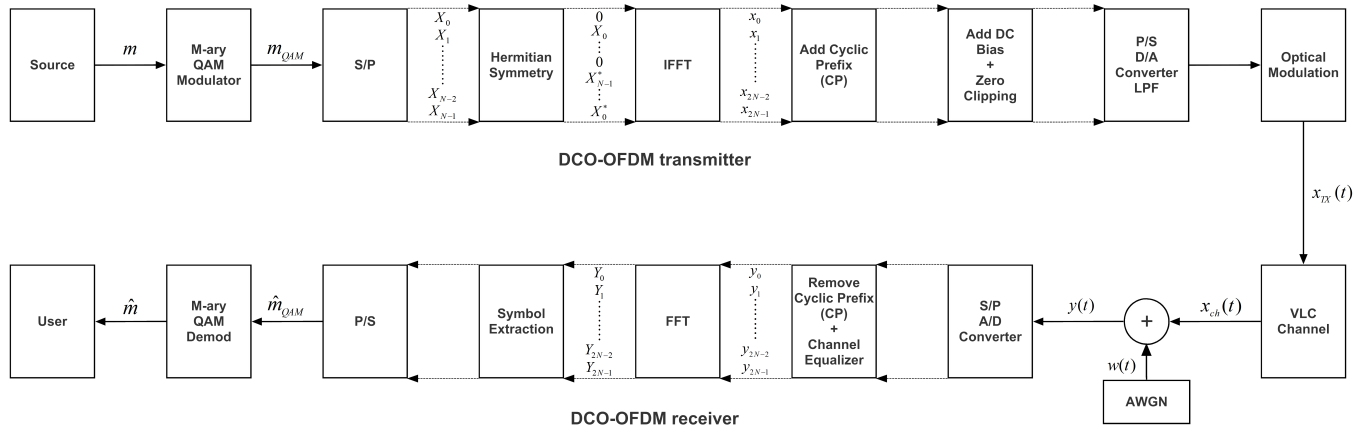


Figure 3.9. DCO Block Diagram

3.1.2.3. DCO-OFDM System Structure. The block diagram of the transmitter and receiver parts of a DCO-OFDM system is shown in Fig. 4. In the DCO-OFDM system, a DC bias is added to the signal to make it positive and, therefore, all the OFDM subcarriers carry data symbols. On the other hand the asymmetrically clipped optical OFDM (ACO-OFDM) technique, another version of the optical OFDM schemes, positivity of the transmitted signal is realized by clipping the original bipolar OFDM signal at zero and transmitting only the positive parts. Consequently,

DCO-OFDM is less average optical power efficient than ACO-OFDM while the use of only half of the subcarriers to carry data in ACO-OFDM makes this scheme less bandwidth efficient than the DCO-OFDM.

The OFDM system consider here has N subcarriers. At the transmitter these subcarriers are assumed to be actively employed to transmit data symbols modulated by either M -level quadrature amplitude shift keying (M-QAM) or phase shift keying (M-PSK). Frequency domain complex-valued vector of data symbols $\mathbf{X} = [X[0], X[1], \dots, X[N-1]]^T$ meets the Hermitian symmetry and the components at the 0^{th} (DC) and $(N/2)^{th}$ subcarriers are set to zero as follows.

$$X[k] = \begin{cases} 0 & , \text{ if } k = 0, \\ X^*[N-k] & , \text{ if } k = 1, 2, \dots, N/2 - 1, \\ 0 & , \text{ if } k = N/2, \end{cases}$$

where $*$ denotes the complex conjugation. Consequently, time-domain signal samples obtained at the output of the IFFT become real-valued due to the Hermitian symmetry [?]. Note that, throughout this paper, lowercase letters will be used for time-domain signals and uppercase for discrete frequency-domain signals. The resulting real, bipolar and anti-symmetric time-domain signal vector $\mathbf{x} = [x[0], x[1], \dots, x[N-1]]^T$ is denoted as

$$x[n] = \frac{1}{N} \sum_{k=0}^{N-1} X[k] e^{j \frac{2\pi kn}{N}} \quad (3.17)$$

where N is the number of points in IFFT and $X[k]$ is the k^{th} component of \mathbf{X} . Due to Hermitian symmetry and zero insertion process at the subcarriers $k = 0$ and $k = N/2$, the number of data

symbols carried by the subcarriers in DCO-OFDM is only $N/2 - 1$. A cyclic prefix (CP) of length N_{cp} is then added to the discrete time samples. N_{cp} must be greater or equal to the maximum channel delay spread. In our simulations, N_{CP} is taken as $N_{CP} \geq L$. After digital-to-analog conversion the electrical signal, $x(t)$ is generated in analog form. Note that $x(t)$ can be modeled approximately as a Gaussian process due to the central limit theorem. It can be easily seen that its mean is zero and the variance can be determined by $\sigma_x^2 = E\{x_k^2\}$. A suitable DC bias is next added to $x(t)$ and the residual negative peaks are clipped resulting in a signal denoted by $x_{DCO}(t)$. Note that since the peak to average ratio of the OFDM samples in the time-domain is substantially high, a large DC bias would be necessary to eliminate the negative part of $x(t)$. However, this increases the optical energy per bit, making the scheme quite inefficient in terms of the optical power. Therefore, instead, a moderate DC bias is employed in real applications and the residual negative signal components are clipped. But this will inevitably generate a clipping noise and based on the level of the clipping noise set by the designer, the BER performance of the scheme will be affected. Usually the DC bias level denoted by V_{DC} is determined by the standard deviation of $x(t)$ as follows, [24].

$$V_{DC} = \rho \sqrt{E\{x^2(t)\}}, \quad (3.18)$$

where ρ is a constant and to be determined from $10 \log(\rho^2 + 1)$ dB for a given distortion level in dB.

On the other hand, since the clipping noise, generated after clipping, falls only on the even subcarriers it does not effect the transmitted symbols carried by odd subcarriers. There is no need to add a DC bias to the clipped signal in the ACO-OFDM technique. Consequently, ACO-OFDM is more power efficient in terms of peak to average power ratio (PAPR) [?] than DCO.

For a large number of subcarriers, the amplitude of the unclipped DCO-OFDM signal can be approximated by a Gaussian distribution [?]. Thus, the amplitude distribution of the clipped signal

$x_{DCO}(t)$ is the half-Gaussian

$$p_{x_{DCO}}(x) = Q(V_{DC}/\sigma_x)\delta(x) + \frac{u(x)}{\sigma_x\sqrt{2\pi}} e^{-(x-V_{DC})^2/2\sigma_x^2}$$

where σ_x is the standard deviation of the unclipped Gaussian distributed signal, $u(\cdot)$ is the unit step function and $Q(x) = 1/\sqrt{2\pi} \int_x^\infty \exp(-t^2/2) dt$. The average transmitted electrical power $P_{elec,DCO}$ of the above clipped signal is given by

$$\begin{aligned} P_{elec,DCO} &= E\{x_{DCO}^2\} = \int_{-\infty}^{\infty} x^2 p_{x_{DCO}}(x) dx \\ &= (\sigma_x^2 + V_{DC}^2) \left(1 - Q(V_{DC}/\sigma_x)\right) \\ &\quad + (\sigma_x V_{DC}/\sqrt{2\pi}) \exp(-V_{DC}^2/2\sigma_x^2) \end{aligned} \quad (3.19)$$

In our computer simulations, as described in the following section, it is assumed that D/A converter and photodetector are ideal so that optical-to-electrical conversion constant ζ and electrical-to-optical conversion constant R are chosen as $\zeta = R = 1$. The received time-domain signal, $y(t)$, contains amplified/attenuated components as well as inter-symbol interference (ISI) due to the real optical channel having the impulse response $h(t)$, the AWGN and the additive clipping noise as follows.

$$y(t) = x(t) \star h(t) + w(t) + n_{clip}(t) \quad (3.20)$$

where \star denotes the linear convolution operation, $h(t)$ is the L -path impulse response of the optical

channel and $w(t)$ is an AWGN and n_{clip} represents an electrical equivalent of the optical clipping noise. Ambient noise radiation is modeled as a DC component and can be filtered out. It is important to notice that the AWGN being added in the electrical domain and overall noise power is denoted by σ_n^2 .

At the receiver, after A/D converter the CP is removed from the discrete-time received signal $y[n]$ then the Fast Fourier Transform (FFT) is taken to convert it back to frequency-domain signal from which the original data is detected by a simple one-tap zero forcing equalizer.

3.1.2.4. Computer Simulation Results. In this section, computer simulation for the bit error rate (BER) performances of DCO-OFDM systems are investigated in the presence of realistic indoor optical channel models obtained by Zemax software and compared with the AWGN channels with quadrature phase shift keying (QPSK) and 16 QAM signaling formats. 256 subcarriers and N_{CP} is equal to the length of the CIR were used in the simulations. For DCO-OFDM systems, [?],

$$\frac{E_{b,elec,DCO}}{N_0} = \frac{x_{DCO}^2(t)}{R_{b,DCO}N_0}. \quad (3.21)$$

where $R_{b,DCO} = \log_2 M/T_s$ is the bit rate of the DCO-OFDM.

Fig.5 is for the case where the realistic channel configuration A is employed in the DCO-OFDM scheme in the presence of an additive Gaussian noise. The plots show the BER versus $E_{b,elec}/N_0$ for QPSK with bias levels chosen as 7 dB and 13 dB. From these plots it is observed that the performance results given in the literature for the BER versus $E_{b,elec}/N_0$ in the presence of only AWGN channels is far being realistic for the real optical communication channels [28]. For comparison purpose, the BER performances of the asymmetrically clipped OFDM scheme with the same channel configuration, obtained in [29], is also included in Fig. 5. We conclude from all these curves presented in Fig. 5 that it is utmost important and necessary to obtain and model realistic indoor optical channel models for efficient design of VLC systems in real applications.

Similar results were obtained in Fig. 6 for the realistic channel configuration B except the BER curves are shifted according to the different properties of the configurations in terms of the room size, coating material types, locations of transmitter and receiver.

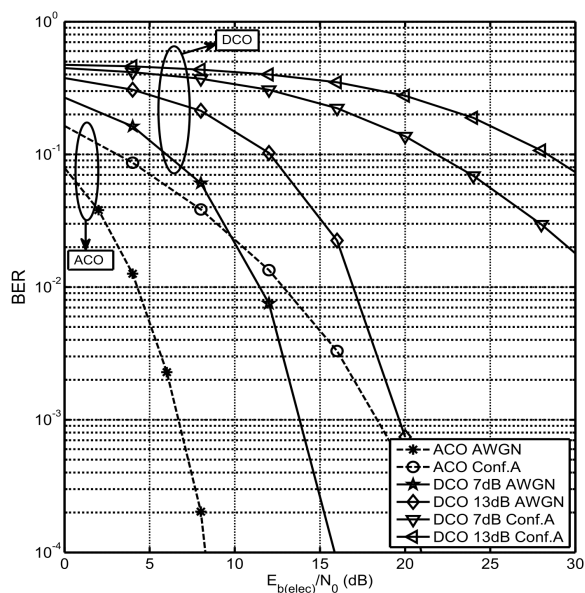


Figure 3.10. BER performance of Configuration A

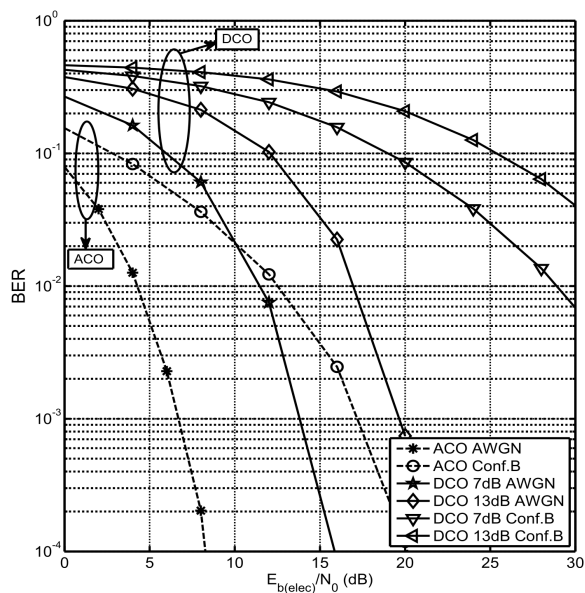


Figure 3.11. BER performance of Configuration B

3.1.2.5. Conclusions. In this paper, DCO-OFDM, a recently developed modulation scheme for IM/DD systems is analyzed in the presence of realistic indoor optical channel models for two different channel configurations obtained by the Zemax software. The BER performance of the ACO-OFDM system was investigated in the presence of the indoor optical channel impulse responses obtained for these two configurations as well as for different bias levels and compared with that of the AWGN channels. It was concluded that there are substantial performance differences between the cases where an indoor optical channel or an AWGN channel model is used. Consequently, we also concluded that it is not suitable to use the performance results of these types of systems solely based on the AWGN channel assumption for the DCO-OFDM scheme in designing such systems.

3.2. MIMO Based Optical OFDM Systems

3.2.1. Enhanced Unipolar OFDM (eU-OFDM)

Visible light communication (VLC) involves the dual use of illumination infrastructure for high speed wireless access. Designing such optical based communication systems, realistic indoor optical channel modeling becomes an important issue to be handled. In this paper, first we obtain new realistic indoor VL channel characterizations and models, in a multiple-input multiple-output (MIMO) transmission scenario, using non-sequential ray tracing approach for the channel impulse responses (CIRs). Practical issues such as number of light emitting diode (LED) chips per luminary, spacing between LED chips, objects inside the room and cabling topology are also investigated. On the other hand, since indoor optical channels exhibit frequency selectivity, multi-carrier communication systems, particularly orthogonal frequency division multiplexing (OFDM) is used to handle the resulting inter-symbol interference in VLC systems. Hence, we propose a new MIMO-OFDM based VLC system, called MIMO enhanced unipolar OFDM (MIMO-eU-OFDM) by combining MIMO transmission techniques with the recently proposed eU-OFDM scheme. The bit error rate (BER) performance of the proposed system is investigated in the presence of the 2×2 and 4×4 realistic MIMO VLC channels and its BER performance is compared with the reference

optical MIMO-OFDM systems.

3.2.1.1. Introduction. Optical wireless communications (OWC) is an up and coming technology to complement wireless radio frequency (RF) systems. OWC comprises VL (visible light) and IR (infra red) regions of the spectrum as indoor/outdoor wireless communications medium. Visible light communications (VLC) is a branch of OWC operating in the (390-750nm) band and providing number of advantages over RF and millimeter wave communications. VLC is a not complex, expensive or scarce technology. It offers almost 10.000 times larger unregulated and RF non-interfering spectrum with improved data security [30]. Moreover, it could be realized by off-the-shelf components which allow to reuse of the existing lightning infrastructure. Therefore, VLC enables secure and free of health concern transmission where RF and millimeter wave communications are physically impossible or prohibited. Recent developments in light emitting diode (LED) manufacturing technologies are leading innovations in solid state lighting (SSL) as a source of illumination while LED's are starting to replace the incandescent and fluorescent lighting. LED's can be modulated at rates several hundred times that of incandescent and fluorescent light sources in such a power efficient way [31]. Intensity Modulation/Direct Detection (IM/DD) is the most practical modulation technique to use in indoor VLC. In IM/DD technique, information is carried by the intensity of the light. Then at the receiver, fluctuations in the intensity converted to electrical signal. Therefore, the signal carrying information by the IM/DD system should be real and non-negative valued. Implementation of the orthogonal division multiplexing (OFDM) signaling employed in IM/DD systems has showed great promise in terms of spectral efficiency and robustness against inter-symbol interference (ISI) [32].

Many of the recent works about optical OFDM (O-OFDM) systems have revealed the fact that each scheme has strengths and weaknesses in different metrics. DC-biased optical OFDM (DCO-OFDM) suffers from poor average optical efficiency. Power efficient asymmetrically clipped optical OFDM (ACO-OFDM) suffers from loss of half degrees of freedom (e.g., spectral efficiency) [33]. Unipolar OFDM, which neither requires DC biasing nor asymmetrically clipping, has

been proposed as an alternative to DCO-OFDM and ACO-OFDM techniques [34]. However, the spectral efficiency of U-OFDM is half of DCO-OFDM, which makes the U-OFDM scheme power inefficient for higher order modulations. Recently, enhanced U-OFDM (eU-OFDM) scheme has been proposed in [35], which utilizes the positive and negative separated frame structure of the U-OFDM and allows multiple U-OFDM information streams superimposed on top of each other in order to not sacrifice from the spectral efficiency. Due to its advantages in terms of power and spectral efficiency, eU-OFDM appears as a strong alternative for future OWC standards. On the other hand, considering the advantages of inherently available multiple-input-multiple-output (MIMO) optical wireless systems, the combination of the aforementioned optical OFDM techniques with MIMO transmission is inevitable [36].

Despite the recent surge of interest in VLC mentioned above, a lot of research problems related modeling of the VLC channel model and performance of the optical modulations schemes in various models still remain open. This work first presents realistic channel models for MIMO VLC systems by considering geometry of the environment, objects inside, the reflection characteristics of the materials as well as the specifications of the sources and receivers by using non-sequential ray tracing approach. The obtained channel impulse responses (CIR's) for MIMO scenario comprises practical issues such as number of LED chips per luminary, spacing between LED chips, objects inside the room and wiring topology. Second, by combining MIMO and eU-OFDM techniques, a new optical OFDM scheme, called MIMO-eU-OFDM, is proposed in this study. The bit error rate (BER) performance of MIMO-eU-OFDM is studied by computer simulations in the presence of 2×2 and 4×4 realistic MIMO VLC channel models and its BER performance is compared with the reference optical MIMO-OFDM systems.

3.2.1.2. Realistic VLC Channel Modeling. We now present a novel and realistic channel modeling approach for VLC that overcomes the limitations of previous works. Our study is based on Zemax[®] which is an optical illumination design software with sequential and non-sequential ray-tracing capabilities [12]. With an accurate description of interactions among rays emitted from the

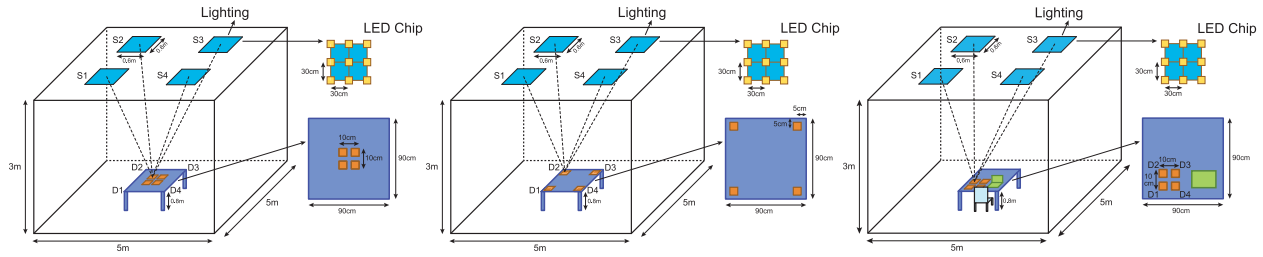


Figure 3.12. Configuration A (receivers located in center), B (receivers located in corners) and C (receivers at the left corner, chair and laptop exists)

LEDs in a user defined environment, the non-sequential ray-tracing is based on tracing the rays along physically realizable paths until they intercept an object. Wavelength dependency, effect of realistic light sources as well as different types of reflections are taken into consideration. Non-sequential ray tracing algorithms allow us to calculate the detected power and path lengths from source to detector for each ray. These are then processed to yield the channel impulse responses (CIRs) for various indoor environments. The line-of-sight (LOS) response depends on the LOS distance. Besides the LOS component, there is a large number of reflections from the ceiling, walls, floor and as well as objects within the environment.

In this work, we particularly focus on a specific MIMO scenario where four luminaries and four detectors are placed on the ceiling and on the table (besides the laptop e.g., USB device) respectively. We present the channel modeling with practical considerations such as number of LED chips per luminary, objects inside the room and cabling topology. After the evaluation of CIRs, we also investigate the effect of the propagation delay of cables on the CIRs. We show that a sparse channel model is obtained as a result of wiring topology of communication access point to luminaries. This type of channel model arises in indoor VLC systems such as homes and offices normally using multiple LED luminaries. Two important issues to modeling of the channel for these environments are number of LED chips and distance between them in each luminary. In fact, the number of LEDs and spacing between them affect the channel parameters such as channel DC gain, root mean square (RMS) delay spread and mean excess delay spread which are used in MIMO systems. However, the only channel models for MIMO VLC systems presented

in literature [32, 33] are obtained by unrealistic conditions such as fixed reflectance for materials, ideal Lambertian pattern for LEDs and by considering empty room.

Table 3.2. Channel Configurations

Parameters	Values
Size of room (m)	$5 \times 5 \times 3$
Number of luminaries	4
Number of chips per luminary	9
Model of each chip	Cree Xlamp® MC-E
Power of each chip	5 W
Luminary positions (m)	(1.3, 0.7, 3) (1.3, -1.3, 3) (-0.7, -1.3, 3) (-0.7, 0.7, 3)
Photodetector (PD) positions	(-0.14, -0.5, 0.8) (-0.14, -0.4, 0.8) (-0.14, -0.5, 0.8) (-0.14, -0.4, 0.8)
View angle of luminary	120°
FOV of PD	85°
Area of PD	1 cm^2
Materials (Wavelength dependent reflectance)	Walls: Plaster, Ceiling: Plaster Floor: Pine wood, Desk: Pine wood Chair: Black gloss paint Laptop: Black gloss paint

We now investigate some realistic indoor channel models and generate their CIRs for MIMO VLC systems consisting of 4 transmit and 4 receive units. The CIRs obtained with the ray tracing method of Zemax® software also enables us to specify the objects located in and the geometry of an indoor as well as the reflection characteristics of the surface materials, specifications of the sources (i.e., LEDs) and receivers (i.e., photodiodes) [24, 23, 37]. We consider a room size of $5 \times 5 \times 3$ meters (see Fig. 1) with single user - 4 transmit and 4 receive units. In [38], an ideal case has been considered in which 100 LED chips per each luminary were employed. However, by a simplifying technique, we can put lesser number of LED chips in each luminary to achieve the same channel parameters [39]. We place four luminaries on the ceiling, each consisting of 9 LED chips with spacing of 30 cm. Each LED chip radiates 5 W with a view angle of 120° . The field of view (FOV) and the area of the detector are 85° and 1 cm^2 , respectively. Four detectors placed on the desk at a height of 80 cm (standard desk height) with equal distances between them (10 cm). The materials of the walls, ceiling, floor, desk, chair and laptop are plaster, plaster, pine wood, pine wood, black gloss paint and black gloss paint [23]. The user is located in a symmetrical position with respect to the transmit units. Additionally, the locations of receiver units placed on the table are randomly selected. In Table I, different parameters of our configuration are given for a MIMO

VLC system.

Table 3.3. Channel parameters for configurations A, B and C

Channel	Configuration A (receivers located in center, $d_{RX} = 0.1$)				Configuration B (receivers located at corners, $d_{RX} = 0.8$)				Configuration C (receivers at the left corner, chair and laptop exists)			
	T_{tr} [ns]	τ_0 [ns]	τ_{RMS} [ns]	H_0	T_{tr} [ns]	τ_0 [ns]	τ_{RMS} [ns]	H_0	T_{tr} [ns]	τ_0 [ns]	τ_{RMS} [ns]	H_0
$h_{1,1}$	40	14.22	10.18	2.17×10^{-4}	37	12.40	8.98	2.94×10^{-4}	39	13.27	9.48	2.46×10^{-4}
$h_{1,2}$	40	14.44	9.79	2.19×10^{-4}	40	15.22	10.40	1.78×10^{-4}	40	13.83	9.90	2.04×10^{-4}
$h_{1,3}$	40	14.52	9.84	2.04×10^{-4}	42	17.28	11.23	1.38×10^{-4}	38	13.23	9.27	2.28×10^{-4}
$h_{1,4}$	40	14.44	9.79	2.19×10^{-4}	40	15.22	10.40	1.78×10^{-4}	39	14.07	9.77	2.02×10^{-4}
$h_{2,1}$	40	14.44	9.79	2.19×10^{-4}	40	15.22	10.40	1.78×10^{-4}	41	16.56	10.73	1.52×10^{-4}
$h_{2,2}$	40	14.22	10.18	2.17×10^{-4}	37	12.40	8.98	2.94×10^{-4}	41	17.20	11.04	1.33×10^{-4}
$h_{2,3}$	40	14.44	9.79	2.19×10^{-4}	40	15.22	10.40	1.78×10^{-4}	40	15.67	10.28	1.55×10^{-4}
$h_{2,4}$	40	14.52	9.84	2.04×10^{-4}	42	17.28	11.23	1.38×10^{-4}	42	17.99	11.44	1.12×10^{-4}
$h_{3,1}$	40	14.52	9.84	2.04×10^{-4}	42	17.28	11.23	1.38×10^{-4}	40	14.51	9.96	1.92×10^{-4}
$h_{3,2}$	40	14.44	9.79	2.19×10^{-4}	40	15.22	10.40	1.78×10^{-4}	41	15.64	10.63	1.60×10^{-4}
$h_{3,3}$	40	14.22	10.18	2.17×10^{-4}	37	12.40	8.98	2.94×10^{-4}	40	15.15	10.52	1.64×10^{-4}
$h_{3,4}$	40	14.44	9.79	2.19×10^{-4}	40	15.22	10.40	1.78×10^{-4}	40	14.91	10.25	1.74×10^{-4}
$h_{4,1}$	40	14.44	9.79	2.19×10^{-4}	40	15.22	10.40	1.78×10^{-4}	37	11.73	8.64	3.32×10^{-4}
$h_{4,2}$	40	14.52	9.84	2.04×10^{-4}	42	17.28	11.23	1.38×10^{-4}	37	12.01	8.56	3.29×10^{-4}
$h_{4,3}$	40	14.44	9.79	2.19×10^{-4}	40	15.22	10.40	1.78×10^{-4}	37	11.79	8.56	3.10×10^{-4}
$h_{4,4}$	40	14.22	10.18	2.17×10^{-4}	37	12.40	8.98	2.94×10^{-4}	38	11.99	8.85	2.90×10^{-4}

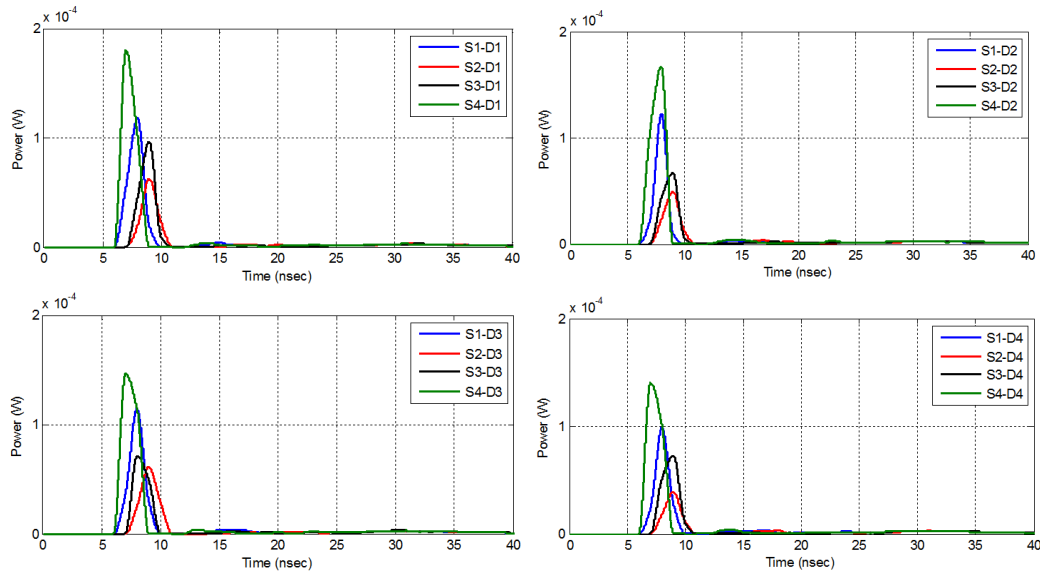


Figure 3.13. The PDP's for configuration C

The three different indoor MIMO-VLC configurations considered in this paper for channel modeling are shown in Fig. 1. Power delay profiles of each channel (totally 16 channels exist)

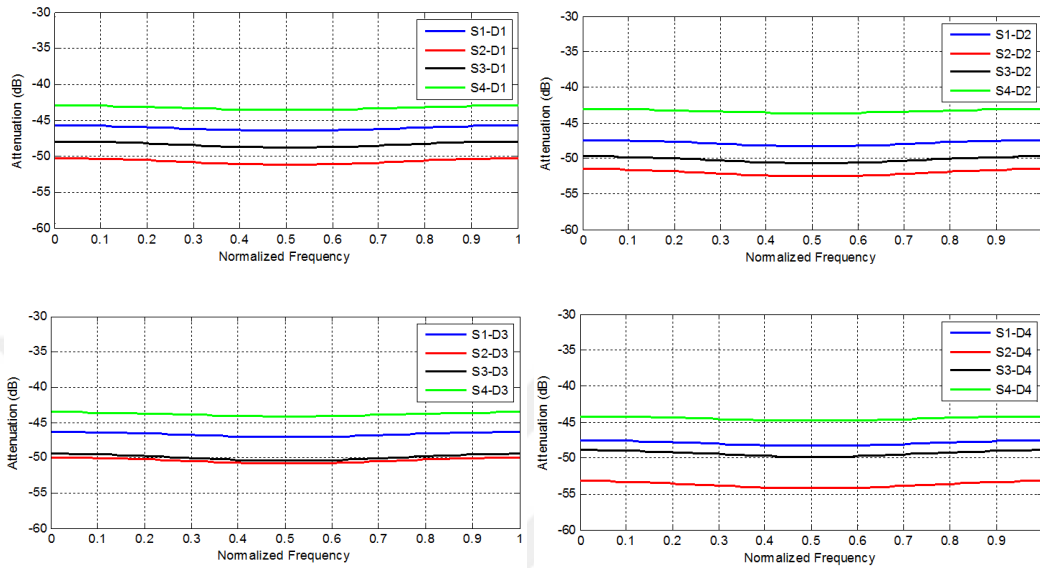


Figure 3.14. Channel frequency responses for configuration C

and their frequency responses are presented in Figs. 2 and 3, respectively. Table II presents the channel parameters of the CIRs between each luminary and each detector. The entire luminaries are assumed to emit light simultaneously. Obviously, all luminaries may not emit light at the same instant because of the difference of wiring topology. Therefore, this fact should be taken into consideration while a channel model is constructed in its general form. As shown in Fig. 4, the signal travels from communication access point to the luminary (array of LED chips) through a wired connection. Based on the simulation parameters, we used four luminaries on top of the ceiling where the dimensions of room is $5 \times 5 \times 3$ meters. Fig. 5 illustrates the wiring topology for our indoor environment model where a CAT-5 cable by length of 2 m between each luminary is employed [40]. This cable introduces a propagation delay of 5 nsecs per meter. Fig. 6 depicts the artificial multipath CIR as seen at the receiver (D1) taking into account the delays caused by cabling (see Fig. 5). Fig. 6 shows the CIR including the delays caused by cabling. We observe that the CIR, obtained in Fig. 6 exhibits a sparse channel model as a result of the wiring between luminaries in indoor VLC.

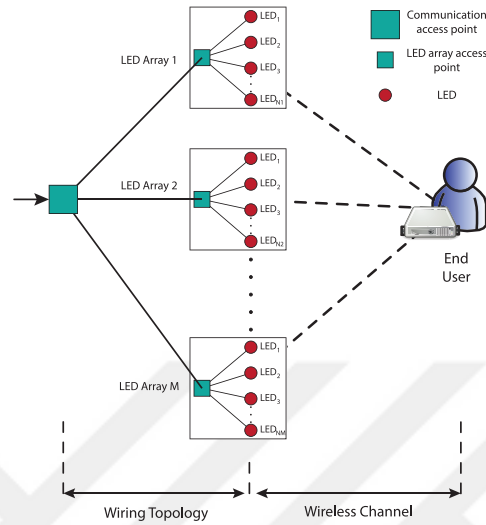


Figure 3.15. Wiring topology between communication access point and luminaries

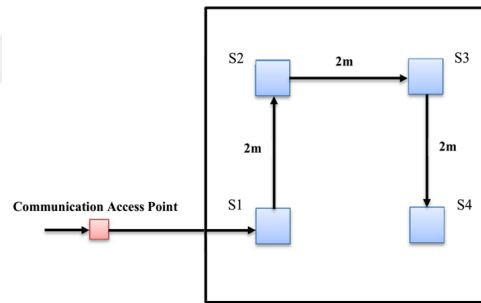


Figure 3.16. Cabling topology in configuration C via CAT-5

3.2.1.3. MIMO Enhanced Unipolar OFDM (MIMO-eU-OFDM) System. U-OFDM [34] has been proposed as an alternative to ACO-OFDM and DCO-OFDM techniques and it neither requires AC nor DC biasing for the operation of optical OFDM. U-OFDM scheme provides a unique solution for the transformation of bipolar OFDM signals obtained after IFFT operation to unipolar signals for their transmission over optical wireless links. In U-OFDM scheme, each bipolar frame is split into two unipolar frames (one positive and one negative frame), and these frames are transmitted one by one. According to U-OFDM principle a bipolar frame as

$$\mathbf{x} = \begin{bmatrix} -1.2 & 4.2 & 3.5 & -2.3 \end{bmatrix} \quad (3.22)$$

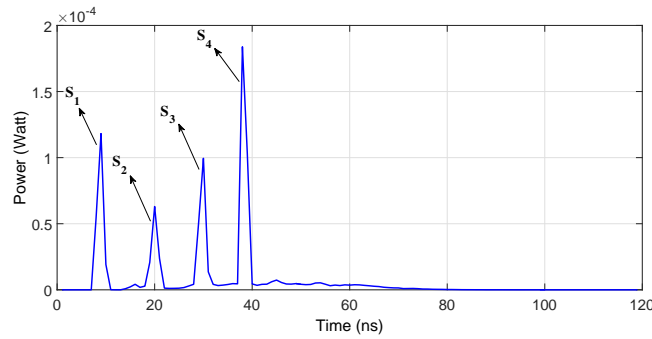


Figure 3.17. Channel impulse response for configuration C including the delays caused by cabling

can be transformed into

$$\mathbf{x} = \begin{bmatrix} \mathbf{x}_P & \mathbf{x}_U \end{bmatrix} = \begin{bmatrix} 0 & 4.2 & 3.5 & 0 & 1.2 & 0 & 0 & 2.3 \end{bmatrix} \quad (3.23)$$

where \mathbf{x}_P and \mathbf{x}_U denote the corresponding positive and negative frame, respectively. At the receiver side, the original bipolar frame can be obtained by subtracting the negative frame from the positive frame. The major drawback of the U-OFDM scheme is its reduced spectral efficiency given as,

$$\eta_U = \frac{\log_2(M)(N_{FFT} - 2)}{4N_{FFT}} \approx \frac{\log_2(M)}{4} \quad (3.24)$$

which is the half of the DCO-OFDM. In (3), M is the size of the considered M -QAM constellation, and N_{FFT} is the FFT size. The factor of $1/4$ comes from the combined effects of Hermitian symmetry and doubling the frame size with positive/negative frames.

eU-OFDM scheme [35, 41] is obtained by the modification of the U-OFDM scheme to achieve a higher spectral efficiency. eU-OFDM scheme doubles the spectral efficiency of U-OFDM and obtains the same spectral efficiency as that of DCO-OFDM by combining several U-OFDM

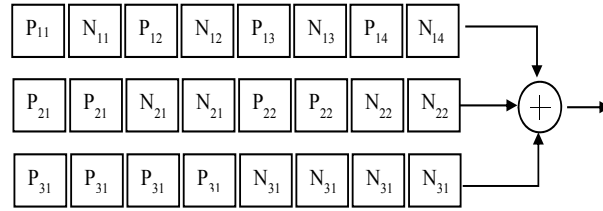


Figure 3.18. eU-OFDM signal generation for $L = 3$ layers

frames in a clever way. Fig. 7 shows the signal generation of eU-OFDM for $L = 3$ layers. As seen from Fig. 7, for the implementation of eU-OFDM scheme, 2^{L-l} bipolar OFDM frames are generated for each layer $l = 1, 2, \dots, L$. Then, these frames are transformed into unipolar frames by U-OFDM principle, where $P_{l,k}$ and $N_{l,k}$ denote the k th positive and negative frame at layer l , respectively. In other words, $P_{l,k}$ and $N_{l,k}$ are generated from the k th bipolar OFDM frame of the corresponding layer. At the first layer ($l = 1$), 2^{L-1} U-OFDM frames are generated and concatenated to obtain the main frame of layer 1. At the second layer, 2^{L-2} U-OFDM frames are generated but positive and negative frames are replicated twice before forming the main frame of this layer. A similar procedure is applied at layer 3 but the corresponding frames are replicated four times for this layer. For the l th layer, each unipolar frame is replicated 2^{l-1} times according to eU-OFDM principle. After the formation of L main frames, these frames are added and used to modulate the intensity of an LED.

At the receiver side, due to the appropriate replication of the U-OFDM frames of the lower layers, the interference of the U-OFDM frames at the lower layers to the U-OFDM frames at a higher layer is eliminated. As an example, for layer 1, each negative frame is subtracted from each positive frame, and the corresponding bipolar frame is obtained. Please note that the structure of eU-OFDM eliminates the interference from lower layers to layer 1 as seen from Fig. 7. After demodulation of the information bits, these bits are modulated again to obtain the main frame of layer 1 and this frame is subtracted from the overall received signal to remove the interference of the signals of these layer to the lower layers. This iterative demodulation procedure continues for other layers [35]. Due to its improved spectral and energy efficiencies, eU-OFDM appears as

a strong alternative to DCO-OFDM. It is shown in [41] that by considering $L = 5$, the spectral efficiency of eU-OFDM reaches 96.8% as that of DCO-OFDM ($\eta_L = \log_2(M)/2$).

Due to the advantages of MIMO transmission techniques, the combination of MIMO and eU-OFDM appears as a promising optical OFDM solution. In Fig. 8, the block diagram of the proposed MIMO-eU-OFDM scheme is presented. In this scheme, eU-OFDM is combined with V-BLAST technique, and considering an optical MIMO system of T LEDs and R PDs, each LED transmits its own eU-OFDM signals to improve the overall throughput of the system. Therefore, the spectral efficiency of the proposed scheme becomes

$$\eta_{new} \approx \frac{T \log_2(M)}{2}. \quad (3.25)$$

Denoting the vector of transmitted signals in a time instance by $\mathbf{x} \in \mathbb{R}^{T \times 1}$, the received signals $\mathbf{y} \in \mathbb{R}^{R \times 1}$ can be given as

$$\mathbf{y} = \mathbf{H}\mathbf{x} + \mathbf{n} \quad (3.26)$$

where $\mathbf{H} \in \mathbb{R}^{R \times T}$ is the channel matrix whose elements are shown in Table I for $T = R = 4$, and \mathbf{n} is the noise vector.

At the receiver side, the interference between the signals transmitted from different LEDs is eliminated by a zero-forcing (ZF) detector, i.e., $\mathbf{z} = \mathbf{H}^{-1}\mathbf{y}$, and each eU-OFDM frame is demodulated in a successive interference cancellation way as in [35]. For the evaluation of the error performance, we consider the average received electrical signal-to-noise ratio (SNR) as [42]

$$SNR = \frac{P_{Rx}^E}{\sigma_n^2} = \frac{1}{\sigma_n^2} \left(\frac{1}{R} \sum_{r=1}^R \sum_{t=1}^T h_{r,t} I \right)^2 \quad (3.27)$$

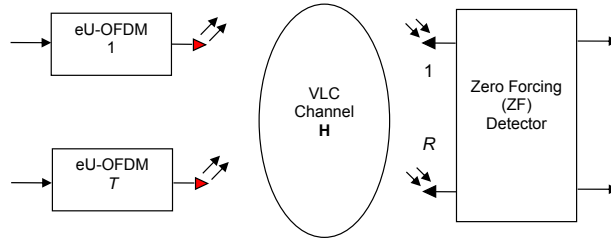


Figure 3.19. MIMO-eU-OFDM system model for $T \times R$ Optical MIMO System

where P_{Rx}^E is the average received electrical power, σ_n^2 is the power of the Gaussian noise samples, I is the mean optical intensity (average optical power of eU-OFDM), which is calculated as

$$I = \frac{1}{\sqrt{2\pi}} \sum_{l=1}^L \frac{1}{\sqrt{2^{l-1}}} \quad (3.28)$$

where unit-energy time-domain signals are considered and the amplitude of the frames at layer l is scaled by $1/\sqrt{2^{l-1}}$.

3.2.1.4. Computer Simulation Results. In this section, we provide computer simulation results for the proposed MIMO-eU-OFDM scheme for realistic indoor optical wireless channels. The BER performance of the proposed scheme is compared with V-BLAST-DCO-OFDM scheme which extends the concept of DCO-OFDM to MIMO systems [36]. For the considered signal constellation, the DC bias value [33] is set as 7 dB for DCO-OFDM. Two MIMO setups are considered: 2×2 and 4×4 . Three different configurations (configurations A, B and C) given in Table I are considered. For 4×4 MIMO channel, the channel coefficients of Table I are used, while for 2×2 MIMO case, we considered the elements correspond to first and third columns and rows of the channel matrix of the 4×4 case. The number of OFDM subcarriers is taken as $N_{FFT} = 128$ and 4-QAM constellation is considered. Number of layers are selected as $L = 5$ for the MIMO-eU-OFDM scheme and ZF detector is used at the receiver. In Fig. 9, the BER performance of the MIMO-eU-OFDM and V-BLAST-DCO-OFDM schemes are given for a 2×2 MIMO system with configurations A, B and C where 2 bits/sec/Hz of spectral efficiency is ob-

tained for both systems. As seen from Fig. 9, the proposed MIMO-eU-OFDM scheme achieves a better BER performance than the V-BLAST-DCO scheme for all considered configurations. In Fig. 10, we compare the BER performance of the MIMO-eU-OFDM and V-BLAST-DCO-OFDM schemes for a 4×4 MIMO setup with configurations A, B and C where 4 bits/sec/Hz of spectral efficiency is obtained for both systems. Similar to 2×2 case, the proposed scheme outperforms the reference scheme for all configurations.

It is interesting to note that due to the structure of the channel matrix with highly correlated elements, the performance of the considered schemes get worse for the 4×4 MIMO system as well as the BER performances of the systems for configurations A and C are worse than the BER performance for configuration B. However, the spectral efficiency is doubled without increasing the constellation size for the 4×4 MIMO system. On the other hand, the results of Figs. 9-10 give insight for the design of future OWC setups, which requires channel matrices with lower correlation among their elements to obtain better BER performance.

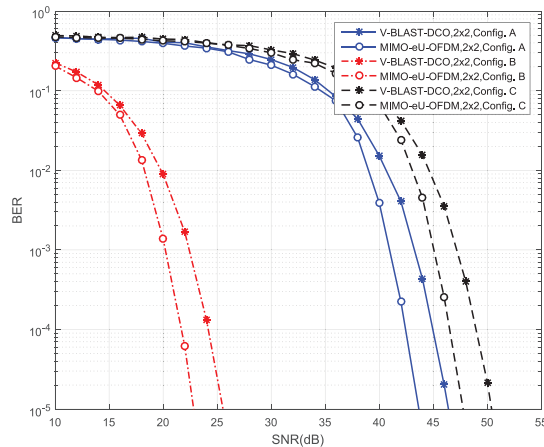


Figure 3.20. Performance of MIMO-eU-OFDM and V-BLAST-DCO-OFDM for 2×2 MIMO system

3.2.1.5. Conclusions. In this work, first, realistic indoor MIMO-VLC channel characterization and modeling were investigated by a non-sequential ray tracing approach. Indoor VLC CIRs for

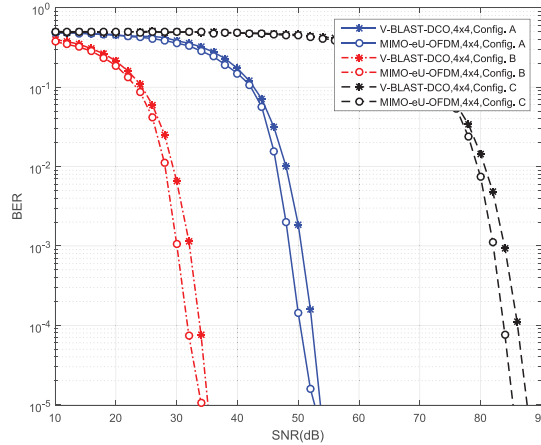


Figure 3.21. Performance of MIMO-eU-OFDM and V-BLAST-DCO-OFDM for 4×4 MIMO system

different MIMO configurations and scenarios were considered by taking some practical challenges into account such as number of LED chips per luminary, spacing between LED chips, objects inside the room and cabling topology. In particular, our results have demonstrated that the wiring topology should be taken into consideration to evaluate the CIRs. Our results have further shown that the CIR in an indoor environment including the propagation delays caused by wiring leads to a frequency selective sparse channel structure.

Second, by combining the eU-OFDM scheme and MIMO transmission techniques, a new VLC system, called MIMO-eU-OFDM was proposed and its BER performance was investigated in the presence of 2×2 and 4×4 realistic indoor MIMO-VLC channels. It was concluded that due to the structure of the channel matrix with highly correlated elements, the performance of the considered schemes has gotten worse for the 4×4 MIMO system. Particularly, we concluded that the BER performances of the systems for configurations A and C are worse than that of the configuration B. However, the spectral efficiency was doubled without increasing the constellation size for the 4×4 MIMO system. Consequently, the performance results obtained in the paper have given insight for the design of future OWC setups, which requires channel matrices with lower correlation among their elements to obtain better BER performance.

3.2.2. Red-Green-Blue OFDM (RGB-OFDM)

In this work, we propose a wavelength division multiplexing (WDM) based new modulation scheme for frequency selective multiple-input-multiple-output (MIMO) optical wireless communication (OWC) channels. The proposed scheme uses red, green, blue LEDs to transmit complex-bipolar valued time domain signal through diagonal channel matrix while preserving the illumination aims by emitting white light. The maximum a posteriori (MAP) estimator of the proposed scheme relies on DFT based eigen decomposition algorithm. It is shown in computer simulations that, proposed scheme achieves better bit-error-rate (BER) performance than existing VLC-MIMO-OFDM schemes due to diagonal channel matrix structure.

3.2.2.1. Introduction. Spectral efficiency for fixed power level is increased by using multiple antenna units in RF communication systems. Capacity of the wireless link is multiplied and spatial channels emerged by multiple transmit antennas (MISO), multiple receive antennas (SIMO) or both (MIMO). Forecasts for near future show that, more than 24 exabytes of mobile data traffic is expected in 2020's. Smart vehicles, drugs, robots and wearable technologies are going to be main challenges for mobile networks. Potential spectrum shortage is pushing researchers and engineering towards finding new and interference-free communication mediums to compensate higher data bandwidth demand. Millimeter wave communications taken into consideration in 5G research and development acts[43]. Optical wireless communications (OWC) especially visible light communications (VLC) offers very practical infrastructure for both communication and illumination in 5G and 5G+ technologies. Occupation of the electromagnetic spectrum up to 300GHz band (millimeter wave) left only bit of spectrum which is innocuous for human body around in the 430-770 THz region (visible light). Using existing lighting structure also for communications could reduce deployment cost significantly. So that, VLC would be one of the hot topics in next 10-15 years for both network access and backhaul levels.

In VLC systems, information carried on the light intensity as small fluctuations and it can be

detected at the transmitter (IM/DD). Since intensity of the light could not be negative and complex valued VLC systems have two main challenges. Conjugate symmetry or better known as Hermitian symmetry one powerful tool to have real output after IFFT operation in exchange for half of the spectral efficiency[44]. Positiveness (unipolarity) of the signal is obtained by different method in different modulation schemes. Simplest and easiest method is called DC biased optical OFDM (DCO-OFDM) uses appropriate level of DC bias to obtain unipolar real signal[45]. Despite the simplicity and broad application of this method, appropriate DC bias level for any modulation order is one of the most important issues. Clearly, larger DC bias reduces the clipping noise however, it is also increases the transmitted signal power which causes DC bias penalty[46]. Since OFDM has high peak-to-average-ratio (PAPR) state-of-the-art technique developed to obtain unipolar signal without using DC bias is called asymmetrically clipped optical OFDM (ACO-OFDM)[18]. In ACO-OFDM, Discrete Fourier Transform (DFT) property used to obtain unipolar and anti-symmetric time domain samples in time by only employing odd numbered subcarriers while even ones are set to zero. Anti-symmetric bipolar signal could be clipped without loss of information while all clipping noise is falling into even subcarriers. Approximately 7dB of gain is obtained by this method however, clipping process in time domain causes half of the spectral efficiency loss compared with DCO-OFDM and 3dB of the penalty at the receiver[28]. Flip OFDM and Unipolar OFDM (U-OFDM) are inspired from non-DC bias idea non-3dB penalty idea [47, 20]. In both methods, obtained bipolar real signal after DFT is split into two frames as, "positive" and "negative" frames. Positive signals are transmitted in the first frame whilst negative ones are set to zero. Absolute value of the negative samples are sent in the second frame while positive ones set to zero. At the receiver, to obtain original bipolar signal, negative frame is subtracted from positive frame.

Recently, both spectral efficiency loss and 3dB penalty solved by using “time-domain superposition”. The idea stems from well-known medium access layer concept called as “successive interference cancellation (SIC)” [48]. Accordingly, positive and negative parts of the real bipolar signal are extracted. In the sequel, polarity of the negative part is inverted and signal is transmitted as two OFDM symbols called "positive" and "negative" frames. Spectral efficiencies of the

methods mentioned above is given in Table 3.4.

Table 3.4. Spectral Efficiencies of various modulation methods

Transmission Method	Spectral Efficiency, η (bits/sec/Hz)
DCO-OFDM	$(\frac{N}{2} - 1)\log_2 M$
ACO-OFDM	$\frac{N}{4}\log_2 M$
Flip-OFDM	$\frac{N}{4}\log_2 M$
U-OFDM	$\frac{N}{4}\log_2 M$
eU-OFDM	$\approx (\frac{N}{2} - 1)\log_2 M$

As it can be seen clearly from Table 3.4, optical modulation schemes could only reached half of the spectral efficiency of the RF systems. In this paper, we propose a simple red-green-blue (RGB) wavelength-division-multiplexing (WDM) based VLC unit to reach spectral efficiency equal to RF systems while keeping illumination purpose of the system by obtaining white light from combination of the RGB colors. To the best of the authors' knowledge it is the first application of non-Hermitian symmetry non-time domain process OFDM structure by using only 3 LEDs.

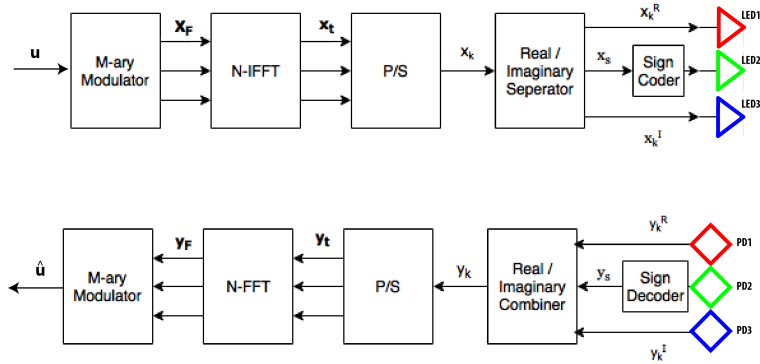


Figure 3.22. RGB OFDM Block Diagram

3.2.2.2. System Structure. The block diagram of RGB OFDM transmitter/receiver structure is given in Fig.3.22. Let u be the binary information stream. \mathbf{X}_F is obtained by simply performing M-QAM constellation mapping where N is the FFT size and M is the QAM constellation size. The input to the IFFT is the complex vector $\mathbf{X}_F = [X_0 X_1 \cdots X_{N-1}]^T$ where $0th$ and $N/2th$ subcarriers are not employed. \mathbf{X}_F requires no Hermitian symmetry unlike the other modulation

schemes. Resulting complex and bipolar valued discrete time domain samples \mathbf{x} , cannot be transmitted through LEDs directly since the IM/DD signals constrained to be real and positive. $\Re - \Im$ separator separates the $\Re(\mathbf{x})$ and $\Im(\mathbf{x})$ parts into two real and positive streams by taking absolute value of them. Resulting discrete time domain signals, x_R and x_I follows $\mathcal{N}_{\mathcal{F}}(0, 1/2)$ for unit power M-QAM constellation where $\mathcal{N}_{\mathcal{F}}$ represents folded Gaussian distribution. Sign information of x_R and x_I streams coded into a x_S vector as 4 level PAM symbols to obtain third stream. Simple look-up table to obtain x_R , x_I and x_S is given in Table 3.5.

Table 3.5. RGB OFDM Signal Generation Rule

Re	Im	x_R	x_S	x_I
+	+	$ \Re(x_k) $	a	$ \Im(x_k) $
+	-	$ \Re(x_k) $	b	$ \Im(x_k) $
-	+	$ \Re(x_k) $	c	$ \Im(x_k) $
-	-	$ \Re(x_k) $	d	$ \Im(x_k) $

As it can be easily seen that from the Table 3.5, probability distributions of x_R and x_I are symmetric and both will follow folded Gaussian given as,

$$f_{x_{R(I)}}(v) = \frac{2}{\sqrt{\pi}} e^{-v^2} u(v) \quad (3.29)$$

where f_{x_R} and f_{x_I} represents the probability density functions of x_R and x_I . Sign information x_S is simply following uniform distributed 4-PAM symbols. Lastly, obtained real and positive discrete time domain samples are fed to red, green and blue LEDs simultaneously. Positive and real discrete time domain samples are transmitted over 3×3 diagonal MIMO channel. Independence of the RGB channels comes from wavelength-division-multiplexing (WDM) provided by RGB filters on photodiodes (PD) at the receiver part. WDM separates each stream from each other while ensuring that white illumination is obtained for illumination purposes.

At the receiver, RGB filtered PDs capture received vector which could be given as,

$$\mathbf{y} = \mathbf{H}\mathbf{x} + \mathbf{n} \quad (3.30)$$

where $\mathbf{y} \in \mathbb{R}^{3 \times 1}$ is received electrical signal vector as $\mathbf{y} = [y_{k,1} \ y_{k,2} \ y_{k,3}]^T$ and $\mathbf{n} \in \mathbb{R}^{3 \times 1}$ is real valued additive white Gaussian noise (AWGN) vector. \mathbf{n} follows, $\mathcal{N}(0, \sigma_n^2)$ where $\mathcal{N}(\mu, \sigma^2)$ denotes the normal distribution with mean μ and variance σ^2 . Transmitted vector, $\mathbf{x} \in \mathbb{R}^{3 \times 1}$ is in the form of,

$$\mathbf{x} = [x_{k,R} \ x_{k,S} \ x_{k,I}]^T. \quad (3.31)$$

3×3 diagonal MIMO optical channel could be represented as,

$$\mathbf{H} = \begin{bmatrix} h_{1,1} & 0 & 0 \\ 0 & h_{2,2} & 0 \\ 0 & 0 & h_{3,3} \end{bmatrix} \quad (3.32)$$

where $h_{r,t}$ denotes the channel impulse response of the optical channel between r^{th} receiver and t^{th} transmitter. In this work, for simplicity non-linear effect of LEDs not considered. LEDs assumed working in their dynamic ranges.

In detection process, sign information $\bar{x}_{k,S}$ is estimated in the first place, from green LED by employing maximum likelihood (ML) estimator,

$$\bar{x}_{k,S} = \arg \min_{x_{k,S}} \|y_{k,2} - h_{2,2} \cdot x_{k,S}\|^2 \quad (3.33)$$

where $x_{k,S} \in \{a, b, c, d\}$. In the sequel, amplitude values for real and imaginary parts, \bar{x}_R and \bar{x}_I are estimated from red and blue LEDs by using *a priori* information that, x_R and x_I have clipped Gaussian distributions in the time domain. MAP estimates of x_R and x_I obtained as,

$$\begin{aligned} \bar{x}_{k,R} &= \arg \max_{\bar{x}_{k,R}} p(x_{k,R} | y_{k,1}), \\ \bar{x}_{k,I} &= \arg \max_{\bar{x}_{k,I}} p(x_{k,I} | y_{k,3}). \end{aligned} \quad (3.34)$$

where $p(x_{k,R}|y_{k,1})$ and $p(x_{k,I}|y_{k,3})$ are the p.d.f s of the $x_{k,R}$ and $x_{k,I}$ conditioned on received signals at the antennas 1, $y_{k,1}$ and 3, $y_{k,3}$ respectively. (3.34) could be written by using Bayes' theorem as,

$$\begin{aligned}\bar{x}_{k,R} &= \arg \max_{x_{k,R}} p(y_{k,1}|x_{k,R})p(x_{k,R}), \\ \bar{x}_{k,I} &= \arg \max_{x_{k,I}} p(y_{k,3}|x_{k,I})p(x_{k,I}).\end{aligned}\tag{3.35}$$

If we plug the p.d.fs in (3.35),

$$\begin{aligned}\bar{x}_{k,R} &= \arg \max_{x_{k,R}} \\ &\frac{1}{\sqrt{2\pi\sigma_n^2}} e^{-(y_{k,1}-h_{1,1}x_{k,R})^2/2\sigma_n^2} \cdot \frac{2}{\sqrt{\pi}} e^{-x_{k,R}^2} u(x_{k,R}), \\ \bar{x}_{k,I} &= \arg \max_{x_{k,I}} \\ &\frac{1}{\sqrt{2\pi\sigma_n^2}} e^{-(y_{k,3}-h_{3,3}x_{k,I})^2/2\sigma_n^2} \cdot \frac{2}{\sqrt{\pi}} e^{-x_{k,I}^2} u(x_{k,I}).\end{aligned}\tag{3.36}$$

Some algebra and dropping constant terms give MAP estimation metrics, x_{MAP}^R and x_{MAP}^I can be defined as,

$$\begin{aligned}\bar{x}_{k,R}^{MAP} &= \left(\frac{y_{k,1}+h_{1,1}}{h_{1,1}^2+2\sigma_n^2}\right)^+ \quad \text{and} \\ \bar{x}_{k,I}^{MAP} &= \left(\frac{y_{k,3}+h_{3,3}}{h_{3,3}^2+2\sigma_n^2}\right)^+\end{aligned}\tag{3.37}$$

where $()^+$ operator and σ_n^2 denote positive estimation and variances of the $n_{k,1}$, $n_{k,2}$ and $n_{k,3}$ respectively.

3.2.2.3. MIMO Channel Model. In this work, we have proposing realistic indoor VLC channel modeling approach to overcome the limitations in [27]. We have employed powerful ray tracing features of the optical design and illuminations software environment. Accordingly, we could model the indoor environment with daily life objects inside (including wavelength dependency

of all materials) by employing real sources (i.e. LEDs) and receivers (i.e. photodiodes). Along with ray tracing approach, we obtained channel impulse responses (CIRs) for non-ideal sources and purely diffuse, specular and mixed type of reflections. Realistic scenario environment selected from IEEE802.15.7r standardization group for the sake of accuracy [49]. Simulation scenario with human bodies and furniture is given in Fig. 3.23. Commercial Cree Xlamp XP-C blue, green, red

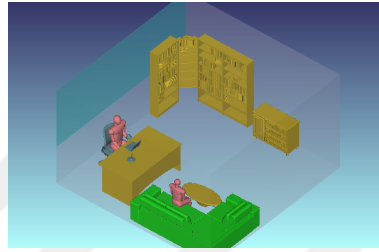


Figure 3.23. Office room scenario

and white LEDs used as a transmitter with viewing angle 120° . By taking, total power emitted per LED chip is 1 Watt we can associate channel DC gain with the average received power at the receiver [?]. Three detectors with red, green and blue filter located in the on the desk surface with the field of view (FOV) and detector area with 85° and 1cm^2 respectively. Relative spectral distributions of the RGB and white LEDs are given in Fig. 3.24. Parameters for simulation scenario

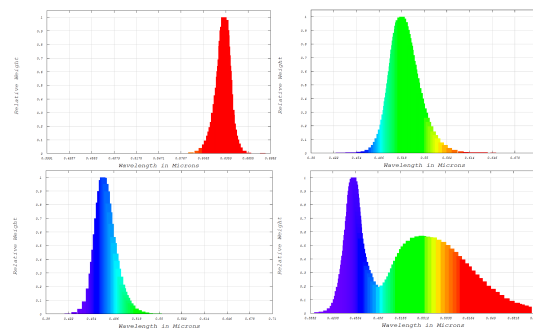


Figure 3.24. Simulated relative spectral distributions of the RGB and white LEDs respectively

given in Table 3.6. CIRs obtained between each transmitter and its corresponding receiver given in Table 3.7. It can be said that channel DC gain and RMS delay spread in scenario with human and furniture are smaller than scenario without human and furniture. This effect is stemmed by change of reflection characteristics of the room by human bodies and furniture [?].

Table 3.6. Simulation Parameters

Room size	5 m × 5 m × 3 m
Materials	Walls: Plaster, Ceiling: Plaster, Floor: Pinewood
Objects	1 desk and a chair paired with desk 1 laptop on the desk, 1 desk light on the desk, 1 library 1 cage, 1 couch, 1 coffee table, window, 2 human bodies
Objects specifications	Desk: Pinewood (Typical height of 0.88m) Chair: Black gloss paint, Laptop: Black gloss paint Cage: Pinewood, Couch: Cotton, Coffee table: Pinewood Human body: Shoes: Black gloss paint, Head & Hands: Absorbing Clothes: Cotton
LED specifications	Brand: Cree XLamp XP-C-blue-green-red-white
Receiver area and FOV	1 cm ² , 85
Location of LEDs (m)	Blue (-0.005,0.01,3) Green (0,0,3) Red (-0.01,0,3) White (0,0,3)
Location of detectors (m)	DBlue (-1.2,1.28,0.88) DGreen (-1.2,1.38,0.88) DRed (-1.3,1.33,0.88) DWhite (-1.25,1.33,0.88)

Table 3.7. Channel Parameters for Office room with secondary light scenario including human body and furniture

Configuration	"Office room with secondary light" scenario with human and furniture			
	T _{ir}	tau0	tauRMS	H0
Red LED	39	14.84	9.07	2.80x10 ⁻⁶
Green LED	32	12.29	6.28	2.78x10 ⁻⁶
Blue LED	29	11.44	4.99	2.83x10 ⁻⁶
White LED	35	13.40	7.77	2.58x10 ⁻⁶

3.2.2.4. Frequency Selective MIMO Channel Model. Ever increasing mobile data demand forces new generation communication systems to achieve higher data rates. Higher data rates causes to channel to be frequency selective. In this part, we have considered frequency selective MIMO channels and equalizers for time domain processed optical wireless communications systems. We assume that proposed system uses cyclic prefix, $L_{cp} \geq L_h$ where L_{cp} and L_h are cyclic prefix length and number of channel taps respectively. Frequency selective MIMO channel matrix can be expressed as,

$$\tilde{\mathbf{H}} = \begin{bmatrix} \mathbf{h}_{1,1} & \mathbf{0} & \mathbf{0} \\ \mathbf{0} & \mathbf{h}_{2,2} & \mathbf{0} \\ \mathbf{0} & \mathbf{0} & \mathbf{h}_{3,3} \end{bmatrix} \quad (3.38)$$

where $\mathbf{h}_{1,1}$, $\mathbf{h}_{2,2}$ and $\mathbf{h}_{3,3}$ are $L_{h1,1}$, $L_{h2,2}$ and $L_{h3,3}$ tap channel vectors obtained for empty room by using sequential ray tracing software. Wavelength characteristics of red, green and blue LEDs are considered for ray tracing approach. At the receiver, received signals can be modeled as,

$$\mathbf{y}_1 = \mathbf{h}_{1,1} \circledast \mathbf{x}_R + \mathbf{n} \quad (3.39)$$

$$\mathbf{y}_2 = \mathbf{h}_{2,2} \circledast \mathbf{x}_S + \mathbf{n} \quad (3.40)$$

$$\mathbf{y}_3 = \mathbf{h}_{3,3} \circledast \mathbf{x}_I + \mathbf{n} \quad (3.41)$$

where \circledast denotes circular convolution operation. It is well known that, circular convolution can be represented by matrix multiplication given as,

$$\mathbf{y}_1 = \mathbf{G}_{1,1} \mathbf{x}_R + \mathbf{n} \quad (3.42)$$

$$\mathbf{y}_2 = \mathbf{G}_{2,2} \mathbf{x}_S + \mathbf{n} \quad (3.43)$$

$$\mathbf{y}_3 = \mathbf{G}_{3,3} \mathbf{x}_I + \mathbf{n} \quad (3.44)$$

where $\mathbf{G}_{1,1}$, $\mathbf{G}_{2,2}$ and $\mathbf{G}_{3,3}$ denotes $N \times N$ circulant channel matrices of frequency selective channel vectors, $\mathbf{h}_{1,1}$, $\mathbf{h}_{2,2}$ and $\mathbf{h}_{3,3}$ respectively.

3.2.2.5. Design of a MAP Estimator. For frequency selective MIMO systems, estimates are vector and matrices. ZF and MAP estimators in Section 2.1.1 are updated to deal with vectoral estimates. At the receiver, again we estimate sign vector as a first step by using simple ZF estimator given as $\bar{\mathbf{x}}_S^{ZF} = \mathbf{G}_{2,2}^{-1} \cdot \mathbf{y}_2$. After equalization, ML detector applied to $\bar{\mathbf{x}}_S^{ZF}$ to detect $\bar{\mathbf{x}}_S$.

If we modify (4) and (5) to vectoral form to obtain MAP estimators for $\bar{\mathbf{x}}_{\mathbf{R}}$ and $\bar{\mathbf{x}}_{\mathbf{I}}$. After some matrix algebra we obtained,

$$\begin{aligned}\bar{\mathbf{x}}_{\mathbf{R}}^{\text{MAP}} &= \arg \max_{\mathbf{x}_{\mathbf{R}}} p(\mathbf{y}_1 | \mathbf{x}_{\mathbf{R}}) p(\mathbf{x}_{\mathbf{R}}) \quad \text{and} \\ \bar{\mathbf{x}}_{\mathbf{I}}^{\text{MAP}} &= \arg \max_{\mathbf{x}_{\mathbf{I}}} p(\mathbf{y}_3 | \mathbf{x}_{\mathbf{I}}) p(\mathbf{x}_{\mathbf{I}}).\end{aligned}\tag{3.45}$$

From (3.45) we can get,

$$\begin{aligned}\bar{\mathbf{x}}_{\mathbf{R}}^{\text{MAP}} &= \\ \arg \max_{\mathbf{x}_{\mathbf{R}}} &\frac{1}{\sqrt{2\pi\sigma_n^2}} e^{-(\mathbf{y}_1 - \mathbf{G}_{1,1}\mathbf{x}_{\mathbf{R}})^T (\mathbf{y}_1 - \mathbf{G}_{1,1}\mathbf{x}_{\mathbf{R}}) / 2\sigma_n^2} \\ &\frac{2}{\sqrt{\pi}} e^{-(\mathbf{x}_{\mathbf{R}})^T (\mathbf{x}_{\mathbf{R}})} \quad \text{and} \\ \bar{\mathbf{x}}_{\mathbf{I}}^{\text{MAP}} &= \\ \arg \max_{\mathbf{x}_{\mathbf{I}}} &\frac{1}{\sqrt{2\pi\sigma_n^2}} e^{-(\mathbf{y}_3 - \mathbf{G}_{3,3}\mathbf{x}_{\mathbf{I}})^T (\mathbf{y}_3 - \mathbf{G}_{3,3}\mathbf{x}_{\mathbf{I}}) / 2\sigma_n^2} \\ &\frac{2}{\sqrt{\pi}} e^{-(\mathbf{x}_{\mathbf{I}})^T (\mathbf{x}_{\mathbf{I}})}.\end{aligned}\tag{3.46}$$

After some matrix algebra and dropping constant terms,

$$\begin{aligned}\bar{\mathbf{x}}_{\mathbf{R}}^{\text{MAP}} &= (\mathbf{K}\mathbf{G}_{1,1}^T \mathbf{y}_1)^+ \quad \text{and} \\ \bar{\mathbf{x}}_{\mathbf{I}}^{\text{MAP}} &= (\mathbf{M}\mathbf{G}_{3,3}^T \mathbf{y}_3)^+ \\ \text{where} & \\ \mathbf{K} &= [1/2 \cdot (\mathbf{G}_{1,1}^T \mathbf{G}_{1,1} + \mathbf{G}_{1,1} \mathbf{G}_{1,1}^T) + 2\sigma_n^2 \mathbf{I}]^{-1} \\ \mathbf{M} &= [1/2 \cdot (\mathbf{G}_{3,3}^T \mathbf{G}_{3,3} + \mathbf{G}_{3,3} \mathbf{G}_{3,3}^T) + 2\sigma_n^2 \mathbf{I}]^{-1}\end{aligned}\tag{3.47}$$

It can be easily seen from (3.47) that, multiplication of two circulant matrices gives also circulant matrix. Moreover, addition operation is not disturbing the circularity of the matrix. So that, matrices \mathbf{K} and \mathbf{M} remain as circulant matrices.

3.2.2.6. Eigenvalue decomposition for circulant matrices. It is well studied in mathematics that, circulant matrices are special case of general Toeplitz matrices. We already know that, \mathbf{H}_{11} and

\mathbf{H}_{33} are circulant matrices. Moreover, $[\sigma_r^2(\mathbf{H}_{11}^T \mathbf{H}_{11} + \mathbf{H}_{11} \mathbf{H}_{11}^T) + 2\sigma_{n_1}]$ and $[\sigma_i^2(\mathbf{H}_{33}^T \mathbf{H}_{33} + \mathbf{H}_{33} \mathbf{H}_{33}^T) + 2\sigma_{n_3}]$ parts in (13) and (14) are also circulant matrices. If we apply basic DFT based eigen decomposition,

$$\mathbf{A}^{-1} = \mathbf{F} \cdot \mathbf{\Lambda}^{-1} \cdot \mathbf{F}^H \quad (3.48)$$

where $\mathbf{\Lambda} = \text{diag}(\lambda_1, \lambda_1, \dots, \lambda_n)$, λ_i 's are eigenvalues of the vector \mathbf{A} and \mathbf{F} called unitary Fourier matrix. We can easily see that, only first row of \mathbf{H}_{11} and \mathbf{H}_{33} is enough to construct all, \mathbf{H}_{11} , \mathbf{H}_{33} , \mathbf{H}_{11}^{-1} and \mathbf{H}_{33}^{-1}

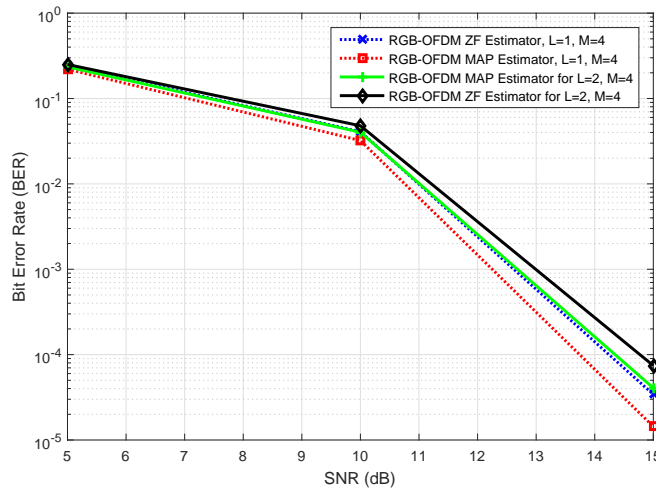


Figure 3.25. BER vs. SNR Results for ZF and MAP Estimators with L=1 and L=2 tap channels

3.2.2.7. Simulations and Results. SNR vs. BER and MSE vs. BER graphs for both ZF and MAP estimator are given in Figs. 3.25 - 3.26.

3.2.2.8. Conclusions. In this paper, we have proposed novel WDM using RGB-OFDM for optical wireless communications systems for both frequency flat and frequency selective MIMO channels. Computer simulations showed that, using *a priori* information that folded Gaussian distributed structure of time domain signals gives remarkable performance augmentation for both frequency

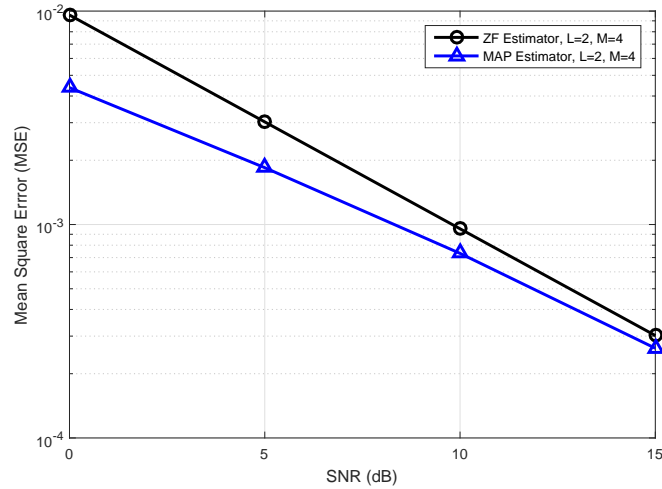


Figure 3.26. MSE vs. BER Result for ZF and MAP Estimator with L=2 tap channel

flat and frequency selective MIMO channels. Also, new approach proposed to overcome matrix inversion complexity of vectorial MAP estimator. As a future study, we are planning to extend time domain MAP estimator for U-OFDM and eU-OFDM systems while they are operating in both frequency flat and frequency selective MIMO channels.

4. Realization of Indoor Optical Wireless Communication Systems

During 3 years of research & development process we have built three progressive versions of OWC link technology between transmitter and receiver parts which are named as "Generations". In the 1st Generation (1G) system simple return-zero on-off keying (RZ-OOK) scheme is employed. In 1G, RS-232 serial communication protocol is taken as guideline to the design process. Full-duplex operation of the system provided up to 64K bits/sec data rate. At the receiver, op-amp circuitry compensated the channel fading effect and simple comparator transformed received signal to RS-232 formatted signal back at the receiver without further symbol detection process. Achieved communication range of interval measured as [9cm, 15cm].

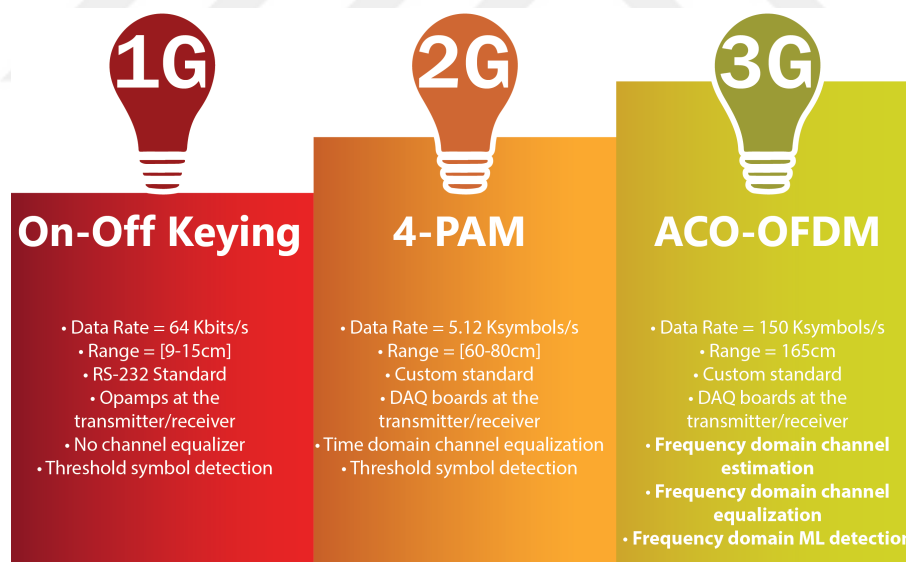


Figure 4.1. 1st, 2nd and 3rd Generation OWC Systems

In the 2G system, OWC link quality and spectral efficiency is raised by utilizing 4 level PAM system with time domain raised cosine filtering. Synchronization and packet transfer protocols of the 2G is implemented in the DAQ boards. At the receiver, channel equalization, symbol extraction and detection algorithms are executed. 2G communications range is measured as, [50cm, 80cm].

Lastly, 3G OWC system with ACO-OFDM is implemented for real life scenario with the 165 cm of separation between transmitter and receiver units. 3G used one of non-DC bias required power efficient ACO-OFDM to transmit data. Moreover, system used frequency domain channel estimation symbol detection. Complexity of the system is dramatically increased while DAQ boards and computer were same. Thus, performance of the O-OFDM highly dependent on the hardware for this generation. Same synchronization and packet transfer protocol used in 2G is also kept. System is operated in 150 000 bits/sec data rate for fixed transmitter and receiver unit separation as 165cm.

4.1. 1st Generation (1G) RZ-OOK Based VLC System

In the first generation, objective was realization of the OWC link between transmitter and receiver parts by using simplest digital modulation scheme. Accordingly digital communications literature is reviewed and ASK, FSK and PSK are taken as candidates. Since VLC systems are based on IM/DD technique and it is not possible to carry information on carrier frequency and phase. That is why particularly binary ASK (OOK) became best option for simplest transmission. OOK systems rely on a basic idea that information is carried on two different amplitude values such as, '0' and '1'. This binary returning to zero scheme called "Return Zero On-Off Keying (RZ-OOK)". Since the amplitude of the signal is not taking any negative values, electrical signal could be directly fed to an LED without further modification. Typical RZ-OOK scheme has shown in the Figs. 4.2 and 4.4.

RZ-OOK is widely used technique in optical systems. It has serious advantage among other modulation methods when moderate data rate is sufficient for designed system. Main advantages of RZ-OOK could be explained as,

- Non-coherent reception at the receiver side.
- Less computational complexity in signal processing and detection at the receiver.
- Noise immunity.

- Compatibility with TTL logic.

4.1.1. Transmitter

Transmitter structure designed for **RZ-OOK! (RZ-OOK!)** transmission is given in Fig. 4.2.

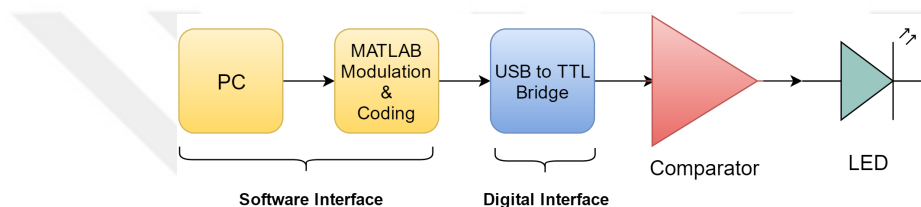


Figure 4.2. RZ-OOK Transmitter Structure

User generated information bits are processed in MATLAB environment to obtain time domain signals which are suitable for IM/DD transmission. CP2102 USB TO UART Bridge used as a D/A converter by converting information in the MATLAB environment to digital data by the means of time domain pulses. Flowchart of the MATLAB audio transmission algorithm is given in Fig. 4.3

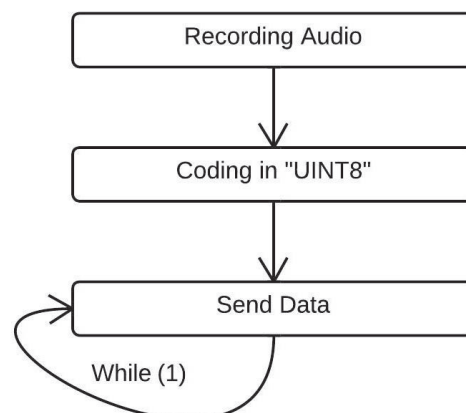


Figure 4.3. Flowchart of RZ-OOK MATLAB audio transmission algorithm

CP2102 is using RS-232 serial communications protocol for communications. Accordingly, one start bit and one stop bit added to each packet to provide frame synchronization. System data rate is optimally kept in 64k bits/sec within LED and photodiode's frequency response interval.

4.1.2. Optical Channel

For this particular design of system received signal modeled as,

$$r(t) = h \cdot x(t) + n(t) \quad (4.1)$$

where r , h , x and n shows received signal, time-invariant optical channel fading coefficient and AWGN respectively. There is no channel equalization algorithm utilized for this system simple comparator op-amp circuit is used to compensate the effects of both optical channel and AWGN.

4.1.3. Receiver

Receiver part is designed to compensate channel fading as well as AWGN. Receiver structure of the system is given in Fig. 4.4. BPW34 Silicon PIN Photodiode captures the OOK signals at the

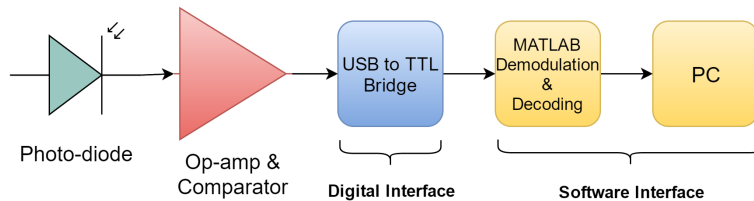


Figure 4.4. RZ-OOK Receiver Structure

receivers. BPW34 converts data carrying optical signal to electrical current between $[35\mu A, 45\mu A]$ range. To extract symbols back received signal is amplified compared with 2.5 threshold voltage by LTC6244HMS8 Dual 50Mhz, Low Noise, CMOS operational amplifier. Comparator part discards the effect of AWGN and shapes time domain signal for A/D conversion process which is compatible to RS-232 protocol. Photograph of receiver circuitry is given in Fig. 4.5. After all time

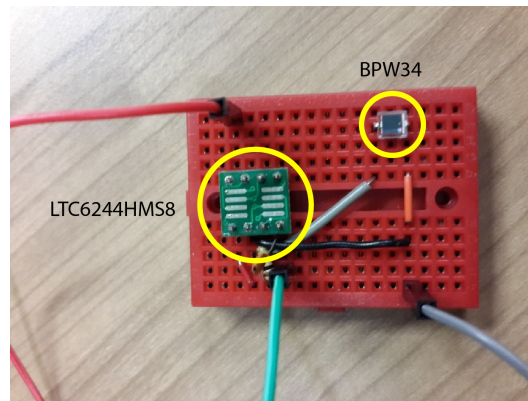


Figure 4.5. Photograph of receiver circuitry

domain processes, CP2102 USB TO UART Bridge decodes received frames and detects symbols consecutively. Detected values are further processed to obtain original data in MATLAB environment. Flowchart of the data reconstruction algorithm for audio in MATLAB is given in Fig. 4.6.

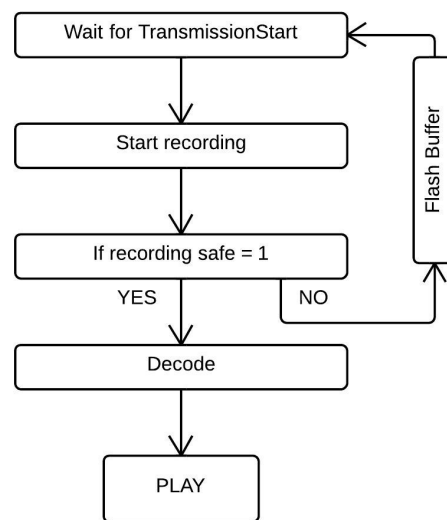


Figure 4.6. Flowchart of RZ-OOK MATLAB receiver algorithm for audio

BER vs SNR analysis utilized to measure system performance for various distance and noise values by transmitting text, voice and image. Photograph of CP2102 USB TO UART Bridge is

given in Fig. 4.7.

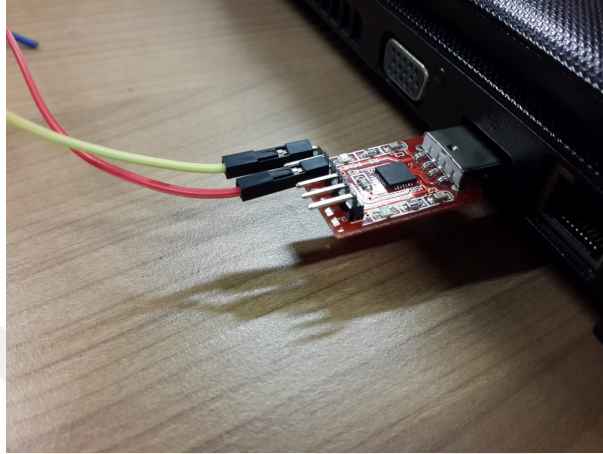


Figure 4.7. Photograph of CP2102 USB TO UART Bridge

Table 4.1. Results for audio transmission with white power LED

	TYPE OF DATA	SIZE	SAMPLING RATE	TYPE OF LED	LOS	LENS	DISTANCE	TIME (SEC)	SUCCESS
1	Audio	73.3 kbyte	12000	White power LED	Yes	No	8 cm	~9.4	Not Detectable
2	Audio	73.3 kbyte	12000	White power LED	Yes	No	9 cm	~9.4	Success
3	Audio	73.3 kbyte	12000	White power LED	Yes	No	10 cm	~9.4	Success
4	Audio	73.3 kbyte	12000	White power LED	Yes	No	12,5 cm	~9.4	Success
5	Audio	73.3 kbyte	12000	White power LED	Yes	No	14,5 cm	~9.4	Partial Success
6	Audio	73.3 kbyte	12000	White power LED	Yes	No	16,5 cm	~9.4	Not Detectable
7	Audio	73.3 kbyte	12000	White power LED	Yes	No	21 cm	~9.4	Not Detectable
8	Audio	73.3 kbyte	12000	White power LED	Yes	No	28 cm	~9.4	Not Detectable

4.1.4. Experimental Results

Experimental results obtained for different parameters and conditions are given in Tables 4.1, 4.2 and 4.3. Success range is between 9cm and 14 cm for first 8 experiments, 24cm – 41 cm for experiments numbered 9 to 17 and 8cm – 11cm for experiments numbered 21 to 25. Signal shapes sent from transmitter and detected at the receiver for various distances given in Fig. 4.9.

Table 4.2. Results for image transmission with white power LED

	TYPE OF DATA	SIZE	DIMENSION	TYPE OF LED	LOS	LENS	DISTANCE	TIME (SEC)	SUCCESS
1	Image	169,2kbyte	[215 x 215 x 3]	White Power LED	Yes	Yes	37,5cm	~21,6	Success
2	Image	169,2kbyte	[215 x 215 x 3]	White Power LED	Yes	Yes	27cm	~21,6	Success
3	Image	169,2kbyte	[215 x 215 x 3]	White Power LED	Yes	Yes	21cm	~21,6	Not Detectable
4	Image	169,2kbyte	[215 x 215 x 3]	White Power LED	Yes	Yes	23,5cm	~21,6	Not Detectable
5	Image	169,2kbyte	[215 x 215 x 3]	White Power LED	Yes	Yes	26cm	~21,6	Success
6	Image	169,2kbyte	[215 x 215 x 3]	White Power LED	Yes	Yes	25cm	~21,6	Success
7	Image	169,2kbyte	[215 x 215 x 3]	White Power LED	Yes	Yes	24cm	~21,6	Success
8	Image	169,2kbyte	[215 x 215 x 3]	White Power LED	Yes	Yes	40cm	~21,6	Success
9	Image	169,2kbyte	[215 x 215 x 3]	White Power LED	Yes	Yes	45cm	~21,6	Data Corrupted

Table 4.3. Results for image transmission with blue power LED

	TYPE OF DATA	SIZE	SAMPLING RATE	TYPE OF LED	LOS	LENS	DISTANCE	TIME (SEC)	SUCCESS
1	Audio	73.3 kbyte	12000	Blue Power LED	Yes	No	6 cm	~9.4	Not Detectable
2	Audio	73.3 kbyte	12000	Blue Power LED	Yes	No	7 cm	~9.4	Not Detectable
3	Audio	73.3 kbyte	12000	Blue Power LED	Yes	No	8 cm	~9.4	Success
4	Audio	73.3 kbyte	12000	Blue Power LED	Yes	No	9 cm	~9.4	Success
5	Audio	73.3 kbyte	12000	Blue Power LED	Yes	No	10 cm	~9.4	Success
6	Audio	73.3 kbyte	12000	Blue Power LED	Yes	No	11 cm	~9.4	Success
7	Audio	73.3 kbyte	12000	Blue Power LED	Yes	No	12,5 cm	~9.4	Partial Success
8	Audio	73.3 kbyte	12000	Blue Power LED	Yes	No	14,5 cm	~9.4	Not Detectable

4.1.5. Conclusions

In conclusion, we were able to transfer data such as text, audio and picture by using VLC between two computers for the first time. Data could be transmitted up to 1 Mbits/sec but frequency response of our non-ideal components obstructs speed of transmission. Photo-diode has the lowest response and it was weakest chain of the designed system. So that, photo-diode (BPW34) assigned our speed of transmission for this design. We used Schmitt trigger and OP-AMP circuitry to increase quality of both transmitted and received data. We observed that color of the light, distance between light and receiver, line of sight or non line of sight, SNR level and BER directly affects

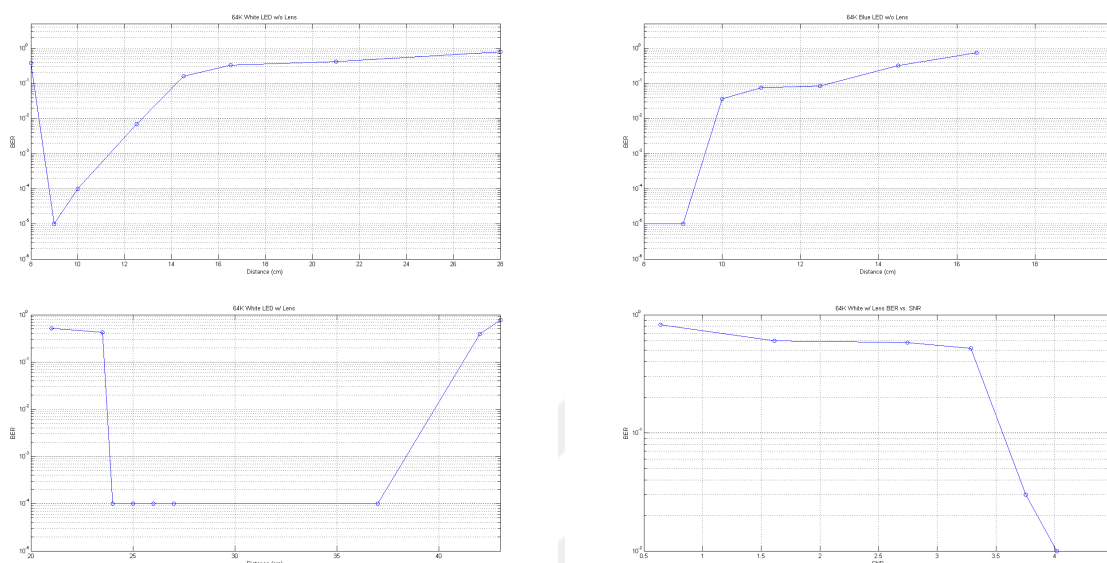


Figure 4.8. Distance vs BER graphs for; 64K white LED w/o lens (upper left), 64K blue LED w/ lens (upper right), 64k white LED w/ lens (lower left) and BER vs SNR graph for 64K white LED w/ lens (lower right).

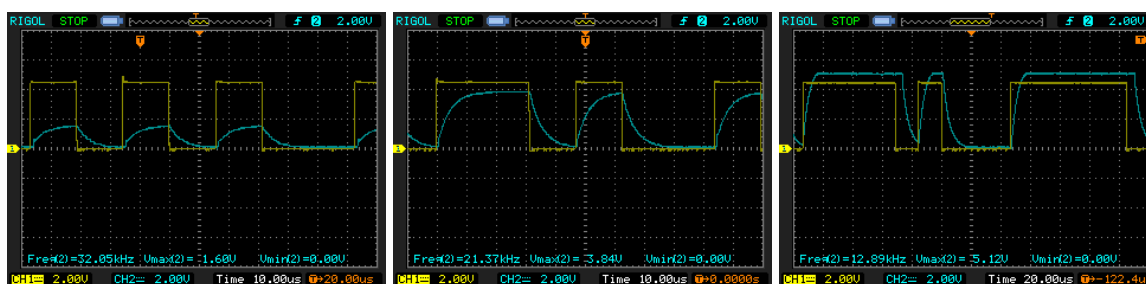


Figure 4.9. Sent and received signal shapes for various distances (yellow is sent signal and blue is received signal)

the quality of transmission. As given in experimental results, we measured quality and speed of data transmission with different colors, distance etc. As a result that we achieved 64,000 bits/sec speed in for an indoor visible light communications application. If components that have better frequency response would increase the speed of data transmission up to 1 Mbits/sec. Multi-path systems can be used to make non-line of side communication in the VLC systems and not just first one but second and more ordered reflections could be considered as a channel impulse response.

4.2. 2nd Generation (2G) 4-PAM Based VLC System

The first generation of the system was based on RS-232 serial communications and OOK signal shape. Conversely, in 2nd generation we have used multilevel PAM modulation rather than ON-OFF Keying modulation. Both systems are still single carrier based and operating in baseband region. Spectral efficiency of 1G was not high enough for realistic transmission cases. So that, we have used multilevel transmission scheme and we have created our own hybrid protocol to be able to synchronize transmitter and receiver part. System structure for 2nd generation PAM based communication system is given in Fig. 4.10.

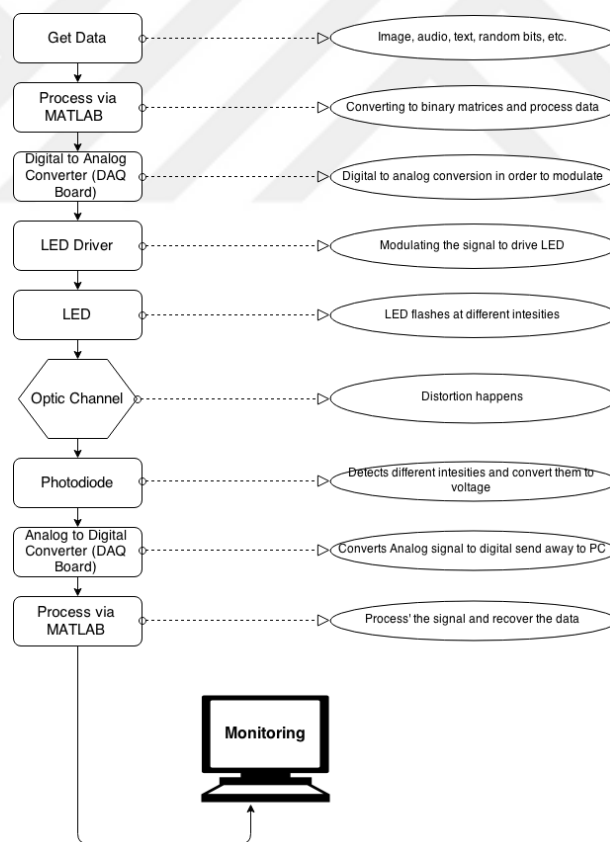


Figure 4.10. PAM based VLC System Schematic

Like OOK modulation, the data is carried on the amplitude but in this particular modulation there are several intensity levels. We have 4 different levels: +1V, +2V, +3V and +4V. Each symbol

corresponds to 2 bits of information.

4.2.1. Transmitter

The system which is designed with transmitter and receiver parts, is firstly used for text transmission. Texts are mostly the information that carries lesser bits than other type of transmission information. Therefore, it is likely to complete the transmission without error. In the transmitter, the string or text processed and turned into blocks that contains 1024 bits inside. Then, the blocks are sent one by one through optic channel. Photograph of the transmitter antenna (LED) for 2nd generation PAM based VLC system is given in Fig. 4.11.



Figure 4.11. Transmitter part of the 2nd generation PAM based VLC system

Simple transmitter encoding look-up table is given in Table 4.4. After the conversion, voltage

Table 4.4. Transmitter loop-up table for 2G system

Bits	Correspondent Voltage
00	1V
01	2V
11	3V
10	4V

values are transferred to digital to analog converter and transferred the analog signal to LED Driver.

The LED Driver drives the current to LEDs in order to succeed the transmission. Discrete-time domain signal after 4-PAM encoding according to table given above is plotted in Fig. 4.12.

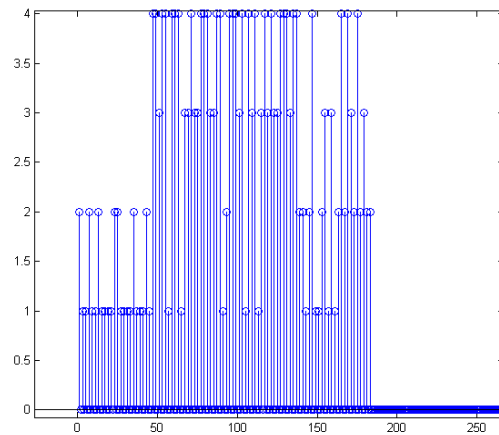


Figure 4.12. String that converted voltage values.

4.2.1.1. DAQ (Data Acquisition) Board. DAQ boards are used in the both sides, transmitter and receiver. General characteristics of the device are as follows. DAQ board is digital converter. After converting the digital datum to analog datum PC sends the modulated datum to LED drive [50]. In the project, we used the ADLINK USB-1902 Data Acquisition Board.

4.2.1.2. LED Current Driver. This device basically transfers the data as numerical value we created in MATLAB and sends to the LED driver. So, to modulate the data we should give the data as an input to LED Driver. The output of the LED Driver fed to the LED. Thus, data modulated is applied to the LED with the help of cables. The brand and model we use as a LED driver is Newport 560b Laser Diode Driver.

4.2.1.3. Power LED. LED driven data is detected from photo-diode LED on the receiver side by flashing at different levels. For example, if the LED flashes at 3 volts, photo-diode that detects the light with particular DC level (e.g. 3.5 volts). LUMINUS SST-50 LEDs are used in the system as a light source [51]. In previous generation VLC system, an ordinary LED utilized. By using power

LED, the distance between the received photo diode and LED could be increased.

4.2.2. Optical Channel

In ideal channel modeling, all the environmental effects could be ignored. In that case, the signal that goes through the channel assumed frequency flat. Moreover, AWGN has no affect on the signal. Due to low noise and Line of Sight (LOS) structure of the system , decision algorithm was simple. In addition to this we had small amount of DC effect that coming from laboratories additional light bulbs. With a simple algorithm, it can be eliminated easily. On the other hand, with the help of our colleagues from Özyeğin University (OZU), we had chance to test our design with their realistic channel model. On that channel model we had 5x5x3 m2 sized room and we have a transmitter on the ceiling and a receiver at the front left side. Room specifications, position of the receiver, transmitter and channel impulse response are given below 4.13.

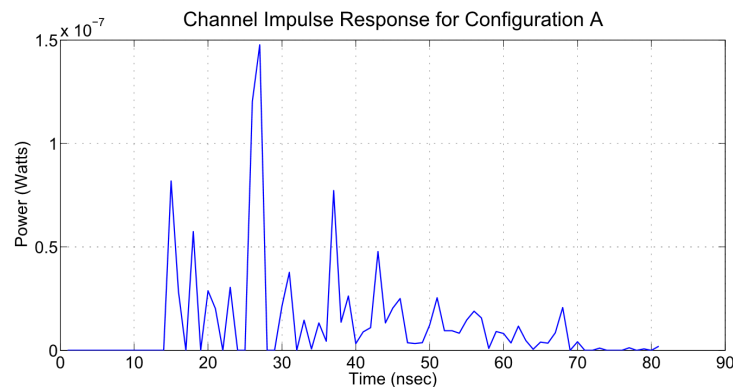


Figure 4.13. CIR obtained by optical illumination software environment

For such a distorted signal that conveyed through channel, equalization would be required to make decisions. Due to large amount of distortions, decision would be nearly impossible if an equalizer would not be used. The type of the equalizer we have used is Zero Forcing and this equalizer have been designed specifically for this simulation. The results of this application will be deeply explained in the following section.

4.2.3. Receiver

On the receiver side, photodiode detects the intensity differences and convert them to currents. Then analog to digital converter, converts the signal do digital values. Sends them to MATLAB and it process the data and recover original information with appropriate codes. Photograph of the receiver antenna (photo-diode) for 2nd generation PAM based VLC system is given in Fig. 4.15. Sequence of the receiver algorithm is following;

- Firstly, we eliminated first 2 and last 2 samples. These are plot samples for starting triggering condition.
- After we obtained raw eliminated "0" data, we extracted DC bias from this signal. Firstly, we found data which are greater than 4. Take mean of them and extracted from 4 to figure out DC level.
- Scaling is very important concept for detection. We determine max and min values of received data ($a = \min$, $b = \max$). Then as we decided our transmitted data includes information 1V, 2V, 3V and 4V. We sent our data from transmitted with pulse amplitude modulation. iv. On the detection process, after max and min value of received data, it is divided 4 parts. Later, we obtained threshold value is $(b-a)/3$. Decision algorithm is visualized in Fig. 4.14.

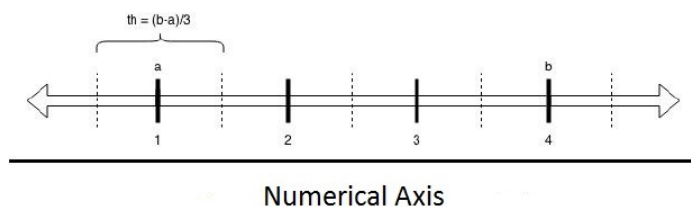


Figure 4.14. Decision algorithm at the receiver

4.2.4. Experimental Results

In this part, we have examined 3 scenarios;



Figure 4.15. Receiver part of the 2nd generation PAM based VLC system

4.2.4.1. SER Graph of 4 level system (Ideal Channel). Here we have SER graph of 4 level system that operates through ideal optic channel. The graph explains the symbol error rate (SER) in different SNR ratios and in different distances. While obtaining this graph, main steps and SER Graph are given below;

- After data is received, noise is generated and added to data.
- Then, data detection process is again implemented.
- Symbol error rate is calculated.
- Moreover, this process is done for different distances which are 50, 60, 70, 80 cm.

4.2.4.2. Comparison of SER Graph in 4 Level System with Realistic Channel and Ideal Channel.

In this case the system operates in two different channel, one is ideal the other one is realistic channel. The graph explains symbol error rate in different SNR ratios and through different optic channels. As clearly seen, there are less errors in ideal channel according to realistic channel.

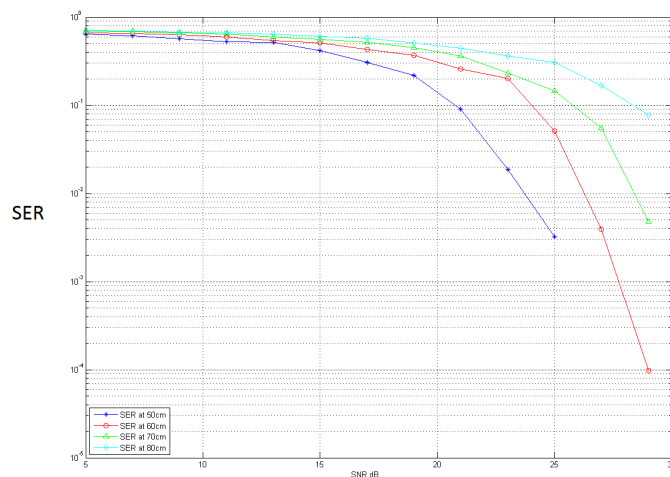


Figure 4.16. 4 Level SER vs. SNR in different distances

4.2.4.3. SER Graph of 8 level system (Ideal Channel). Here we have SER graph of 8 level system that operates through ideal optic channel. The graph explains the symbol error rate (SER) in different SNR ratios and in different distances. While obtaining this graph, main steps and SER Graph are given below;

- After data is received, noise is generated and added to data.
- Then, data detection process is again implemented.
- Symbol error rate is calculated.
- Moreover, this process is done for different distances which are 60, 70, 80 cm.

4.2.5. Conclusions

In this project, technical background information is gathered from lots of relevant papers this technology is examined in deeply. Optical communication system is constructed by using DAQ Cards, Power LED, Led Driver, Photodiode and PCs. After trial and error process, hardware section is completed, then the appropriate software part is written via MATLAB. We have tested our system design with three types of document: Text, audio, and image.

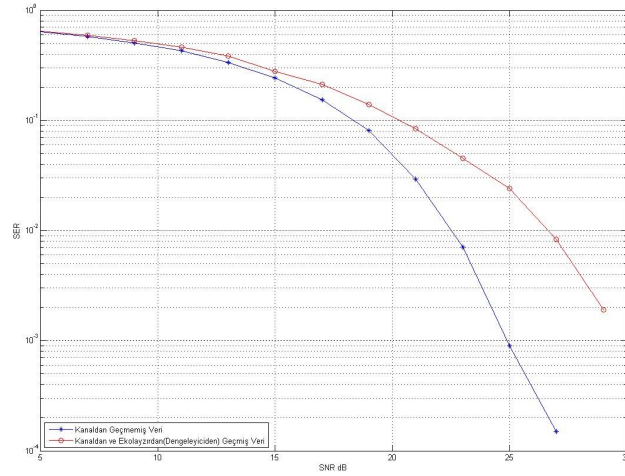


Figure 4.17. 4-Level SER vs. SNR, Ideal vs. Realistic Channel

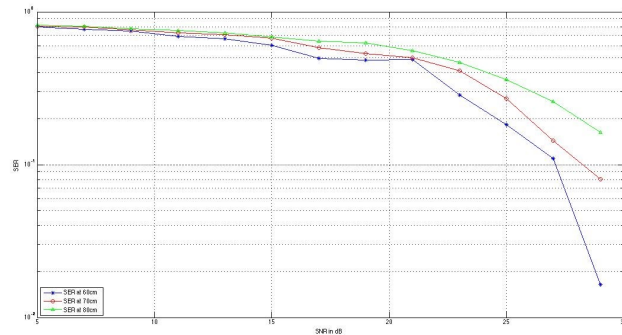


Figure 4.18. 8 Level SER vs. SNR in different distances

According to optical communication concept, it is succeed for sending 3 different documents which are text, audio and image respectively from one computer and all data was received properly from the second computer. Moreover, the first version of this system has been also constructed last year as bachelor project as we call VLC 1st generation. 1st generation was based on RS-232 serial communication. In the system, baseband communication is used as we did in our system, we called that 2nd generation. In the 1st generation, it has been used ON-OFF Keying modulation by using USB protocol between two computers. Conversely, in 2nd generation we have used PAM modulation along with ON-OFF Keying Modulation. The efficiency with ON-OFF Keying Modulation was not enough for transmission so we have used PAM. In addition to this, with “1”s

and “0”s we have added to each column and trigger condition we have used, we have created our own hybrid protocol to be able to synchronize transmitter and receiver part. Finally, it is built a primitive prototype of a simple visible light communication system. In applications such as traffic management, indoor areas, visible light communication is desirable for security and it provides high data rates. Although there are technical challenges to be solve, quick technical development can make this technology low cost, high data rate and efficient version [52].

4.3. 3rd Generation (3G) OFDM Based Optical Wireless Communication System

In the earlier Bachelor of Science (BS) projects done in the Electric and Electronic department of Kadir Has University, the other teams have used “On-Off Keying” and “Phase Amplitude Modulation” techniques. Text data and images have been sent with these techniques with the help of Matlab, current source, led, diode, oscillator and etc. The main objective of our project is to implement a new version of a visible light communication system (Called 3rd generation VLC), employing orthogonal frequency division multiplex (OFDM) with “Quadrature Amplitude Modulation (QAM)” technique to make the process faster, to increase data rate, to decrease the bandwidth waste and to solve inter symbol interference (ISI) problems. In addition to the technical improvements, we have reset the transmission environment which was on the horizontal position, to vertical position to apply the experimental structure for real life applications [53, 54].

Indoor VLC systems is one of the applications of optical communication systems. In this system the communication is provided in a short range with a high energy efficiency. In comparison with the other systems, indoor VLC system is not affected by the channel noise caused by the sun light, which is a very important advantage of indoor VLC. The working principles of indoor VLC systems is shown below in Fig. 4.19.

RF communication is the most popular one because it has good coverage. However we need more bandwidth due to the rapidly increasing traffic volume in wireless network and also we are

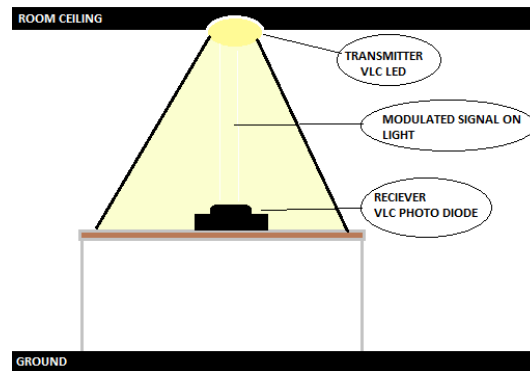


Figure 4.19. Basic Indoor VLC System Working Principle

running out of bandwidth in RF spectrum. Where the RF communication is limited or not enough, VLC provides both communication and illumination. Table 2.2 shown differences between VLC and RF communication. VLC systems use the IEEE 802.15.7 standard, with high data rates up to 96 Mbits/second.

4.3.1. Optical OFDM for VLC in IM/DD Systems

Orthogonal frequency division multiplexing (OFDM) is used extensively in wired and wireless broadband communication systems to bring a solution to intersymbol interference (ISI) caused by dispersive channel. OFDM signals are designed for intensity modulation/direct detection (IM/DD) systems which must be real and non-negative. There are several different forms of OFDM for IM/DD systems such as: asymmetrically clipped optical OFDM (ACO OFDM), DC biased optical OFDM (DCO-OFDM), and other forms based on ACO-OFDM and DCO-OFDM [6]. Block diagram of the designed ACO-OFDM system is given in Fig. 4.20.

4.3.2. Implementation of the Optical OFDM System

The VLC systems implemented in previous projects carried on at the Kadir Has University were designed in such a way that data communication was established by using the same physical structure. However, they were set up in a horizontal position where the LED and the photodiode

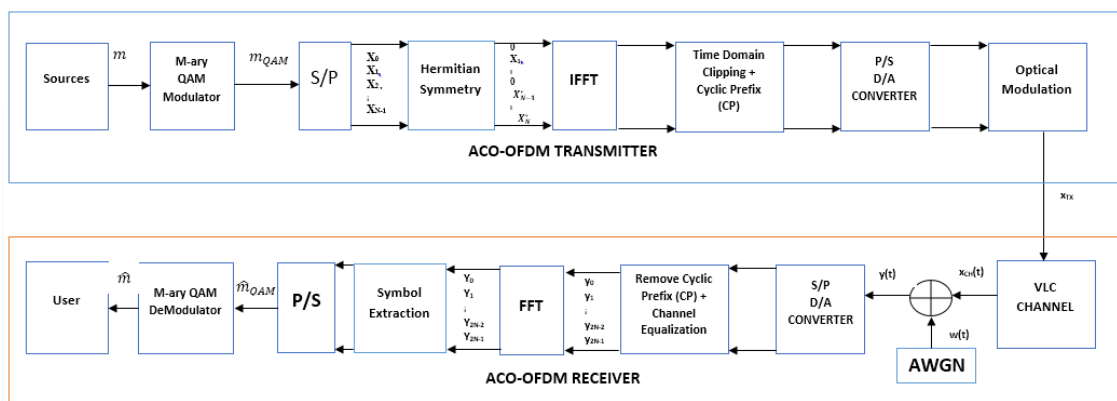


Figure 4.20. Block diagram of receiver-transmitter parts of an ACO-OFDM system

used for the transmission of data were located much closed to each other. Also the illumination which is one of the main purposes of the system were not properly demonstrated due to the horizontal working area. So that the previous projects does not seem to be suitable for real life application. In addition, the position of the system was causing some differences in the channel estimation and in signal to noise ratio (SNR). The general views of the previous projects are shown below in the Figure 4.21.

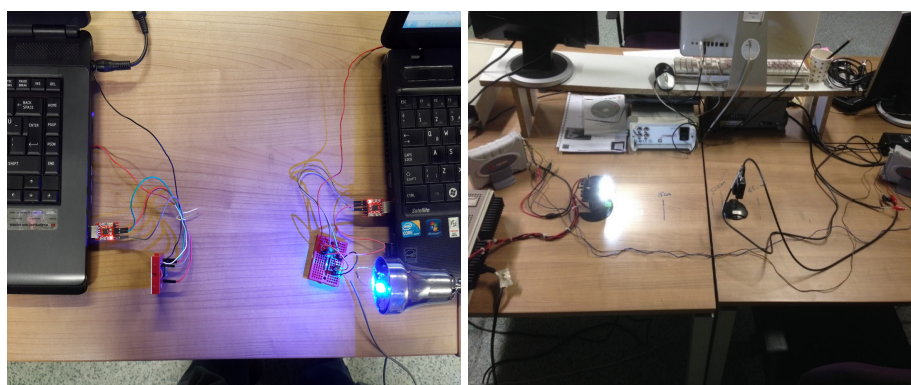


Figure 4.21. 1G (left) and 2G (right) VLC Systems

In the 3rd generation system's setup we have made some modifications in order to provide better communication performance and high data speeds. The setup process is explained step by step in the following sections.

4.3.3. Transmitter

The project setup is basically consist of 3 parts: signal generation, transmission of data, and receiver. The project area, including the setup can be seen in the Fig. 4.22.

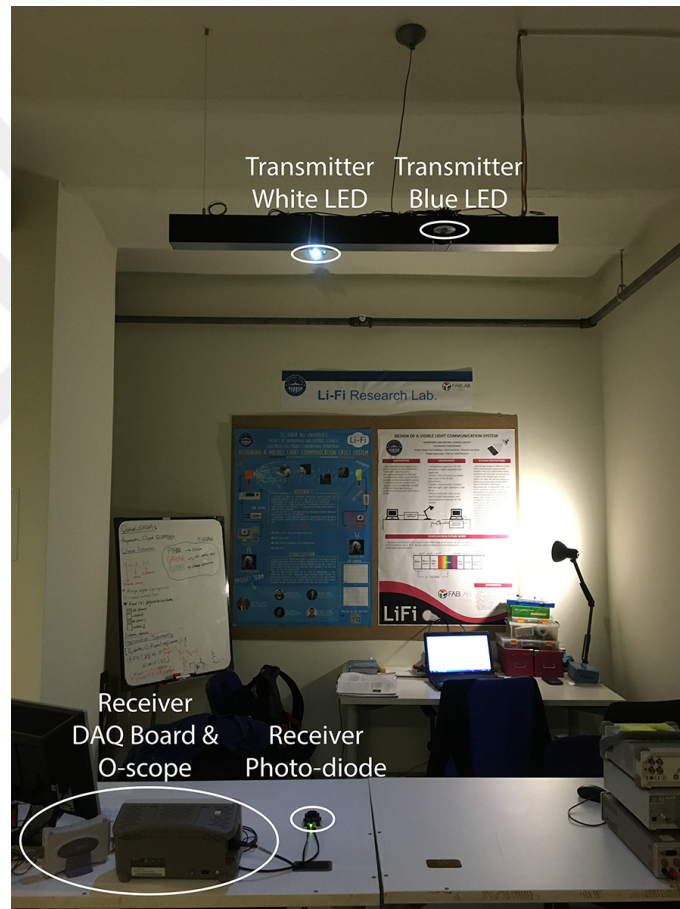


Figure 4.22. The general view of third generation VLC system

4.3.3.1. Choosing the LED Positions. To determine the LED positions, we have taken into account the height and power level which would be suitable to maintain a daily life. In this project there are two Power LEDs used, which provides white and blue light. LEDs are located on the ceiling in place of a normal light source, and the essential connections were made with the power source. The final forms of the LEDs are shown in the Fig. 4.23.

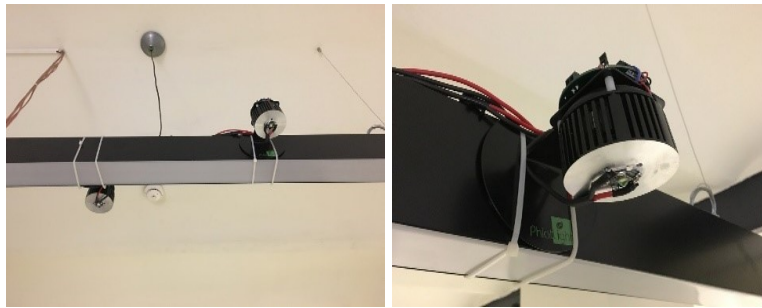


Figure 4.23. LED light sources

4.3.3.2. Amplifier and Use of Current Source as Bias. Since the LEDs used in this project are Power LEDs, they require more power than the normal LEDs. The signals transmitted from the system cannot provide enough power. In order to solve this problem, 560B LASER DIODE DRIVER current source model was used as an amplifier. Moreover, in the cases where a fixed direct current value is required to provide communication via light with that fixed direct current value, this current source allows us to determine a Bias value as digital or analog conversion. The current source is shown in Fig. 4.24.



Figure 4.24. 560B Laser Diode Driver as a current source

4.3.3.3. ADLINK DAQ Board. It is not possible to transmit digital data directly to the light source or receive an analog information directly from the digital system. Hence a converting device is required. In this project ADLINK USB-1902 which has the property of converting analog to digital and digital to analog, is used. The speed of transmitting symbols via ADLINK is limited

to 250K symbols per second. The connections and the ADLINK converting device is shown in Fig. 4.25.



Figure 4.25. ADLINK USB-1902 device and input/output connections

3rd generation VLC system, has similar blocks that RF OFDM has. The main block diagram of the setup is shown in the Fig. 4.26.

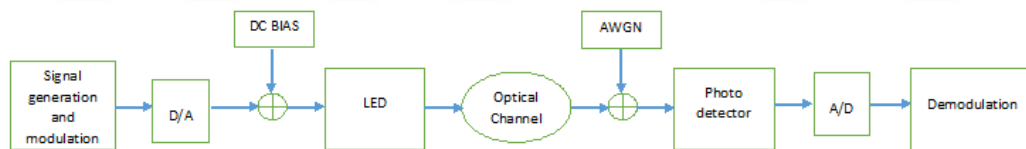


Figure 4.26. Demonstration of how the system works

- In the system, firstly the signals are generated by using MATLAB environment.
- A/D and D/A hardware are serving as bridges between MATLAB and real life domains.
- For having reliable output current is used as a medium to loading information on the LEDs rather than voltage. So that, “Newport 560B Laser Diode Driver” current source is utilized.
- The LED light sources, where the wavelengths of the sources change according to their colors, adds the signals generated up on the light with bias.

4.3.4. Visible Light Communications Channel

Channel Estimation is one of the most important part of the Optical Wireless Communications (OWC). Data is transmitted between the LED (transmitter) and the photo-diode (receiver) on

light intensity in IM/DD systems, in the presence of an optical channel as shown in Figure 4.27.



Figure 4.27. ACO OFDM Block Diagram for channel estimation

There are several ways of channel estimation, and in this project Least Square (LS) method was used. In order to detect the transmitted data we should know the channel parameters. Since the data might be distorted due to some effects on the channel such as: reflection and refraction, caused from the objects in the transmission area, fading of the signal, (Additive White Gaussian Noise) AWGN and etc[27, 25]. The Estimation of channel will allow us to apply demodulation and decoding to receive data properly. The LED is being used during this project is a white LED which is considered as a wide-band source, where the Infrared Sources (IR) are monochromatic. Thanks to the frequency selective behavior of VLC channel, we can obtain higher data rates [9, 24]. The FIR filter effect described by “channel taps” of the channel gives us the ability of frequency selectivity. Channel taps enable us to have a control over the distortion removing of the received signal. Channel estimation in VLC will be detailed in following chapters.

4.3.5. Receiver

- The lights beams coming from the light source, reaches the receiving part by passing through an optical channel. The channel has reflection and refraction effects plus Additive White Gaussian Noise (AWGN). Power of the AWGN depends on thermal effects, extrinsic light sources and front end amplifications.
- Received signal is the form of $y = \mathbf{H}x + \mathbf{n}$ where y , \mathbf{H} , x and \mathbf{n} represents received signal at the receiver, channel impulse response matrix, transmitted signals at the transmitter and

AWGN respectively.

- In order to process received signal, signals are detected by the photo detector and A/D converter converts time domain signals from analog to digital domain. The both A/D and D/A processes are provided by ADLINK USB – 1902 hardware.
- Digital signals are further processed to obtain information conveying stream back. Procedure is detailed in the following sections.

4.3.6. ACO-OFDM Modulation and Demodulation Processes

We now examine the physical stages of the designed system. In this project, ACO-OFDM is used for transmission link. User bits are projected onto M-QAM symbol space by taking Hermitian symmetry and odd subcarrier utilization into consideration. IFFT results real and anti symmetric discrete time-domain samples by courtesy of state-of-the-art DFT property. Obtained time domain anti-symmetric symbol could be clipped without a information loss. All the process could be reverted and transmitted symbols could be obtained back at the receiver. Basic block diagram of the system is given in Fig. 4.28.

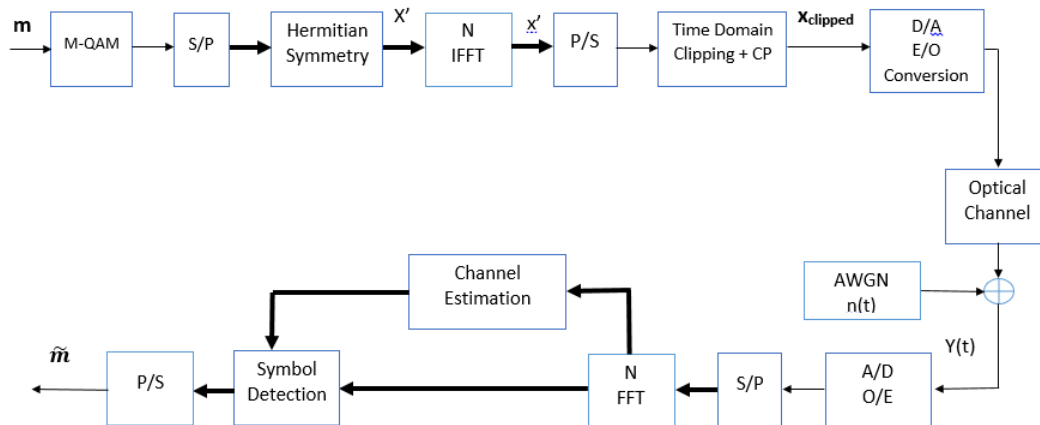


Figure 4.28. Block diagram of ACO-OFDM system

Time domain clipping process is investigated in Fig. 4.29.

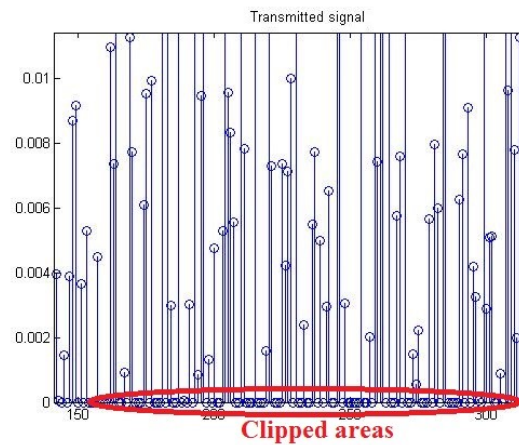


Figure 4.29. Block diagram of ACO-OFDM system

Destructive effect of the channel compensated in the frequency domain with simple one-tap equalizer. However, before that procedure channel needs to be estimated in the frequency domain by inserting known pilots to the data stream. That pilots are extracted and used for channel estimation procedure. Both channel estimation and equalization are executed in the frequency domain.

4.3.7. VLC System Based on LTE Standard

Our system is designed according to current Long Term Evaluation (LTE) Standard. System parameters are chosen as,

$$\begin{aligned}
 N &= \text{Useful Symbols} \\
 F_{\text{sampling}} &= \text{Sampling rate of A/D Link Devices} \\
 \Delta f &= \text{Sub-carrier spacing} \\
 \text{Sampling Rate : } f_{\text{sampling}} &= N * \Delta f \approx \text{Bandwidth} \\
 \max(f_{\text{sampling}}) &= 250000 \\
 \min(N) &= 256 \\
 \max(\delta f) &= 976 \text{ Hz}
 \end{aligned} \tag{4.2}$$

First and last 4 symbols of the OFDM frame are used as both synchronization and cyclic prefix. Remained 1016 symbols are used for data transmission.

4.3.8. Experimental Results

In the project test stage is implemented by the Monte Carlo method. The number of Monte Carlo runs in our simulations is chosen as 10. So that we averaged our results for 10 trials. Transmitted and received data are depicted in Fig. 4.30.

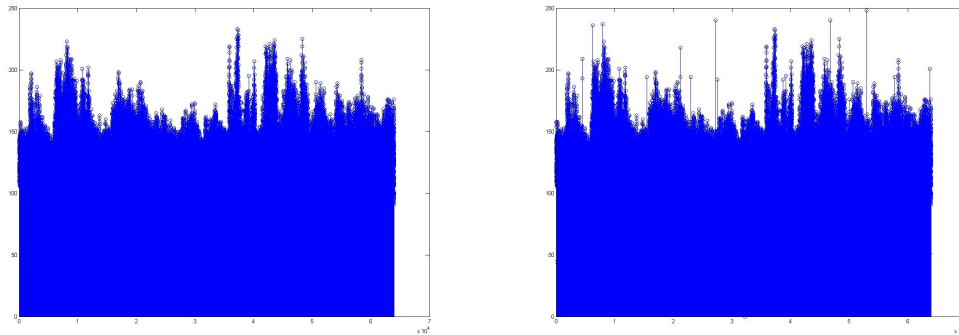


Figure 4.30. Message signal and received message signal

We have observed symbol errors which is proving that system is working well. It is observed from the results that, channel impulse response has dominant effect on the SER. Experimental

results for various parameters are given in the Tables below.

Table 4.5. Results for, DC Bias: 280mA, sample rate: 150K, N: 2048

Test #	SubCarrier	Pause(sec)	Modulation	# of Sysmbol Loses	% of Sysmbol Loses	Time
TEST 1	2048	0,033	QPSK	1100	1,719	47
TEST 2	2048	0,032	QPSK	1147	1,792	47
TEST 3	2048	0,03	QPSK	1168	1,825	47
TEST 4	2048	0,034	QPSK	1119	1,748	47
TEST 5	2048	0,029	QPSK	1152	1,8	39
TEST 6	2048	0,028	QPSK	1190	1,859	39
TEST 7	2048	0,035	QPSK	961	1,502	47
TEST 8	2048	0,036	QPSK	1241	1,939	47
TEST 9	2048	0,037	QPSK	1020	1,594	47
TEST 10	2048	0,039	QPSK	997	1,558	47
TEST 11	2048	0,035	QPSK	934	1,459	47

Table 4.6. Results for, DC Bias: 280mA, sample rate: 100K, N: 2048

Test #	SubCarrier	Pause(sec)	Modulation	# of Sysmbol Loses	% of Sysmbol Loses	Time
TEST 12	2048	0,021	QPSK	2816	4,4	39
TEST 13	2048	0,018	QPSK	2703	4,223	39
TEST 14	2048	0,019	QPSK	2389	3,733	39
TEST 15	2048	0,02	QPSK	3468	5,419	39
TEST 16	2048	0,028	QPSK	3456	5,4	39
TEST 17	2048	0,029	QPSK	3154	4,928	39
TEST 18	2048	0,03	QPSK	3059	4,78	39
TEST 19	2048	0,031	QPSK	3279	5,123	39
TEST 20	2048	0,032	QPSK	2926	4,572	39

Tests are conducted for two DC bias levels as, 280mA and 500mA. It has observed that, 500mA DC bias gives better symbol error rate (SER). More power at the receiver decreases SER for given SNR level.

In Table 4.10 64 QAM is investigated. For 64 QAM symbol error rate increases dramatically.

In Table 4.12 experiments are conducted for N=1024. This configuration gave the most reliable communication link in terms of symbol error.

For the sake of capturing system limits, test are also conducted without front-end devices

Table 4.7. Results for, DC Bias: 280mA, sample rate: 100K, N: 4096

Test #	SubCarrier	Pause(sec)	Modulation	# of Sysmbol Loses	% of Sysmbol Loses	Time
TEST 21	4096	0,028	QPSK	3315	5,18	27,95
TEST 22	4096	0,032	QPSK	3083	4,817	30
TEST 23	4096	0,034	QPSK	2762	4,316	31,95
TEST 24	4096	0,035	QPSK	3148	4,919	31,9534
TEST 25	4096	0,037	QPSK	2367	3,698	31,959878
TEST 26	4096	0,037	QPSK	2578	4,028	31,8
TEST 27	4096	0,038	QPSK	2801	4,377	31,95
TEST 28	4096	0,039	QPSK	2948	4,606	31,952381
TEST 29	4096	0,04	QPSK	3103	4,848	31,959
TEST 30	4096	0,03	QPSK	2632	4,113	30,29
TEST 31	4096	0,029	QPSK	2808	4,388	29,8
TEST 32	4096	0,028	QPSK	3071	4,798	28

Table 4.8. Results for, DC Bias: 500mA, sample rate: 150K, N: 2048, M: 4

Test #	SubCarrier	Pause(sec)	Modulation	# of Symbol Loses	% of Symbol Loses	Time
TEST 1	2048	0,039	QPSK	868	1,357	47
TEST 2	2048	0,036	QPSK	748	1,17	45
TEST 3	2048	0,035	QPSK	823	1,286	48
TEST 4	2048	0,034	QPSK	775	1,28	42
TEST 5	2048	0,032	QPSK	765	1,196	40
TEST 6	2048	0,031	QPSK	747	1,167	39
TEST 7	2048	0,03	QPSK	749	1,17	38

Table 4.9. Results for, DC Bias: 500mA, sample rate: 150K, N: 2048, M: 16

Test #	SubCarrier	Pause(sec)	Modulation	# of Symbol Loses	% of Symbol Loses	Time
TEST 8	2048	0,03	16QAM	6763	10,56	19,97
TEST 9	2048	0,036	16QAM	7069	11,045	19,97
TEST 10	2048	0,028	16QAM	6607	10,3	19,97
TEST 11	2048	0,024	16QAM	7062	11,03	19,97
TEST 12	2048	0,024	16QAM	5903	9,223	19,97
TEST 13	2048	0,026	16QAM	6340	9,906	19,97

Table 4.10. Results for, DC Bias: 500mA, sample rate: 150K, N: 2048, M: 64

Test #	SubCarrier	Pause(sec)	Modulation	# of Symbol Loses	% of Symbol Loses	Time
TEST 14	2048	0,026	64QAM	16182	25	9
TEST 15	2048	0,03	64QAM	13086	20	8
TEST 16	2048	0,03	64QAM	14627	22	8,5

(LEDs and photo-diodes). Results are given in Table 4.13.

Table 4.11. Results for, DC Bias: 500mA, sample rate: 150K, N: 4096, M: 4

Test #	SubCarrier	Pause(sec)	Modulation	# of Symbol Loses	% of Symbol Loses	Time
TEST 18	4096	0,03	QPSK	1320	2,062	19,99
TEST 19	4096	0,032	QPSK	1391	2,174	23
TEST 20	4096	0,029	QPSK	1196	1,86	20
TEST 21	4096	0,027	QPSK	1431	2,35	18
TEST 22	4096	0,024	QPSK	1513	2,36	17

Table 4.12. Results for, DC Bias: 500mA, sample rate: 150K, N: 1024, M: 4

Test #	SubCarrier	Pause(sec)	Modulation	# of Symbol Loses	% of Symbol Loses	Time
TEST26	1024	0,03	QPSK	418	0,653125	80
TEST27	1024	0,03	QPSK	305	0,4765625	81
TEST28	1024	0,03	QPSK	235	0,3671875	81
TEST29	1024	0,03	QPSK	256	0,4	80
TEST30	1024	0,03	QPSK	333	0,5203125	80
TEST31	1024	0,03	QPSK	266	0,415625	80
TEST32	1024	0,2	QPSK	301	0,4703125	80

Table 4.13. QPSK wire modulation with various subcarriers

Test #	SubCarrier	Pause(sec)	Modulation	# of Symbol Loses	% of Symbol Loses	Time
TEST 1	2048	0,02	QPSK	741	1,15	0,22
TEST 2	2048	0,018	QPSK	563	0,879	0,22
TEST 3	4096	0,026	QPSK	893	1,39	0,22
TEST 4	1024	0,3	QPSK	96	0,15	0,22
TEST 5	1024	0,32	QPSK	49	0,076	0,22

We have completed all the tests given above successfully. It is proven that the system works fine with ACO-OFDM technique. The tests shows that the best quality is obtained with 1024 subcarriers but the transmission duration was too long. The duration can be made as short as possible by increasing the number of subcarrier, but in such case the quality decreases.

4.3.9. Conclusions & Future Works

In this project OFDM is investigated in very wide sense. OFDM transmission algorithm and suitable hardware changes are done during preparation phase. Audio and text data are successfully transmitted in realistic real life scenario by employing ACO-OFDM with frequency domain

channel estimation & symbol detection. It has been observed that, channel consisting of free-space optics and front-end non-linearity is most dominant error source in the entire system. Especially, non-linear front-end characteristics needs special care in the future works. Unlike 1st and 2nd generation systems multi-carrier system is employed to increase spectral efficiency. It is shown that, as a proof-of-the-concept ACO-OFDM could be realized in real life scenario in the laboratory with 150 Kbits/sec data rate with high reliability [55].

Developments in solid state lighting technologies have given great opportunity to VLC systems. Gigabits of data rates are achieved in the laboratory environments. Novel OFDM techniques are developed to carry information on the light intensity while combating ISI in the channel. This new technology could be used in wide variety of the cases such as in aircraft cabins, smartphones, shopping malls, chemical plants, hospitals etc. It is already known that, biggest part of the data traffic is occurring in indoor environment. As a result, VLC has great chance to survive in the future technology market.

5. Conclusions

VLC is up and coming technology for 5G+ and further generations. It is predicted that we could see full-duplex connected LiFi network in the near future. Necessity to complementary technology to existing RF structure would be more crucial in next 10 years of period. In this thesis, it has shown that VLC is feasible, reliable and cheap technology and biggest candidate for new generation wireless communications. Besides, practical applications proofs the concept of VLC-OFDM applications in real life. All these promising results pushes all the researchers to make VLC real in next generations.

APPENDIX A:

• Hermitian Symmetry Property

OWC systems are using LEDs or lasers to transmit information. As long as information is carried on the light intensity we have two main restrictions. Transmitted signal must be both real and positive valued (unipolar). We want to obtain completely real signal after IDFT operation in OFDM. We can simply deduce that, discrete time domain signal $x[n]$ must be real. Accordingly, DFT/IDFT pair is defined as,

$$\begin{aligned} DFT : \quad X[k] &= \sum_{n=0}^{N-1} x[n] e^{-j2\pi kn/N} \text{ where } k = 0, 1 \dots, N-1 \\ IDFT : \quad x[n] &= \frac{1}{N} \sum_{k=0}^{N-1} X[k] e^{j2\pi kn/N} \text{ where } n = 0, 1 \dots, N-1 \end{aligned} \quad (\text{A.1})$$

We can easily see that,

$$X[N-k] = \sum_{n=0}^{N-1} x[n] e^{-j2\pi(N-k)n/N} = \sum_{n=0}^{N-1} x[n] \underbrace{e^{-j2\pi Nn/N}}_{e^{-j2\pi n}=1} \underbrace{e^{-j2\pi(-k)n/N}}_{e^{j2\pi kn/N}} \quad (\text{A.2})$$

where $k = 0, 1 \dots, N-1$

$$X[N-k] = \sum_{n=0}^{N-1} x[n] e^{j2\pi kn/N}$$

Since $x[n]$ is real. Then, $x^*[n] = x[n]$ where $*$ denotes complex conjugation operation. So that,

$$\begin{aligned} (X[k])^* &= (\sum_{n=0}^{N-1} x[n] e^{-j2\pi kn/N})^* = \\ \sum_{n=0}^{N-1} (x[n])^* (e^{-j2\pi kn/N})^* &= \sum_{n=0}^{N-1} x^*[n] e^{j2\pi kn/N} = \sum_{n=0}^{N-1} x[n] e^{j2\pi kn/N} \end{aligned} \quad (\text{A.3})$$

where $k = 0, 1 \dots, N-1$

As a result,

$$X[k] = X^*[N-k] \quad (\text{A.4})$$

- **Folded Gaussian Distribution**

Normal distribution is defined as,

$$f(x) = \frac{1}{\sqrt{2\pi\sigma^2}} e^{-\frac{(x-\mu)^2}{2\sigma^2}} \quad (\text{A.5})$$

where $\text{var}(x) = E\{(x - \mu)^2\} = \int (x - \mu)^2 f(x) dx$ and
 $\text{mean}(x) = E\{x\} = \int x f(x) dx$.

One part of the Normal distribution folded on the other,

$$f_{FN}(x; \mu, \sigma) = \underbrace{\frac{1}{\sqrt{2\pi\sigma^2}} e^{-\frac{(x-\mu)^2}{2\sigma^2}}}_{\text{Shifted to } x=\mu} + \underbrace{\frac{1}{\sqrt{2\pi\sigma^2}} e^{-\frac{(x+\mu)^2}{2\sigma^2}}}_{\text{Shifted to } x=-\mu} \quad (\text{A.6})$$

We are looking for special case of Folded-Normal distribution ($\mu = 0$) is Half-Normal distribution. If X follows an ordinary normal distribution, $Y = |X|$ follows half normal distribution. So, if Z follows a Normal distribution than Clipped-Normal distribution will be $Z = \lfloor X \rfloor = \frac{Y}{2}$

$$f_Z(x; \sigma) = \frac{1}{\sqrt{2\pi\sigma^2}} e^{-\frac{(x-\mu)^2}{2\sigma^2}} \quad (\text{for } x > 0) \quad (\text{A.7})$$

where $E\{Z\} = \mu_Z = \frac{\sigma\sqrt{2}}{\sqrt{\pi}}$ and $\text{var}(Z)$

- **Parseval's Theorem for DFT**

$$\sum_{n=0}^{N-1} |x[n]|^2 = \frac{1}{N} \sum_{k=0}^{N-1} |X[k]|^2$$

$$NP_{x_n} = P_{X[k]}$$

N(time-domain power) = (frequency-domain power)

- **Jacobian Transformation**

For a given integral of the form,

$$\int \int_R = f(x, y) dx dy \quad (\text{A.8})$$

For a continuous 1-to-1 transformation from (x,y) to (u,v) as $x = x(u, v)$ and $y = y(u, v)$.

Where region R (in the xy plane) mapped onto region R' (in the uv plane) by,

$$\int \int_R = f(x, y) dx dy = \int \int_{R'} = f(x(u, v), y(u, v)) J(u, v) du dv \quad (\text{A.9})$$

where $J(u, v)$ named as Jacobian determinant and defined as,

$$J(u, v) = \begin{vmatrix} \frac{\partial x}{\partial u} & \frac{\partial x}{\partial v} \\ \frac{\partial y}{\partial u} & \frac{\partial y}{\partial v} \end{vmatrix}$$

Fundamental integrals required in power calculations

- **Definite Gaussian Integral,**

$$\begin{aligned} I &= \int_{-\infty}^{\infty} e^{-\alpha x^2} dx \\ I^2 &= \left(\int_{-\infty}^{\infty} e^{-\alpha x^2} dx \right) \left(\int_{-\infty}^{\infty} e^{-\alpha y^2} dy \right) = \left(\int_{-\infty}^{\infty} e^{-\alpha x^2} dx \right) \left(\int_{-\infty}^{\infty} e^{-\alpha y^2} dy \right) \\ I^2 &= \int_{-\infty}^{\infty} \int_{-\infty}^{\infty} e^{-\alpha(x^2+y^2)} dx dy \quad [x = r \cos \theta, y = r \sin \theta] \end{aligned} \quad (\text{A.10})$$

If we apply Jacobian Transformation to map (x,y) plane to (u,v) plane,

$$J(u, v) = \begin{vmatrix} \frac{\partial x}{\partial r} & \frac{\partial x}{\partial \theta} \\ \frac{\partial y}{\partial r} & \frac{\partial y}{\partial \theta} \end{vmatrix} = \begin{vmatrix} \cos \theta & -r \sin \theta \\ \sin \theta & r \cos \theta \end{vmatrix} = r \cos^2 \theta - (-r \sin^2 \theta) = r(\cos^2 \theta + \sin^2 \theta) = r$$

$$I^2 = \int_{-\infty}^{\infty} \int_{-\infty}^{\infty} e^{-\alpha(x^2+y^2)} dx dy = \int_0^{\infty} \int_0^{2\pi} e^{-\alpha r^2} r dr d\theta = \int_0^{2\pi} \left[\frac{e^{-\alpha r^2}}{-2\alpha} \right]_{r=0}^{\infty} d\theta = \left[\left[\frac{\theta e^{-\alpha r^2}}{-2\alpha} \right]_{r=0}^{\infty} \right]_{\theta=0}^{2\pi}$$

$$I^2 = \frac{\pi}{\alpha} \Rightarrow I = \sqrt{\frac{\pi}{\alpha}}.$$
(A.11)

- $\int x e^{-\alpha x^2} dx,$

We already know that, $e^{u(x)} = \int u'(x) e^{u(x)} dx.$

$$\int x e^{-\alpha x^2} dx = -\frac{1}{2\alpha} e^{-\alpha x^2} + c$$
(A.12)

- Definite integral $\int_{-\infty}^{\infty} x^2 e^{-\alpha x^2} dx,$

Which could be obtained from, $-\frac{d}{d\alpha} J.$ Where, $J = \int_{-\infty}^{\infty} e^{-\alpha x^2}$ equals to simple Gaussian integral.

So that, $-\frac{d}{d\alpha} (\sqrt{\frac{\pi}{\alpha}}) |_{\alpha} = \frac{\sqrt{\pi}}{2\sqrt{\alpha^3}}.$

- Second solution to definite integral $\int_{-\infty}^{\infty} x^2 e^{-\alpha x^2} dx,$

$$\int_{-\infty}^{\infty} (-x)(-x) e^{-\alpha x^2} dx = \frac{1}{2\alpha} \int_{-\infty}^{\infty} (-x) \underbrace{(-2\alpha x) e^{-\alpha x^2}}_{u'(x)e^{u(x)}} dx. \text{ From integration by parts,}$$

$$[u = -x, dv = (-2\alpha x) e^{-\alpha x^2} dx \Rightarrow du = -dx, v = e^{-\alpha x^2}]$$

$$-\frac{1}{2\alpha} [x e^{-\alpha x^2}]_{x=-\infty}^{\infty} - \frac{1}{2\alpha} \int_{-\infty}^{\infty} e^{-\alpha x^2} (-dx) = -\frac{1}{2\alpha} [x e^{-\alpha x^2}]_{x=-\infty}^{\infty} + \frac{1}{2\alpha} \int_{-\infty}^{\infty} e^{-\alpha x^2} dx$$

$$= -\frac{1}{2\alpha} [x e^{-\alpha x^2}]_{x=-\infty}^{\infty} + \frac{1}{2\alpha} \sqrt{\frac{\pi}{\alpha}}. \text{ First term, } \frac{1}{2\alpha} [x e^{-\alpha x^2}]_{x=-\infty}^{\infty}$$

$$= \frac{1}{2\alpha} \left(\underbrace{\lim_{x \rightarrow +\infty} \frac{x}{e^{\alpha x^2}}}_{\lim_{x \rightarrow +\infty} \frac{1}{2\alpha x e^{\alpha x^2}} = 0} + \underbrace{\lim_{x \rightarrow -\infty} -\frac{x}{e^{\alpha x^2}}}_{\lim_{x \rightarrow -\infty} \frac{1}{-2\alpha x e^{\alpha x^2}} = 0} \right) = \frac{1}{2\alpha} (0 + 0) = 0$$

$$\int_{-\infty}^{\infty} x^2 e^{-\alpha x^2} dx = \frac{\sqrt{\pi}}{2\sqrt{\alpha^3}}$$
(A.13)

- $\int x^3 e^{-\alpha x^2} dx$

Integration by parts, $[u = x^2, dv = x e^{-\alpha x^2} dx \Rightarrow du = 2x dx, v = -\frac{1}{2\alpha} e^{-\alpha x^2}]$

$$\int x^3 e^{-\alpha x^2} dx = -\frac{1}{2\alpha} x^2 e^{-\alpha x^2} + \frac{1}{\alpha} \int x e^{-\alpha x^2} dx = -\frac{1}{2\alpha} x^2 e^{-\alpha x^2} - \frac{1}{2\alpha^2} x^2 e^{-\alpha x^2}$$

$$\int x^3 e^{-\alpha x^2} dx = -\frac{1}{2\alpha} e^{-\alpha x^2} (x^2 + 1/\alpha) + c \quad (\text{A.14})$$



REFERENCES

1. A. Bell, "Photo phone-transmitter," Dec. 14 1880, uS Patent 235,496. [Online]. Available: <http://www.google.com/patents/US235496>
2. R. Peach, C. Visone, G. Burdge, H. Corporation, J. Vickers, T. Leclerc, P. Sauer, L. Andrews, R. Phillips, J. E. Valencia, and J. Kiriazes, "Performance of a 10 gbps fso system implementing novel beam tracking and a dynamic buffering modem," in *2012 IEEE Photonics Society Summer Topical Meeting Series*, July 2012, pp. 111–112.
3. F. R. Gfeller and U. Bapst, "Wireless in-house data communication via diffuse infrared radiation," *Proceedings of the IEEE*, vol. 67, no. 11, pp. 1474–1486, Nov 1979.
4. Z. Pi and F. Khan, "An introduction to millimeter-wave mobile broadband systems," *IEEE Communications Magazine*, vol. 49, no. 6, pp. 101–107, June 2011.
5. A. B. Flores, R. E. Guerra, E. W. Knightly, P. Ecclesine, and S. Pandey, "Ieee 802.11af: a standard for tv white space spectrum sharing," *IEEE Communications Magazine*, vol. 51, no. 10, pp. 92–100, October 2013.
6. J. Armstrong, "Ofdm for optical communications," *Journal of Lightwave Technology*, vol. 27, no. 3, pp. 189–204, Feb 2009.
7. S. Dissanayake and J. Armstrong, "Comparison of ACO-OFDM, DCO-OFDM and ADO-OFDM in IM/DD systems," *Lightwave Technology, Journal of*, vol. 31, no. 7, pp. 1063–1072, April 2013.
8. B. Ranjha and M. Kavehrad, "Hybrid asymmetrically clipped OFDM-based IM/DD optical wireless system," *Optical Communications and Networking, IEEE/OSA Journal of*, vol. 6,

- no. 4, pp. 387–396, Apr. 2014.
9. K. Lee, H. Park, and J. R. Barry, “Indoor channel characteristics for visible light communications,” *IEEE Communications Letters*, vol. 15, no. 2, pp. 217–219, February 2011.
 10. F. Miramirkhani and M. Uysal, “Channel modeling and characterization for visible light communications,” *IEEE Photonics Journal*, vol. 7, no. 6, pp. 1–16, Dec 2015.
 11. “Aster spectral library—version 2.0. [online].” <http://speclib.jpl.nasa.gov>, accessed: 20-05-2016.
 12. “Zemax 13 release 2, radiant zemax llc. [online].” <http://www.zemax.com/>, accessed: 20-05-2016.
 13. “Cree leds. [online].” <http://www.zemax.com/>, accessed: 20-05-2016.
 14. “Osram leds. [online].” <http://www.zemax.com/>, accessed: 20-05-2016.
 15. C. Chen, D. A. Basnayaka, and H. Haas, “Downlink performance of optical attocell networks,” *Journal of Lightwave Technology*, vol. 34, no. 1, pp. 137–156, Jan 2016.
 16. J. B. Carruthers and J. M. Kahn, “Multiple-subcarrier modulation for non-directed wireless infrared communication,” in *Global Telecommunications Conference, 1994. GLOBECOM '94. Communications: The Global Bridge., IEEE*, vol. 2, Nov 1994, pp. 1055–1059 vol.2.
 17. Y. Tanaka, T. Komine, S. Haruyama, and M. Nakagawa, “Indoor visible communication utilizing plural white leds as lighting,” in *Personal, Indoor and Mobile Radio Communications, 2001 12th IEEE International Symposium on*, vol. 2, Sep 2001, pp. F-81–F-85 vol.2.
 18. J. Armstrong and A. J. Lowery, “Power efficient optical ofdm,” *Electronics Letters*, vol. 42,

- no. 6, pp. 370–372, March 2006.
19. N. Fernando, Y. Hong, and E. Viterbo, “Flip-ofdm for optical wireless communications,” in *Information Theory Workshop (ITW), 2011 IEEE*, Oct 2011, pp. 5–9.
 20. D. Tsonev, S. Sinanovic, and H. Haas, “Novel unipolar orthogonal frequency division multiplexing (u-ofdm) for optical wireless,” in *Vehicular Technology Conference (VTC Spring), 2012 IEEE 75th*, May 2012, pp. 1–5.
 21. M. S. Islam, D. Tsonev, and H. Haas, “A generalized solution to the spectral efficiency loss in unipolar optical ofdm-based systems,” in *2015 IEEE International Conference on Communications (ICC)*, June 2015, pp. 5126–5131.
 22. ———, “On the superposition modulation for ofdm-based optical wireless communication,” in *2015 IEEE Global Conference on Signal and Information Processing (GlobalSIP)*, Dec 2015, pp. 1022–1026.
 23. F. Miramirkhani, M. Uysal, and E. Panayirci, “Novel channel models for visible light communications,” in *Proc. SPIE*, vol. 9387, 2015, pp. 93 870Q–93 870Q–13. [Online]. Available: <http://dx.doi.org/10.1117/12.2077565>
 24. E. Sarbazi, M. Uysal, M. Abdallah, and K. Qaraqe, “Indoor channel modelling and characterization for visible light communications,” in *2014 16th International Conference on Transparent Optical Networks (ICTON)*, July 2014, pp. 1–4.
 25. S. K. Wilson and J. Armstrong, “Transmitter and receiver methods for improving asymmetrically-clipped optical ofdm,” *IEEE Transactions on Wireless Communications*, vol. 8, no. 9, pp. 4561–4567, September 2009.
 26. L. Chen, B. Krongold, and J. Evans, “Performance analysis for optical ofdm transmission in

- short-range im/dd systems,” *Journal of Lightwave Technology*, vol. 30, no. 7, pp. 974–983, April 2012.
27. J. M. Kahn and J. R. Barry, “Wireless infrared communications,” *Proceedings of the IEEE*, vol. 85, no. 2, pp. 265–298, Feb 1997.
 28. J. Armstrong and B. J. C. Schmidt, “Comparison of asymmetrically clipped optical ofdm and dc-biased optical ofdm in awgn,” *IEEE Communications Letters*, vol. 12, no. 5, pp. 343–345, May 2008.
 29. A. Yesilkaya, H. F. Alsan, F. Miramirkhani, E. Panayirci, H. Senol, and M. Uysal, “Modeling of visible light channels and performance analysis of aco-ofdm,” in *2015 23rd Signal Processing and Communications Applications Conference (SIU)*, May 2015, pp. 2102–2105.
 30. H. Haas, “High-speed wireless networking using visible light,” *SPIE Newsroom*, Apr. 2013.
 31. T. Lee and A. Dentai, “Power and modulation bandwidth of GaAs-AlGaAs high-radiance LED’s for optical communication systems,” *Quantum Electronics, IEEE Journal of*, vol. 14, no. 3, pp. 150–159, Mar. 1978.
 32. J. Armstrong, “OFDM for optical communications,” *Lightwave Technology, Journal of*, vol. 27, no. 3, pp. 189–204, Feb. 2009.
 33. S. Dissanayake and J. Armstrong, “Comparison of ACO-OFDM, DCO-OFDM and ADO-OFDM in IM/DD systems,” *Lightwave Technology, Journal of*, vol. 31, no. 7, pp. 1063–1072, Apr. 2013.
 34. D. Tsonev, S. Sinanovic, and H. Haas, “Novel unipolar orthogonal frequency division multiplexing (U-OFDM) for optical wireless,” in *Vehicular Technology Conference (VTC Spring), 2012 IEEE 75th*, May 2012, pp. 1–5.

35. D. Tsonev and H. Haas, "Avoiding spectral efficiency loss in unipolar OFDM for optical wireless communication," in *Communications (ICC), 2014 IEEE International Conference on*, June 2014, pp. 3336–3341.
36. T. Fath and H. Haas, "Performance comparison of MIMO techniques for optical wireless communications in indoor environments," *Communications, IEEE Transactions on*, vol. 61, no. 2, pp. 733–742, Feb. 2013.
37. F. Miramirkhani and M. Uysal, "Channel modeling and characterization for visible light communications," *Photonics Journal, IEEE*, vol. 7, no. 6, pp. 1–16, Dec. 2015.
38. K. Lee, H. Park, and J. Barry, "Indoor channel characteristics for visible light communications," *Communications Letters, IEEE*, vol. 15, no. 2, pp. 217–219, Feb. 2011.
39. J. Ding, K. Wang, and Z. Xu, "Impact of LED array simplification on indoor visible light communication channel modeling," in *Communication Systems, Networks Digital Signal Processing (CSNDSP), 2014 9th International Symposium on*, July 2014, pp. 1159–1164.
40. R. Kizilirmak and M. Uysal, "Single color networks: OFDM-based visible light broadcasting," in *Computer, Communications, and Control Technology (I4CT), 2015 International Conference on*, Apr. 2015, pp. 544–549.
41. D. Tsonev, S. Videv, and H. Haas, "Unlocking spectral efficiency in intensity modulation and direct detection systems," *Selected Areas in Communications, IEEE Journal on*, vol. 33, no. 9, pp. 1758–1770, Sept. 2015.
42. R. Mesleh, H. Elgala, and H. Haas, "Optical spatial modulation," *Optical Communications and Networking, IEEE/OSA Journal of*, vol. 3, no. 3, pp. 234–244, Mar. 2011.
43. T. S. Rappaport, S. Sun, R. Mayzus, H. Zhao, Y. Azar, K. Wang, G. N. Wong, J. K. Schulz,

- M. Samimi, and F. Gutierrez, "Millimeter wave mobile communications for 5g cellular: It will work!" *IEEE Access*, vol. 1, pp. 335–349, 2013.
44. E. Dubois and A. Venetsanopoulos, "Convolution using a conjugate symmetry property for the generalized discrete fourier transform," *IEEE Transactions on Acoustics, Speech, and Signal Processing*, vol. 26, no. 2, pp. 165–170, Apr 1978.
45. M. Z. Afgani, H. Haas, H. Elgala, and D. Knipp, "Visible light communication using ofdm," in *2nd International Conference on Testbeds and Research Infrastructures for the Development of Networks and Communities, 2006. TRIDENTCOM 2006.*, 2006, pp. 6 pp.–134.
46. M. Zhang and Z. Zhang, "An optimum dc-biasing for dco-ofdm system," *IEEE Communications Letters*, vol. 18, no. 8, pp. 1351–1354, Aug 2014.
47. N. Fernando, Y. Hong, and E. Viterbo, "Flip-ofdm for unipolar communication systems," *IEEE Transactions on Communications*, vol. 60, no. 12, pp. 3726–3733, December 2012.
48. X. Wang and H. V. Poor, "Iterative (turbo) soft interference cancellation and decoding for coded cdma," *IEEE Transactions on Communications*, vol. 47, no. 7, pp. 1046–1061, Jul 1999.
49. "VLC channel models by the ongoing vlc standardization group ieee802.15.7r."
50. "Adlink, [Online]," <http://www.adlinktech.com/DAQ/USBDAQ.php>, accessed: 11-05-2016.
51. "Luminus, [Online]," <http://www.luminus.com/products/SST-50.html>, accessed: 11-05-2016.
52. H. I. Ayalp, M. E. Kazanc, B. Mekiker, and M. Ozdemir, "Design of a visible light communication system," in *GE 400 ENGINEERING DESIGN AND PROJECT*, Spring 2015.

53. M. Uysal and H. Nouri, "Optical wireless communications 2014; an emerging technology," in *2014 16th International Conference on Transparent Optical Networks (ICTON)*, July 2014, pp. 1–7.
54. T. Komine and M. Nakagawa, "Fundamental analysis for visible-light communication system using led lights," *IEEE Transactions on Consumer Electronics*, vol. 50, no. 1, pp. 100–107, Feb 2004.
55. P. Hanci, C. Sarikaya, and E. Havan, "Design of a new generation visible light communication system," in *GE 400 ENGINEERING DESIGN AND PROJECT*, Spring 2016.

A.1. Curriculum Vitae

Anil Yesilkaya received the B.Sc. degree in electronics engineering from Kadir Has University, Istanbul, Turkey, in 2014 with first class honors. He was an exchange student in second year of the B.Sc. in Montana State University, Bozeman, United States. He is currently, M.Sc. student from electronics engineering at Kadir Has University with first class honors. He is expected to finish M.Sc. degree in July, 2015. His research interests include optical wireless communications, channel estimation, optimization and artificial intelligence.

A.2. Publications

A.2.1. National Journal Papers

- A. Yeşilkaya, F. Miramirkhani, H. F. Alsan, E. Başar, E. Panayırıcı, M. Uysal, “Modelling of Visible Light Channels and Performance Analysis for Optical OFDM Systems”, Journal of Electrical, Electronics, Biomedical and Computer Engineering. (Accepted in November, 2015)

A.2.2. International Conference Papers

- A. Yesilkaya, O. Karatalay, A. S. Ogrenci, E. Panayırıcı, "Channel Estimation for Visible Light Communications Using Neural Networks", IEEE International Joint Conference on Neural Networks (IJCNN2016), 24-29 July, Vancouver, Canada.
- A. Yesilkaya, F. Miramirkhani, E. Basar, E. Panayırıcı, M. Uysal, " Performance of MIMO Enhanced Unipolar OFDM with Realistic Indoor Visible Light Channel Models", IEEE Wireless Communications and Networking Conference (WCNC2016), 3-6 April, 2016, Doha, Qatar.

- A. Yesilkaya, H. F. Alsan, F. Miramirkhani, E. Panayirci, Habib Senol, and Murat Uysal, "Performance Analysis of DCO-OFDM Systems in the Presence of Realistic Indoor Visible Light Channels", European Conference on Networks and Communications (EuCNC2015), June 29-July 2, 2015, Paris, France.

A.2.3. National Conference Papers

- A. Mamus, A. Yesilkaya, E. Panayirci, "Modeling and Equalization of Indoor Visible Light Channels", Signal Processing and Communications Applications Conference (SIU), 2016 24th, Zonguldak.
- A. Yesilkaya, H. F., E. Panayirci, "VLC Sparse Channel Estimation in the Presence of Non-Gaussian Clipping Noise", Signal Processing and Communications Applications Conference (SIU), 2016 24th, Zonguldak.
- A. Yesilkaya, H. F. Alsan, F. Miramirkhani, E. Panayirci, H. Senol and M. Uysal, "Modeling of visible light channels and performance analysis of ACO-OFDM", Signal Processing and Communications Applications Conference (SIU), 2015 23th, Malatya, 2015, pp. 2102-2105.